Stony Brook University

Studies in Perturbative QCD

A Dissertation Presented

by

Sahap Mert Aybat

to

The Graduate School

in Partial Fulfillment of the Requirements

for the Degree of

Doctor of Philosophy

in

Physics

Stony Brook University

May 2007

Stony Brook University

The Graduate School

Sahap Mert Aybat

We, the dissertation committee for the above candidate for the Doctor of Philosophy degree, hereby recommend acceptance of the dissertation.

George Sterman - Dissertation Advisor
Professor, C. N. Yang Institute for Theoretical Physics

Alfred S. Goldhaber - Chairperson of Defense
Professor, C. N. Yang Institute for Theoretical Physics

Clark McGrew
Assistant Professor, Department of Physics and Astronomy

William Kilgore - Outside Member
Senior Scientist, High Energy Theory Division,
Brookhaven National Laboratory

This dissertation is accepted by the Graduate School.

Lawrence Martin
Dean of the Graduate School

Abstract of the Dissertation
Studies in Perturbative QCD

by

Sahap Mert Aybat

Doctor of Philosophy

in

Physics

Stony Brook University

2007

Quantum Chromodynamics (QCD) is the fundamental theory of strong interactions. One of the reasons why QCD has been very successful is the factorization properties of high energy QCD processes. In quantum field theories, factorization is the separation of short and long distance effects. In the first part of this thesis, we will first develop a systematic understanding of the long distance effects in QCD, and then review the proof of factorization for semi-inclusive hadronic scattering cross sections. We will also discuss how we use this result to make cross section predictions in perturbative QCD.

Cross sections for (semi-)inclusive processes get large logarithmic corrections in perturbative QCD, associated with certain kine-

matic regions in phase space. It is useful to resum these large corrections to all orders in perturbation theory. In the second part of this thesis we will study the resummation of these large corrections for partonic scattering amplitudes. The main result of this thesis will be the computation of the two-loop soft anomalous dimension matrix, which is needed for the resummation of next-to-next-to leading logarithmic corrections.

To my parents.

Contents

List of Figures

Acknowledgements

First and foremost, I would like to thank my thesis advisor George Sterman, for all his support and advice during my graduate studies. I don't think there is any other field in physics I would have enjoyed working on more than perturbative QCD and I don't think I could possibly have learned it better from anyone other than George Sterman.

I would like to thank Lance J. Dixon for a very useful and a fruitful collaboration. His help was crucial for the completion of my project.

I would like to thank all the faculty members of the C.N. Yang Institute for Theoretical Physics and especially Prof. Peter van Nieuwenhuizen from whom I have taken almost all my advanced graduate level courses. It has been a unique experience to learn a countless list of topics in theoretical physics from him and his insights will always be a source of inspiration.

To all my friends : unfortunately you are too many to list in these pages but I thank every single one of you very much, for being excellent friends.

Last, but not least I would like to thank my parents, for their infinite love and support. I would be nowhere without you!

Chapter 1

Prologue: QCD as a Theory of Strong Interactions

1.1   A brief history of QCD

Throughout the history of humankind, one of the very important questions we have always asked is "what is the matter made out of and how does it interact with other matter?" Our quest for answering this question goes back to as early as around 450 BC when Democritus in ancient Greece proposed that the matter is made out of the "indivisible" or the "uncuttable" atoms. Even today, particle physicists continue this quest for a better understanding of the fundamental properties of the nature and probably this search will continue as long as the humankind exists.

Our latest understanding of what the matter is made out of is summarized by the Standard Model (SM) of particle physics, and according to the SM, the matter that we can see directly is made out of leptons and quarks. We understand the interactions of these fundamental particles and therefore the

interactions of matter in terms of four different forces. The first one is the gravitational force. Ironically, even though gravity is the interaction we have observed and known about for the longest time, it is the one that gives today's theoretical physicists the most headache. It is one of the aims of string theory to describe gravity in the world of sub-atomic particles. Classically, however, our understanding goes back to the seventeenth century, when Newton for the first time gave a mathematical description of gravity and its determination of the orbits of planets. Today we believe that the most accurate classical description is due to Einstein, through his theory of general relativity of 1915.

The second force in our list is electromagnetism. The classical theory of electromagnetism was developed during the 19th century and the complete mathematical description was given by J. C. Maxwell. It describes the motion of charged particles in the presence of electric and magnetic fields and how these fields are generated by charges and currents. The relativistic quantum field theory of electromagnetism, which we call quantum electrodynamics (QED) was developed much later in 1940's by Richard Feynman, Freeman Dyson, Julian Schwinger, and Sin-Itiro Tomonaga, and for which Feynman, Schwinger and Tomonaga were awarded with the 1965 Nobel Prize in physics.

The last two forces in our list of fundamental interactions are the weak and strong nuclear forces. Soon after the discovery of the neutron in 1932, it was shown that it decays in about 15 minutes when it is outside the nucleus. This decay mode, also known as the β-decay, which is given by $n \rightarrow p^+ + e^- + \bar{\nu}_e$, is due to the weak interactions. The strong nuclear force, or the strong interactions, are the ones that are responsible for the binding of the quarks

inside the nucleons and the binding of nucleons inside the nucleus.

Developments in high energy acclerators and the discovery of the pion and other mesons in the fifties prompted the studies of the structure of nucleons. The application of quantum mechanics to fields, which resulted in quantum field theory in the late twenties worked very well for the treatment of electrodynamics. For the case of the weak interactions, an effective theory with four-fermion "Fermi" interactions was quite successful at tree level [1, 2]. This theory, however, is not renormalizable and therefore had only limited predictive power. In the absence of renormalization, it was also not known whether one could describe the strong interactions by a consistent quantum field theory [3].

Until the mid sixties, attempts of explaining the strong interactions with a quantum field theory failed. As a result, people tried out different approaches. Among these were "S-matrix theories" [3, 4]. The main idea was to describe the particle states in terms of the analytic properties of the S-matrix which were measured in scattering experiments, instead of in terms of local fields which are not directly measurable in general. Along this path the Regge pole theory was developed by Regge in 1959 [5, 6]. Even though a large amount of experimental data can still be understood best in such theories, the drawback was that the fundamental principles included in these theories were not adequate to be truly predictive.

Apart from the lack of a complete fundamental theory to explain strong dynamics, there was another chaos in the particle physics community due to the discovery of a large number of hadrons. One of the triumphs of the early

sixties was the discovery of what we know today as an approximate symmetry of the hadrons, flavor SU(3), by Gell-Mann and Y. Neeman [7]. This discovery resolved the chaos, by explaining the baryon spectrum, and eventually led to the concept of quarks as the constituents of hadrons, through the constituent quark model [8].

Around the same time, the idea of color was developed by Greenberg in 1964 [9] and Han and Naumbu in 1965 [10]. This new quantum number for the quarks was introduced to resolve problems in the quark model with Fermi statistics for the spin 1/2 quarks, especially after the discovery of Δ^{++} which was composed of three up quarks with parallel spins. This new idea also suggested the existance of a local nonbelian gauge theory, a type of theory which was developed originally by Yang and Mills [11] many years before but which was not popular in the meantime.

A very important period in this brief history is the late sixties, when deep inelastic scattering (DIS) experiments were started at SLAC. One of the results of these experiments was the observation that the proton has a charged substructure which is much smaller than itself.

Probably the most striking result of these early DIS experiments was that the structure functions $F(x, Q^2)$ were approximately independent of the scale Q^2. This is called scaling [12, 13, 14]. One of the very crucial observations was that the parton model developed by Feynman in 1969 [15] and Bjorken and Paschos in 1969 [16], could reproduce this important result of the DIS experiments. The parton model not only explained scaling but also identified partons as quarks with spin-1/2 through the Callan-Gross relation [17] for the

structure functions in the parton model. The quantum field-theoretical justification of the parton model is highly nontrivial and requires an asymptotically free theory, in other words a theory whose coupling decreases as the distance scale decreases.

In the early seventies much happened in favor of field theory. t'Hooft and Veltman prooved the renormalizablity of the spontaneously broken Higgs models and unbroken Yang-Mills theories for which they were awarded with the 1999 Nobel Prize in physics [18, 19, 20]. With this, nonabelian gauge theories started becoming popular. Along with renormalizability, one of the most crucial properties of such theories is that they can be asymptotically free, which was indeed signalled in the DIS experiments. A new tool, operator product expansion, was developed by Wilson [21] which was used for the analysis of DIS. Renormalization group started to become popular once again. It started to become clear that a nonabelian gauge theory was actually consistent with what was known at that time.

1.2 Quantum Chromodynamics

Today we believe that the fundamental theory of strong interactions is given by quantum chromodynamics (QCD), which is a nonabelian gauge theory with the gauge symmetry group SU(3). It is described by the following

Lagrange density

$$\mathcal{L} = -\frac{1}{2} tr \left(F_{\mu\nu} F^{\mu\nu} \right) + \sum_f \bar{q}_{f,i} (i \not{\partial} \delta_{ij} + i g_s \not{A}^a (T_a^{(F)})_{ij} - M_f \delta_{ij}) q_{f,j}$$

$$-\frac{1}{2\xi} (\partial_\mu A^{a,\mu})^2 + \partial_\mu b_a (\partial^\mu \delta_{ab} + g_s f_{abd} A_b^\mu) c_d . \tag{1.1}$$

Here the quark fields $q_{f,i}$ with flavor f ($f = 1, \cdots, n_f$), color i ($i = 1, \cdots, N$) and mass M_f are given by Dirac spinors in the fundamental representation of SU(N) (with N=3 for QCD) where $\bar{q}_{f,i} = q_{f,i}^\dagger \gamma^0$. The A_μ^a ($a = 1, \cdots, N^2 - 1$) are the Lie algebra-valued gluon vector fields in the adjoint representation of SU(N). The $T_a^{(F)}$ are the generators of the group SU(N) in the N-dimensional defining representation, which obey the commutation relation

$$\left[T_a^{(F)}, T_b^{(F)} \right] = i f_{abc} T_c^{(F)} , \tag{1.2}$$

where the f_{abc} are the totally antisymmetric structure functions. The non-abelian Lie algebra-valued field strengths $F_{\mu\nu} \equiv F_{\mu\nu}^a T_a^{(F)}$ are given by

$$F_{\mu\nu} = \partial_\mu A_\nu - \partial_\nu A_\mu + i g_s [A_\mu, A_\nu] . \tag{1.3}$$

Note that we have written the QCD Lagrange density in a covariant gauge with an arbitrary gauge parameter ξ. In this gauge the gluon propagator $G^{\mu\nu,ab}$ is given by

$$G^{\mu\nu,ab}(k, \xi) = \frac{\delta^{ab}}{k^2} \left[-g^{\mu\nu} + (1 - \xi) \frac{k^\mu k^\nu}{k^2} \right] . \tag{1.4}$$

Later on we will often choose $\xi = 1$, also known as the Feynman gauge. Another useful gauge choice is the axial gauge with the gauge fixing function $n \cdot A = 0$ where n is a fixed vector. For this physical gauge the gluon propagator

is given by

$$G^{\mu\nu,ab}(k,n,\xi) = \frac{\delta^{ab}}{k^2} \left[-g^{\mu\nu} + \frac{n^\mu k^\nu + k^\mu n^\nu}{n \cdot k} - n^2 \left(1 + \xi \frac{k^2}{n^2} \right) \frac{k^\mu k^\nu}{(n \cdot k)^2} \right] . \quad (1.5)$$

Finally in Eq. (1.1), b_a and c^a are the anti-ghost and the ghost fields, whose Lagrange density can be obtained by the Fadeev-Popov procedure of Ref. [22].

The diagramatic Feynman rules for perturbative QCD are obtained from the Lagrange density given in Eq. (1.1) following the standard techniques in quantum field theory given in Ref. [23]. These rules can be found in the same reference.

Now that we have discussed a brief history of QCD and written down the QCD Lagrange density, we will focus on some of the very important properties of the theory: confinement, asymptotic freedom and infrared safety. Confinement in QCD is the phenomenon that color charged quarks or gluons do not exist in isolation, as asymptotic states. The confined quarks always form particle-antiparticle pairs, mesons, or triplets to form baryons that are color neutral. There is no proof in perturbative QCD (the regime in QCD where the rules of perturbation theory are applicable) which shows, from first principles, that QCD is a confining theory, although the asymptotic freedom of the coupling suggests that might be the case. However, we know that the reason is due to the nonabelian nature of the theory. Confinement must be understood within the nonperturbative regime of QCD. Numerical methods of lattice QCD, which were developed by Wilson, 1974 [24]; Kogut and Susskind, 1975 [25]; Creutz, 1983 [26], are examples of studies in nonperturbative QCD.

Asymptotic freedom is the property that the running coupling of QCD

decreases as the length scales over which it is measured decreases and likewise increases as the length scale increases. Gross, Politzer and Wilczek were awarded with the 2004 Nobel Prize in physics for their discovery of asymptotic freedom in the theory of strong interactions [27, 28, 29]. We can understand why QCD is an aymptotically free theory with the following physical picture. One can calculate the dielectric constant of a medium, ϵ, in terms of the magnetic permeability, μ, by using $\mu \epsilon = 1$, in units where the speed of light c is one. In classical electrodynamics, magnetic fields arise from electric currents, and due to Lenz's law, when there is an external magnetic field the response of a system is to generate electric currents such that the magnetic field is decreased. Therefore classically all media have $\mu < 1$ and with the above relation $\epsilon > 1$, which corresponds to electric screening. However in QCD, gluons also carry color charge, and behave like color magnetic dipoles, alligning themselves along an external field and therefore increasing its magnitude so that $\mu > 1$. This is the anti-screening of gluons for the QCD vacuum. We can understand the asymptotic freedom of QCD because the anti-screening of the gluons overcomes the screening of quarks as long as there are not too many quarks.

Due to the renormalization properties of a quantum field theory, the strength of the coupling depends on (runs with) the renormalization scale. This running is described by the relation

$$\frac{\partial}{\partial \ln \mu} g(\mu)|_{g_0} \equiv \beta(g(\mu)), \tag{1.6}$$

where μ is the renormalization scale, and where the bare coupling g_0 is held

fixed in the derivative. The *beta function* $\beta(g)$ of QCD is determined to one loop from the renormalization constant of the coupling, Z_g, by

$$
\begin{aligned}
\frac{\partial}{\partial \ln \mu} g(\mu) &= \frac{\partial}{\partial \ln \mu}(Z_g\, g_0) \\
&= -g\left[\beta_0 \frac{\alpha_s}{4\pi} + \beta_1 \left(\frac{\alpha_s}{4\pi}\right)^2 + \cdots\right] \\
&= \frac{\partial}{\partial \ln \mu}\left[g_0 - \ln(\mu^2/M^2)\left(\frac{g_0^3}{8\pi^2}\left(\frac{11N}{3} - \frac{2n_f}{3}\right)\right) + \cdots\right] \\
&= -\frac{g^3}{16\pi^2}\left(\frac{11}{3}N - \frac{2}{3}n_f\right) + \cdots,
\end{aligned}
\tag{1.7}
$$

where M^2 is a UV cutoff. With this one loop beta function we can solve Eq. (1.7) easily with the famous result

$$
\begin{aligned}
g^2(\mu) &= \frac{g^2(\mu_0)}{1 + \beta_1 \frac{g^2(\mu_0)}{16\pi^2}\ln(\mu^2/\mu_0^2)} \\
&\equiv \frac{16\pi^2}{\beta_1 \ln(\mu^2/\Lambda_{\mathrm{QCD}}^2)},
\end{aligned}
\tag{1.8}
$$

where we have defined

$$
\Lambda_{\mathrm{QCD}} \equiv \mu_0 e^{-8\pi^2/2\beta_1 g^2(\mu_0)}.
\tag{1.9}
$$

From Eq. (1.7) for QCD, β_1 is given by

$$
\beta_1 = 11 - \frac{2}{3}n_f.
\tag{1.10}
$$

We can see from Eq. (1.8) that as the momentum scale decreases, or as the corresponding distance scale increases, the perturbative coupling grows. As we have observed above, this is just what we need to justify in field theory the parton model.

Finally we would like to talk about the idea of infrared safety. In QCD, quantities that are dominated by the short distance behaviour of the theory

are called infrared (IR) safe quantities [30]. These quantities cannot depend on light quark or gluon masses, and should be free of infrared divergences due to long distance behaviour of the theory. They can therefore be calculated with the methods of perturbation theory. The infrared divergences will be the subject matter of the next chapter where we will define what they are and from what regions in the momentum space they originate.

In QCD, a physical quantity $\sigma(Q^2/\mu^2, \alpha_s(\mu^2), m^2/\mu^2)$, where Q is a large invariant such that $Q >> \Lambda$, m is the light quark or gluon masses and μ is the renormalization scale, is IR safe if in the large μ limit it behaves as

$$\lim_{\mu \to \infty} \sigma \left(\frac{Q^2}{\mu^2}, \alpha_s(\mu^2), \frac{m^2(\mu^2)}{\mu^2} \right) = \hat{\sigma} \left(\frac{Q^2}{\mu^2}, \alpha_s(\mu^2) \right) + \mathcal{O} \left(\left(\frac{m^2}{\mu^2} \right)^a \right) , \ a > 0 \, .$$

(1.11)

In words, σ should have a finite limit as $m/\mu \to 0$ with Q/μ fixed. It is in the essence of perturbative QCD to identify such infrared quantities and seperate them from long distance-dependent, infrared divergent quantities. This kind of separation of long and short distance dynamics for a physical quantity is called *factorization* and it will be the subject matter of Chapter 3 of this thesis.

For an inclusive hadronic scattering, $A + B \to X$, we will show that many cross sections have such a factorization. For such a cross section $\sigma_{AB \to X}$, we may write

$$\sigma_{AB \to X} = \sum_{a,b} \int_0^1 \frac{dx_a}{x_a} \frac{dx_b}{x_b} \, f_{a/A}(x_a, \mu) \, \hat{\sigma}_{ab}(x_a, x_b, \mu) f_{b/B}(x_b, \mu) + \text{corrections} \, ,$$

(1.12)

with corrections that vanish as energy scale $Q \to \infty$. The fs are the parton distribution functions for partons in hadrons. These give the distribution of

partons in hadrons with momentum fractions $x_{a,b}$. Parton distribution functions are universal, in other words process independent, and they are obtained from experiment. $\hat{\sigma}$ is a *partonic cross section* which is perturbatively calculable.

We will study the formal proof for the factorization of inclusive hadron-hadron scattering cross-sections in great detail in the following chapters.

1.3 Outline of the thesis

Factorization in quantum field theory (QFT) is the separation of long and short distance dynamics. QCD gains its predictive power as the theory of strong interactions through factorization. It is the purpose of this thesis to review the proof of factorization for semi-inclusive hadronic cross sections and to show how we use this result to make cross section predictions in perturbative QCD.

In order to separate the long and short distance effects, we first need to understand the origin of long distance enhancements. We will call these enhancements IR divergences. In Chapter 2 of this thesis we will focus on the IR singularities originating from individual Feynman diagrams that contribute to cross sections. It will be our goal to find a systematic way of identifying the regions in momentum space that contribute to IR enhancements for hadronic processes. We will start with a discussion of the analytic structure of Feynman integrals which will lead us to the idea of *pinch singular surfaces*. It is these surfaces in the parameter space that contribute to the IR singularities. By

considering the pinch singular surfaces we will find a set of infrared power counting rules for gauge theories which will enable us to identify the *leading regions* in momentum space which give the dominant contribution to the long distance enhancements.

After identifying the leading regions in momentum space, in Chapter 3 we will demonstrate the proof of factorization of the long distance dynamics due to these leading regions and the short distance effects. The proof has three main steps. Final state cancellations, factorization of collinear gluons from the hard part and the factorization and cancellation of soft gluons. We will explain each of these steps in considerable detail. We will see that unitarity and gauge invariance will play crucial roles in each of these steps. At the end of Chapter 3 will will have the full factorized form of the semi-inclusive hadronic scattering cross section. As we will see, it is written as a convolution of parton distribution functions and a hard scattering function. We will discuss how we obtain the parton distribution functions from experiment and how we calculate the hard scattering function in perturbation theory.

In the last chapter, Chapter 4, of this thesis we will concentrate on partonic $2 \rightarrow n$ scattering amplitudes. As we will see, partonic scattering amplitudes are crucial for the calculation of the hard scattering functions. Due to the factorization of Chapter 3, it is guarranteed that the virtual and real corrections to the cross section cancel. However, in certain regions of phase space this cancellation is not complete, and due to this incomplete cancellation there are often large logarithmic contributions to the cross section. As we will discuss in great detail, one can sum these large logarithmic corrections to

all orders in perturbation theory. This procedure is referred to as *resummation*. For hadronic scattering processes, resummation of large logarithms, or in the case of partonic scattering amplitudes, resummation of poles requires an anomalous dimension matrix, called *soft anomalous dimension*. The main goal of this thesis is to compute this matrix at two loop level and this we will explain in Chapter 4.

Chapter 2

Pinch Surfaces and Infrared Power Counting

The main idea for the factorization of QCD cross sections, as briefly discussed in Chapter 1, is to separate the perturbative short distance effects from the nonperturbative long distance dynamics. In order to achieve that goal, however one needs to understand the long distance (therefore low energy, or 'Infrared") behaviour for the QCD cross sections. One way to proceed is to study the analytic structure of Feynman diagrams, which will lead us to a set of infrared power counting rules. By means of the infrared power counting rules we will be able to identify the regions in momentum space, for the diagrams that contribute to the cross section, that enhance the infrared behaviour of the cross section. We will start our discussion with the study of the analytic structure of Feynman integrals.

2.1 Analytic Structure of Feynman Integrals: Infrared Divergences

We can write an arbitrary Feynman diagram $\mathcal{G}(\{p_i\})$ with external lines carrying momenta $\{p_i\}$ and an arbitrary number of loops with loop momenta $\{q_j\}$ using Feynman parametrization as

$$\mathcal{G}(\{p_i\}) = \prod_{\text{lines k}}^{P} \int_0^1 d\alpha_k \, \delta(\sum_k \alpha_k - 1) \prod_{\text{loops l}} \int d^n q_l \, D(\alpha_k, q_l, p_i)^{-P} \, N(\alpha_k, q_l, p_i) \,,$$

$$(2.1)$$

where

$$D(\alpha_k, q_l, p_i) = \sum_j \alpha_j \left[l_j^2(q, p) - m_j^2 \right] + i\epsilon \,. \qquad (2.2)$$

$N(\alpha, q, p)$ is the product of all the overall factors in the numerator, which include color factors, symmetry factors, powers of α_s and so on. We would like to find out the singularities of $\mathcal{G}(\{p_i\})$ that are associated with the infrared divergences. The integrand of $\mathcal{G}(\{p_i\})$ is singular at the zeros of the denominator $D(\alpha, q, p)$. However, finding the zeros of D is not enough. $\mathcal{G}(\{p_i\})$ is defined in terms of contour integrals in complex space over the loop momenta q and the Feynman parameters α, and the whole integrand is an analytic function of the external momenta and the integration parameters. Therefore one can, assuming that the integrals can always be done one at a time while keeping the rest of the integration parameters fixed, deform the contour of integration away from the zeros of D, provided that the deformed contours do not cross any other singularities. Such a contour deformation to avoid the poles is, however, not possible under two circumstances.

1. If one of the poles coincides with one of the end points of the Feynman parameter integrals, one cannot use contour deformation to avoid that pole, since the end points of these integrals are fixed. We call these types of singularities *end point singularities.*

2. If two or more poles coincide at a point on either side of the contour, then one cannot deform the contour away from one of the poles without crossing the other singularity. We will call this type of singularities *pinch singularities.*

We see that in order to find the singularities of $\mathcal{G}(\{p_i\})$ we not only look for the zeros of D but also look for the ones that are pinched. Since D is quadratic in the loop momenta q_l, these two conditions can be written as

$$
\begin{aligned}
D(\alpha_k, q_l, p_i)|_{\zeta=\zeta_0} &= 0\,, \\
\frac{\partial}{\partial q_l^\mu} D(\alpha_k, q_l, p_i)|_{\zeta=\zeta_0} &= 0\,,
\end{aligned}
\tag{2.3}
$$

where $\zeta \in \{\alpha_k, q_l\}$ are elements of the set of points in the parameter space for the integrals, and $\zeta_0 \in \zeta$ are points for which D is zero. Using Eq. (2.2) we see that the first line of Eq. (2.3) is satisfied when for each line either its Feynman parameter vanishes, i.e. $\alpha_j = 0$ or it is on-shell, i.e. $l_j(k, p)^2 = m_j^2$. The second line in Eq. (2.3) is satisfied when the derivative of D vanishes at $D = 0$. These two conditions were put into an explicit form by Landau and are summarized as the Landau equations [31]

$$
\text{either} \ \ \alpha_j = 0\,, \forall j \quad \text{or} \quad l_j(q, p)^2 = m_j^2\,,
$$

$$
\text{and} \sum_{\text{lines}\,j} \epsilon_{jm}\, \alpha_j\, l_j^\mu(q, p) = 0\,,
\tag{2.4}
$$

where ϵ_{km} is $+1$ (-1) if the loop momentum q_m is flowing in the same (opposite) direction as the line momentum l_j.

For an arbitrary Feynman diagram $\mathcal{G}(\{p_i\})$, using Eq. (2.4) we know that in order to get an infrared singularity one of the necessary conditions is to have on-shell lines, or vanishing Feynman parameters for lines that are off-shell.

For a diagram with an arbitrary number of off-shell lines, we now construct another diagram where every off-shell line with $\alpha_i = 0$ is reduced to a point. We refer to such diagrams as *reduced diagrams*. The Landau equations, given in Eq. (2.4), describe a very useful physical picture for these reduced diagrams as we see by the following reasoning, due originally to Coleman and Norton [32].

In configuration space we can think of each on-shell line as propagating freely between two vertices that have a space-time separation given by

$$\Delta x_i^\mu \equiv \alpha_i \, l_i^\mu(p, q) \,, \tag{2.5}$$

where we have interpreted each Feynman parameter α_i as the ratio of the Lorentz invariant time of propagation to the energy of the particle[1]:

$$\alpha_i = \Delta x_i^0 / l_i^0 \,. \tag{2.6}$$

Then we have

$$\Delta x_i^\mu = \Delta x_i^0 \, \beta_i^\mu \,, \tag{2.7}$$

---

[1] Note that the Feynman parameters as we have introduced originally do not have any dimensions, which is not the case here. However, one can always rescale them with a dimensionfull constant so that they have the appropriate dimensions.
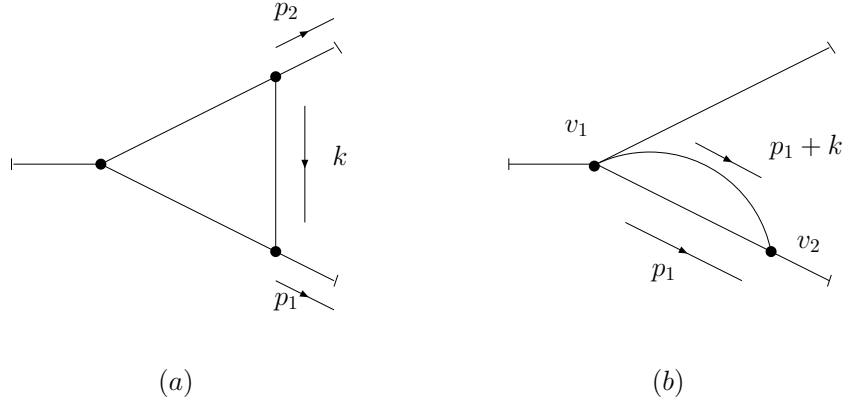
Figure 2.1: a) The scalar massless triangle diagram. b) CO region correspond-ing to Eq. (2.14)

with

$$\beta_i^\mu = \left(1, \frac{\vec{l_i}}{l_i^0}\right),$$ (2.8)

the four-velocity of a particle with momentum l_i^μ. Now let's define

$$\Delta x_{ab} \equiv x_a - x_b,$$ (2.9)

where we have labelled each vertex of the loop as $x_1, x_2, \cdots, x_n$ with space-time separation between each vertex $\Delta x_{12}, \Delta x_{23}, \cdots, \Delta x_{n1}$. Notice that by definition Δx_{ab} have translational invariance. Given these identifications the requirement in the second line of Eq. (2.4) is identical to

$$\Delta x_{12} + \Delta x_{23} + \cdots + \Delta x_{n1} = 0, \, \forall \, \text{loops},$$ (2.10)

which corresponds to a physical picture in which on-shell particles with mo-menta l_i propagate freely between vertices in a loop of n lines.

Now let's see how we can apply our considerations so far to a simple con-crete example. We will consider the scalar massless one-loop triangle diagram

in Fig. 2.1 a. The one-loop momentum space Feynman integral in dimensional regularization with $n = 4 - 2\varepsilon$ dimensions is proportional to

$$
\begin{aligned}
I_\Delta^{\text{scalar}} \quad &\propto \quad \int \frac{d^n k}{(2\pi)^n} \frac{1}{k^2 + i\epsilon} \frac{1}{(p_1 - k)^2 + i\epsilon} \frac{1}{(p_2 + k)^2 + i\epsilon} \\
&= \quad 2 \int_0^1 d\alpha_1 \, d\alpha_2 \, d\alpha_3 \, \delta(1 - \alpha_1 - \alpha_2 - \alpha_3) \int \frac{d^n k}{(2\pi)^n} \frac{1}{D^3(p_1, p_2, k, \alpha_i)} \, ,
\end{aligned}
$$
(2.11)

with

$$
D(p_1, p_2, k, \alpha_i) = \alpha_1 k^2 + \alpha_2 (p_1 - k)^2 + \alpha_3 (p_2 + k)^2 + i\epsilon \, .
$$
(2.12)

In order to find the pinched singular points for this diagram, we apply the Landau equations, Eq. (2.4) to the denominator given in Eq. (2.12). We find

$$
\begin{aligned}
D(p_1, p_2, k, \alpha_i) &= 0 \, , \\
\alpha_1 k^\mu - \alpha_2 (p_1 - k)^\mu + \alpha_3 (p_2 + k)^\mu &= 0 \, .
\end{aligned}
$$
(2.13)

There are three non-trivial solutions to the system of equations. They are given by

$$
\begin{aligned}
k = \rho \, p_1 \, , \qquad \alpha_1 \rho &= \alpha_2 (1 - \rho) \, , \\
\alpha_3 &= 0 \, ,
\end{aligned}
$$
(2.14)

$$
\begin{aligned}
k = -\rho' \, p_2 \, , \qquad \alpha_1 \rho' &= \alpha_2 (1 - \rho') \, , \\
\alpha_2 &= 0 \, ,
\end{aligned}
$$
(2.15)

$$
k = 0 \, , \qquad \alpha_2 = \alpha_3 = 0 \, ,
$$
(2.16)

where ρ and ρ' are positive real numbers,

$$0 \; < \; \rho < 1$$

$$0 \; < \; \rho' < 1 \,. \tag{2.17}$$

The momentum space regions corresponding to the solutions given in Eqs. (2.14) and (2.15) are called *collinear regions* (CO) since for both cases the loop momentum k is proportional to one of the external momenta. The region of momentum space where the loop momentum is vanishingly small, which corresponds to the solution given in Eq. (2.16) is called the *soft region* (IR). The physical picture corresponding to the collinear region given in Eq. (2.14) is illustrated in Fig. 2.1 b. At vertex v_1, two on-shell lines are created and they propagate freely to vertex v_2, where they combine to give the external line. With further simple analysis one can show that the lightlike four-velocities of the propagating lines β_k and β_{p_1+k} are equal. One can draw an analogous physical picture for the collinear region corresponding to Eq. (2.15).

2.2   Pinch Surfaces

In the previous section we have seen that for an arbitrary Feynman diagram, in order to have IR/CO enhancements, the denominator for the Feynman integral given in Eq. (2.2) has to satisfy the Landau equations, Eq. (2.4) at points $\zeta_0 \in \{q, \alpha\}$ for which D vanishes. The set of points $\zeta_0 = \{q_0, \alpha_0\}$ form surfaces in the (q, α) space. Each such surface that produces an IR/CO singularity is called a *pinch surface*. Each pinch surface has a corresponding

reduced diagram. A pinch surface is a multidimensional subspace in the (q, α) space. One can parametrize a pinch surface and its complementary space by a set of *intrinsic parameters* $\{x_i\}$ and a set of *normal variables* $\{y_i\}$, respectively [33].

Our aim is to write the integrals in $\mathcal{G}(\{p_i\})$ near the pinch surfaces such that every denominator is a homogeneous function of the normal variables that vanish there. This is referred to as the *homogeneous integral* [33]. The homogeneous integral in the above set of variables is of the form

$$J \sim \int_C \prod_{i=1}^{n} dy_i \, y_i^{-a_i} \int \prod_{j=1}^{m} dx_j \, I(\{x\}, Y) \,, \tag{2.18}$$

where the contour C passes through the point $\{y_i\} = 0$ and Y represents various ratios formed by y's. In order to put a bound on the integrals we write the normal variables in terms of a scaling variable λ, for example by inserting

$$\int_0 d\lambda \, \delta \left(\lambda - \sqrt{\sum_{i=1}^{n} y_i^2} \right) = 1 \tag{2.19}$$

in Eq. (2.18) and then changing variables to $y_i' = y_i \, \lambda$. For vanishing λ the power counting estimate of J in Eq. (2.18) can be written as

$$J \sim \int_0 d\lambda \, \lambda^{p-1} \,, \tag{2.20}$$

where

$$p = n - \sum_{i=1}^{n} a_i \,. \tag{2.21}$$

For $p \leq 0$ the integral J is divergent, and we say that J is logarithmically divergent for $p = 0$.
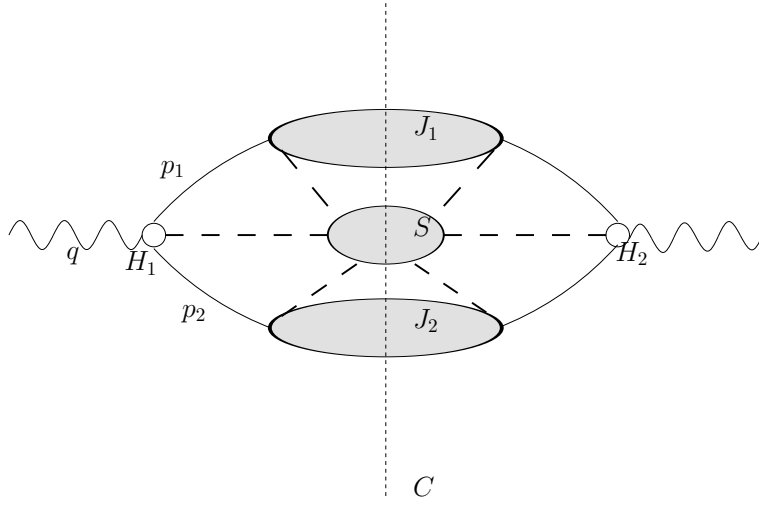
Figure 2.2: A generic reduced cut vacuum polarization graph. The dashed lines represent scalar and/or vector lines.

2.3 Infrared Power Counting

In this section we will review the infrared power counting rules derived in Ref. [33] considering cut vacuum polarization diagrams in Fig. 2.2. A cut diagram is constructed by linking amplitudes, M_1, with complex conjugate amplitudes, M_2^*, such that the on-shell final states are cut by a single vertical line leaving M_1 to the left and M_2 to the right of the cut [23]. Our discussion below treats the cut diagrams that contribute to the cross sections in e^+e^- annihilation or Z^0 decay. The more general cases of lepton-hadron and hadron-hadron scatterings are in Refs. [34, 33] and below.

The physical picture that leads to the reduced cut diagram of Fig. 2.2 is quite straighforward. Two jets labelled by J_1 and J_2 are formed after the decay of the vector boson, each with momenta p_j. The only possible interactions

between the jets is via soft particles with zero momentum. There cannot be any exchange of finite momentum particles because once the two jets are formed at the hard vertex H, they travel away from each other with the speed of light and therefore can never meet again. All off-shell, short distance contributions are in the hard subdiagrams H_1 and H_2.

We are now ready to specify the set of normal variables for the pinch surfaces of Fig. 2.2. For the case of cut vacuum polarization diagrams we choose [2]

1. All four components k^μ for the internal loop momentum in subdiagram S and for loops that connect S to the jets. We take all $k_i^\mu \sim \lambda$.

2. The invariant mass l^2 and the product $l \cdot p$ for each loop momentum l in the jet with total momentum p_j. Here $l^2 \sim l \cdot p \sim \lambda$ while $l_T \sim \lambda^{1/2}$. Also the total invariant mass for each jet, $p_j^2 \sim \lambda$.

Having identified the normal variables, we can start our discussion of the power counting. First we consider theories without vector particles. We construct the homogeneous integral by keeping terms with the lowest power of normal variables in both numerator and denominator. With the above choice of normal variables, denominators of soft lines will be quadratic in the normal variables whereas the denominators of jet lines will be linear.

Now consider an arbitrary reduced cut vacuum polarization diagram, as in Fig. 2.2 with J finite-momentum jet and S zero-momentum soft lines, $L^{(s)}$

---

[2]For a detailed discussion of this choice of normal variables see Ref. [33].

soft loops and $L^{(j)}$ internal jet loops and K jets. Then the power p of Eq. (2.21) is given by

$$p = \left(4L^{(s)} + 2L^{(j)} + K\right) - (2S + J) + N^{(j)} + N^{(s)}, \qquad (2.22)$$

where $N^{(j)}$ is due to the numerator factors from jet lines and vertices and $N^{(s)}$ is due to the numerators of soft lines and vertices. K corresponds to the variables p_j^2 with $j = 1 \cdots K$. One can rewrite $4L^{(s)} - 2S + N^{(s)}$ as

$$4L^{(s)} - 2S + N^{(s)} = 4 - b - \frac{3}{2}f - 2b - f + 4(b + f - 1), \qquad (2.23)$$

where b and f are the number of soft boson and fermion lines attached to the jets. On right hand side of the above equation, the terms $4 - b - \frac{3}{2}f$ are due to the dimension of the soft subdiagram S, without external lines; the terms $-2b - f$ are due to the dimension of all the soft lines that connect S to the jets; and finally the terms $4(b + f - 1)$ are due to the dimension of the $b + f - 1$ independent soft loops that connect S to the jets. Substituting Eq. (2.23) into Eq. (2.22) we get

$$p = \left(2L^{(j)} + K - J + N^{(j)}\right) + b + \frac{3}{2}f. \qquad (2.24)$$

Writing $N^{(j)}$

$$N^{(j)} = \sum_{i=1}^{K} n_i^{(j)}, \qquad (2.25)$$

as a sum over contributions from individual jets, we can rewrite p further as

$$p = \sum_{i=1}^{K} \left(2l_i^{(j)} + n_i^{(j)} - j_i + 1\right) + b + \frac{3}{2}f. \qquad (2.26)$$

Next we relate the number of lines and vertices in each jet by

$$2j_i = \sum_{\alpha \geq 3} \alpha \chi_{i,\alpha} + \sum_{\beta \geq 2} \beta y_{i,\beta} + \gamma_i + \delta_i, \qquad (2.27)$$

and by the Euler's identity

$$l_i = j_i - \nu_i + 1 \,. \tag{2.28}$$

Eq. (2.27) simply counts the number of ends of the lines in jet i, $2\,j_i$. In Eq. (2.27), $\chi_{i,\alpha}$ is the number of soft vertices in jet i with α jet lines and no soft lines attached, $y_{i,\beta}$ is the number of soft vertices (vertices which connect zero momentum lines) with one or more soft lines, in addition to β jet lines, and γ_i and δ_i are the number of lines of jet i attached to the hard vertices H_1 and H_2 respectively. Finally ν_i is the total number of vertices in the ith jet. This quantity can be written in the above notation as

$$\nu_i = \sum_\alpha \chi_{i,\alpha} + \sum_\beta y_{i,\beta} + 2 \,, \tag{2.29}$$

where the 2 accounts for the hard vertices H_1 and H_2. Combining Eqs. (2.27)-(2.29) one finds an expression for the contribution of each jet to the power p of Eq. (2.21),

$$2l_i^{(j)} + n_i^{(j)} - j_i + 1 = \frac{1}{2}\sum_{\alpha \geq 3}(\alpha - 4)\chi_{i,\alpha} + \frac{1}{2}\sum_{\beta \geq 2}(\beta - 4)y_{i,\beta} + \frac{1}{2}(\gamma_i + \delta_i - 2) + n_i^{(j)} \,. \tag{2.30}$$

We next turn our attention to the numerator term $n_i^{(j)}$.

We can put a lower bound on the numerator factors $n_i^{(j)}$ by observing the following. Consider first Yukawa-like theories, with only scalar bosons. In such theories numerator momenta only arise from fermion propagators in combinations like

$$(\not{p} + \not{k})(a_1 + a_2\gamma_5)\not{p} = (a_1 - a_2\gamma_5)(\not{p} + \not{k})\not{p} \,, \tag{2.31}$$

where k is the momentum for a spin zero particle that couples to the fermions, and a_1 and a_2 are constants describing the scalar and pseudo-scalar couplings of the scalar bosons.

By simple, direct calculation one can see that $(\not{p} + \not{k})\not{p}$ vanishes at least as fast as the transverse components of $(p + k)$ and p. This gives a factor of $\lambda^{1/2}$. Then in physical gauges we have, for z_i the number of vertices at which scalar or collinear bosons attach to jet fermions,

$$n_i^{(j)} \geq \frac{1}{2}\chi_{i,3} + \frac{1}{2}z_i \, . \tag{2.32}$$

Substituting Eq. (2.30) and Eq. (2.32) into Eq. (2.26) we find

$$
\begin{aligned}
p \; \geq \; & \sum_{i=1}^{K} \left[\frac{1}{2}\sum_{\alpha \geq 4}(\alpha - 4)\chi_{i,\alpha} + \frac{1}{2}\sum_{\beta \geq 4}(\beta - 4)y_{i,\beta} + \frac{1}{2}\left(\gamma_i + \delta_i - 2\right) \right] \\
& + \sum_{i=1}^{K}\left(-\frac{1}{2}\,y_{i,3} + \frac{1}{2}\,z_i - y_{i,2} \right) + b + \frac{3}{2}\,f \, .
\end{aligned}
\tag{2.33}
$$

On the other hand

$$
\begin{aligned}
\frac{1}{2}\left(b + f\right) \; &\geq \; \frac{1}{2}\sum_{i-1}^{K}(y_{i,3} + y_{i,2}) \, , \\
\frac{1}{2}\,f \; &\geq \; \frac{1}{2}\sum_{i=1}^{K}(y_{i,2} - z_i) \, ,
\end{aligned}
\tag{2.34}
$$

so that

$$
p \geq \sum_{i=1}^{K} \left[\frac{1}{2}\sum_{\alpha \geq 4}(\alpha - 4)\chi_{i,\alpha} + \frac{1}{2}\sum_{\beta \geq 4}(\beta - 4)y_{i,\beta} + \gamma_i + \delta_i - 2 \right] + \frac{1}{2}\left(b + f\right) .
\tag{2.35}
$$

We will postpone the discussion of the implications of Eq. (2.40) until the next section. For now, we recall that $\gamma_i \geq 1$ and $\delta_i \geq 1$ are the number

of jet lines attached to the hard vertices, so that p is positive semi-definite. This consideration will play a central role in identifying the leading regions of momentum space. However, before that we still need to discuss the more interesting case of theories with vector particles.

For the case of gauge theories, in the numerator, instead of terms of the form given in Eq. (2.31), jet vertices that couple fermions to vectors give combinations of the form

$$(\not{p} + \not{k})\gamma_\mu\not{p} = -\gamma_\mu(\not{p} + \not{k})\not{p} + 2(p + k)_\mu\not{p}. \tag{2.36}$$

As before, the first term contributes a factor of $\lambda^{1/2}$ when p and k are jet momenta. The second term, however, is unsuppressed at the pinch surface when it is contracted with terms in the hard part H or when k is soft. When k is a jet momentum, however, it corresponds to an unphysical scalar polarization for the vector line. Similar considerations apply to three gluon vertices coupling jet lines. When both p and k are jet momenta these contributions also vanish as fast as $\lambda^{1/2}$. We can see this by contracting k_μ with an axial gauge propagator

$$k_\mu \left(-g^{\mu\nu} + \frac{n^\mu k^\nu}{n \cdot k} + \frac{k^\mu n^\nu}{n \cdot k} - n^2 \frac{k^\mu k^\nu}{(n \cdot k)^2} \right) \frac{1}{k^2} = \frac{n^\nu}{n \cdot k} - n^2 \frac{k^\nu}{(n \cdot k)^2} \leq \lambda^{1/2}. \tag{2.37}$$

However, they are unsuppressed if k is a soft line or k_μ is contracted with momenta in H.

We know that contributions from unphysical degrees of freedom cancel in a sum of gauge invariant sets of diagrams via Ward identities, although,

in covariant gauges these contributions are present for individual diagrams. [3]
Because of this, we can effectively drop terms with longitudinal polarizations
and the remaining terms will still give a factor of $\lambda^{1/2}$. On the other hand,
when line k is soft at the pinch surface, there is no suppression, in contrast to
the case of soft scalars.

In summary, for the case of gauge theories in physical gauges we can
modify Eq. (2.32) as

$$n_i^{(j)} \geq \frac{1}{2}\chi_{i,3} + \frac{1}{2}z_i^{(0)} , \qquad (2.38)$$

where $z_i^{(0)}$ is the number of soft scalar lines emitted at three point vertices by
jet lines. Using this relation and same kind of reasoning as before we end up
with the following bound on p

$$
\begin{aligned}
p \;\geq\; & \frac{1}{2}\sum_{i=1}^{K}\left[\sum_{\alpha\geq 4}(\alpha-4)\chi_{i,\alpha} + \sum_{\beta\geq 4}(\beta-4)y_{i,\beta} + \gamma_i + \delta_i - 2\right] \\
& + \frac{1}{2}\sum_{i=1}^{K}\left[b_i^{(0)} + \left(b_i^{(1)} - z_i^{(1)}\right)\right] + \frac{1}{2}f ,
\end{aligned} \qquad (2.39)
$$

where $b^{(0)}$ and $b^{(1)}$ are the soft scalar and vector lines. $z_i^{(1)}$ is the number of
soft vector lines emitted at three point vertices by the jet lines.

2.4   Leading Regions

In the previous section we have seen that if there are no vector particles
with soft momenta attaching the jet lines then we get the following bound on

---

[3]This actually leads to power divergences in general but we shall elaborate on
this in the next section.

p:

$$p \geq \sum_{i=1}^{K} \left[\frac{1}{2} \sum_{\alpha \geq 4} (\alpha - 4)\chi_{i,\alpha} + \frac{1}{2} \sum_{\beta \geq 4} (\beta - 4)y_{i,\beta} + \gamma_i + \delta_i - 2 \right] + \frac{1}{2}(b + f).$$

(2.40)

The first very important observation, already made following Eq. (2.40), is that $p \geq 0$. Therefore the divergences associated to the pinch surface in question are at worst logarithmic when $p = 0$, and there are no divergences at all for $p > 0$. Furthermore Eq. (2.40) supplies us with a set of very restrictive necessary conditions for the logarithmic divergences. These conditions are

$$b = f = 0,$$

$$\gamma_i = \delta_i = 1,$$

$$\chi_{i,\alpha} = 0, \quad \alpha > 4.$$

(2.41)

In words, the reduced diagram of a divergent point can have no soft lines, each jet must constitute a self energy and no soft vertex may be of higher order than 4. Note that $y_{i,\beta} = 0$ (i.e. no jet vertices that couple to soft lines) is implied by the first line of the above equation. Such a pinch singular surface is described in Fig. 2.3.

From the previous section, the bound on p for gauge theories is given by

$$p \geq \frac{1}{2} \sum_{i=1}^{K} \left[\sum_{\alpha \geq 4} (\alpha - 4)\chi_{i,\alpha} + \sum_{\beta \geq 4} (\beta - 4)y_{i,\beta} + \gamma_i + \delta_i - 2 \right]$$
$$+ \frac{1}{2} \sum_{i=1}^{K} \left[b_i^{(0)} + \left(b_i^{(1)} - z_i^{(1)} \right) \right] + \frac{1}{2} f.$$

(2.42)

The analogous necessary conditions for logarithmic divergences can be written
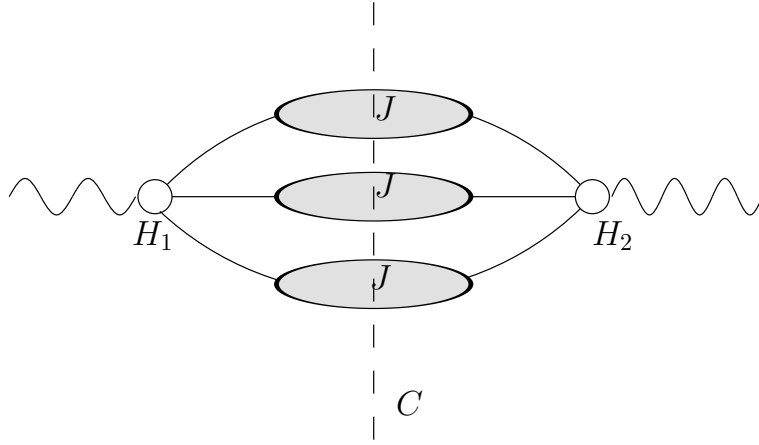
Figure 2.3: Leading pinch singular surface for a cut vacuum polarization graph for theories with no vector particles.

as

$$
\begin{aligned}
b_i^{(1)} &= z_i^{(1)} \,, \\
b_i^{(0)} &= f = 0 \,, \\
\gamma_i &= \delta_i = 1 \,, \\
\chi_{i,\alpha} &= y_{i,\beta} = 0 \,, \quad \alpha > 4 \,.
\end{aligned}
\tag{2.43}
$$

We see that for the case of theories with vector particles, the reduced diagram of a divergent pinch surface may have soft lines, provided that only vector lines attach to jet lines, and then only at three point vertices. Also soft fermion and scalar loops must not connect directly to finite energy lines, although both may appear inside the soft subdiagram, S.

As we have pointed out, these considerations apply when we use physical gauges. However, one can instead use covariant gauges, like the Feynman

gauge. In this case, for gauge theories we modify Eq. (2.32) as

$$n_i^{(j)} \geq \frac{1}{2} \chi_{i,3} + \frac{1}{2} z_i^{(0)} - \frac{1}{2}(\gamma_i - 1) - \frac{1}{2}(\delta_i - 1) \, , \qquad (2.44)$$

where γ_i and δ_i are maximum number of scalar polarized jet lines attached to hard scattering vertices in Feynman gauge. In this case the bound on p of Eq. (2.42) is modified as

$$
\begin{aligned}
p \; \geq \; & \frac{1}{2} \sum_{i=1}^{K} \left[\sum_{\alpha \geq 4} (\alpha - 4)\chi_{i,\alpha} + \sum_{\beta \geq 4} (\beta - 4)y_{i,\beta} \right] \\
& + \frac{1}{2} \sum_{i=1}^{K} \left[b_i^{(0)} + \left(b_i^{(1)} - z_i^{(1)} \right) \right] + \frac{1}{2} f \, ,
\end{aligned} \qquad (2.45)
$$

which now implies that there is no restriction on the number of scalar polarized jet lines attaching the hard vertices.

2.5 Extensions to hadron-hadron scattering

In the following chapter we are going to rely on the above considerations to discuss factorization for high energy QCD cross sections. We will mainly be considering the Drell Yan process where a parton from hadron A and another parton from hadron B annihiliate to produce a virtual photon (or the neutral electroweak boson Z^0), which then decays into a lepton pair with momentum Q and an unknown final state X. Before doing that, however, we would like to first apply Eq. (2.43) to the case of the Drell Yan process to identify the leading pinch singular surfaces diagramatically [35, 34, 36, 37, 38]. Fig. 2.4 shows some examples of these surfaces. In the center of mass frame for the incoming hadrons, we assume that hadron A moves in $+z$ direction and hadron

B in $-z$ direction. We assume that a sum over final states has been carried out. Then a leading pinch singular surface, the momentum k of an internal line can be

1. vanishing in all four components, $k^\mu = 0$ which is denoted by S for soft in figures;

2. collinear to the A-jet, therefore with large plus momentum component, k^+;

3. collinear to the B-jet, therefore with large minus momentum component, k^-;

4. none of the above which is denoted by H for hard in figures. These lines are off-shell by an amount Q^2 after the sum over final states.

One of the leading pinch singular surfaces is such that all quark lines are parts of the A and B jets right up to the hard annihilation vertices and all the gluon lines are soft (i.e. with vanishing momenta in all components). Such a pinch singular surface is shown in Fig. 2.4a. Another leading pinch singular surface is shown in Fig. 2.4b where one of the gluons is interpreted as a constituent of hadron B, and therefore a part of the B-jet, and a soft gluon connects the two jets. Fig. 2.4c shows a pinch singular surface where a collinear gluon from the B-jet enters the hard part taking the quark line to which it attaches to off-shell. This pinch singular surface is leading only in a covariant gauge, and such a singularity is not present in physical gauges since the gluon is scalar polarized at the pinch surface. Finally, in Fig. 2.4d a leading pinch singular

surface is shown where all the gluon lines are off-shell by an amount Q^2, and therefore belong to the hard part. Notice we do not consider jets at wide angles in the figures separately from H. We will return to this point in the next chapter when we discuss the final state cancellations.
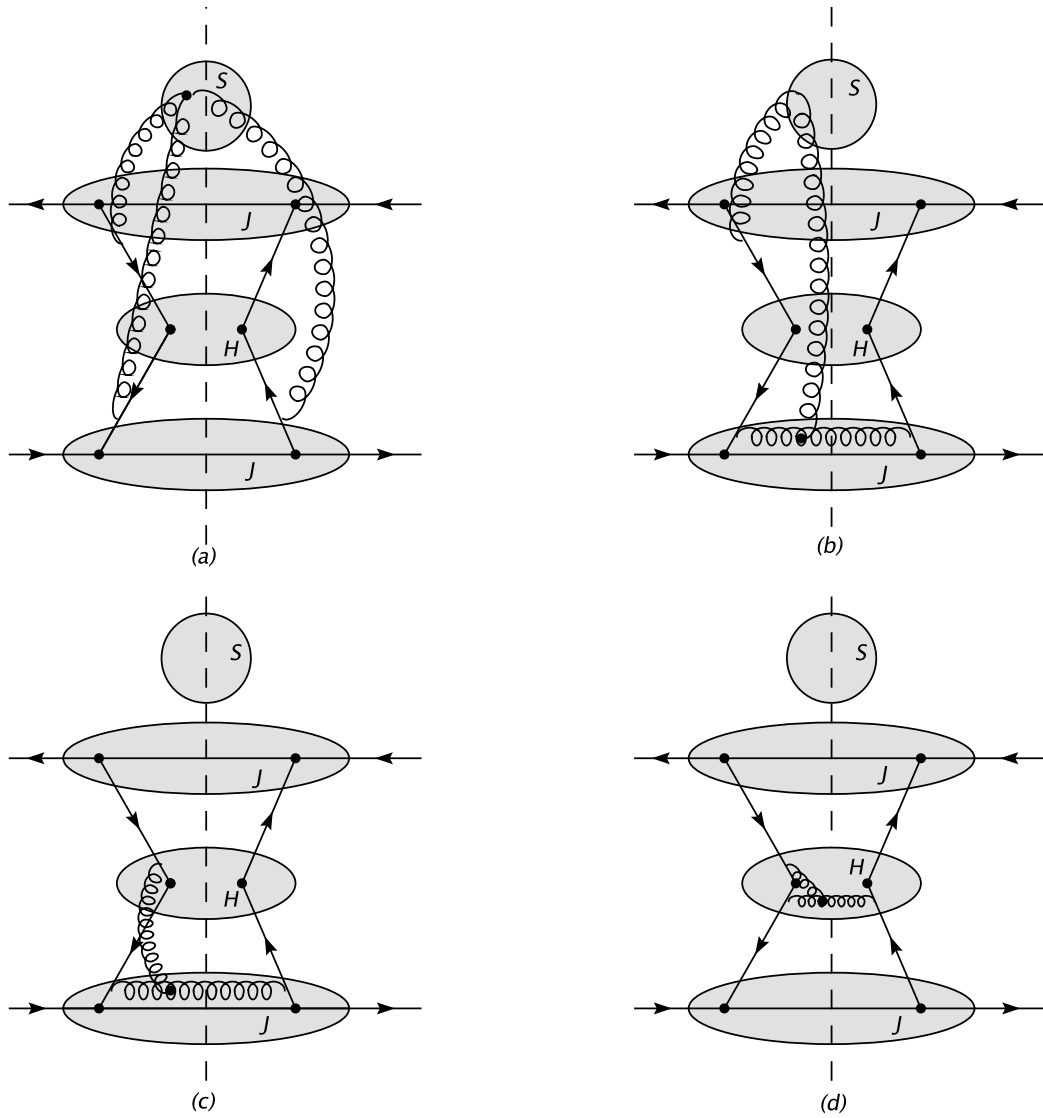
Figure 2.4: Examples of leading pinch singular surfaces for the same cut diagram that contributes to Drell-Yan cross section

Chapter 3

Factorization for QCD Cross Sections

Factorization is the separation of long distance from the short distance effects order by order in perturbation theory. As we discussed in Chapter 1, QCD is an asymptotically free theory of strong interactions, and for this reason short distance effects in QCD (corresponding to high energies) are perturbatively calculable. For a scattering process, in order to achieve this goal one needs to understand the regions in momentum space that contribute to the long distance dynamics, and this we have done in the previous chapter. The predictive power of perturbative QCD comes from the fact that the long distance behaviours of the scattering processes in QCD are universal. Therefore, once factored out and determined by experiment, these long distance pieces can be used to make cross section predictions for other processses. The case of simgle-particle inclusive cross sections in e^+e^- annilihilation was studied and factorization for these proceses were shown in Refs. [36, 39]. For Deep Inelastic Scattering (DIS), factorization was first discussed to all orders in perturbation theory in Refs. [35, 34, 36, 37, 38, 40]. The analysis has been

extended to hadron-hadron scattering in Refs. [41, 42]. In this chapter, following Refs. [41, 42], we will consider the following hadron-hadron scattering, and present the arguments for factorization:

$$h_A(p_A) + h_B(p_B) \rightarrow l\,\bar{l}(Q^\mu) + X \,, \tag{3.1}$$

where hadron A with momentum p_A scatters off hadron B with momentum p_B to give a lepton pair and an unknown final state X. The factorized form of the differential cross section for this process is given by

$$\frac{d\sigma_{AB\rightarrow l\bar{l}+X}}{dQ^2\,dy} = \sum_{a,b} \int_0^1 \frac{d\xi_A}{\xi_A} \frac{d\xi_B}{\xi_B}\, f_{a/A}(\xi_A, Q^2)\, H_{ab}(x_A/\xi_A, x_B/\xi_B, Q^2) f_{b/B}(\xi_B, Q^2)\,, \tag{3.2}$$

where

$$y = \frac{1}{2}\ln(Q^+/Q^-)\,, \quad x_A = e^y\sqrt{Q^2/s}\,, \quad x_B = e^{-y}\sqrt{Q^2/s}\,. \tag{3.3}$$

The sum is over a, b, the parton types, and the $f(\xi, Q)$ are parton distribution functions, which describe the long distance behaviour of the cross section. They are not perturbatively calculable and therefore must be obtained from experiment. They give the distribution of partons inside the hadron with momentum fraction ξ. H_{ab} is the perturbative hard-scattering function, which we calculate to a specific order in perturbation theory. It describes the short distance dynamics. As one can see from Eq. (3.2), the differential cross section for this process is given by a convolution of functions that describe different dynamics.

As we have stated above, one of the key properties of a factorized cross section as in Eq. (3.2) is that the parton distribution functions fs are process

independent. This requires that the two partons entering the hard scattering are not correlated in momentum, spin or color. As we shall see in the following sections, the essence of the proofs for factorization is to show that this is indeed the case. The argument in the case of color is particularly subtle. In order to motivate this, let's consider the following physical picture for a Drell-Yan process in the center of mass (c.m.) frame of the two hadrons that approach each other with large momenta in $\pm z$ directions. Each hadron is composed of a finite number of partons that are confined in a region of space with transverse size $L \sim 1$ fm and a Lorentz-contracted longitudinal size $(m/P)L$ with P the hadron's momentum.

In the Drell-Yan process, two partons, one from each hadron, annihilate at a hard interaction vertex to form a virtual photon of momentum Q, where Q^2 is large ($Q^2 >> \Lambda_{\mathrm{QCD}}$). First of all we would like to observe that in the leading contribution, only one parton from each hadron takes part in this hard interaction. To verify this note that the hard interaction takes place in a region of space with transverse area of dimension on the order of $1/Q$. The probability for a second parton to be in this area is (interaction area)/(cross sectional area of hadron) $\sim 1/(L^2 Q^2)$ which is suppressed for large Q.

Now consider the exchange of soft gluons with momenta $q << Q$. Naively, if these gluons have momentum components as small as $q^\mu \sim 1/L$, then these fields can extend to a distance on the order of L ahead of the colliding hadrons therefore giving them enough time, on the order of L/c before the hard interaction, to interact with the parton of the other hadron. This would spoil the factorization of Eq. (3.2), because it would mean that the colors of the partons

taking part in the hard interaction could become correlated.

It has been argued in Ref. [43] that classically such color correlations do not arise. One can easily verify that the vector potential corresponding to a point charge as in the case of the Drell Yan process is actually a pure gauge. Even a vector potential that is a pure gauge does have an effect on a charged particle in the gauge theory. A phase $e \int A_\mu dx^\mu$ is acquired by a particle moving through potential A_μ from infinity to the interaction point. This phase, however, does not depend on the path, but only on the endpoints if A_μ is a pure gauge. In the following sections, we will see that by the use of gauge invariance, the effects of initial state interactions via soft gluons factor, and the phase mentioned above can be included in the definition of the parton distribution functions.

Having discussed this heuristic argument for factorization as in Eq. (3.2), we will continue with the demonstration of the proof of factorization following Refs. [41, 42]. The proof has three main steps:

1. cancellation of final state interactions using time ordered perturbation theory,

2. factorization of collinear gluons from the hard part H,

3. soft gluon factorization and cancellation.
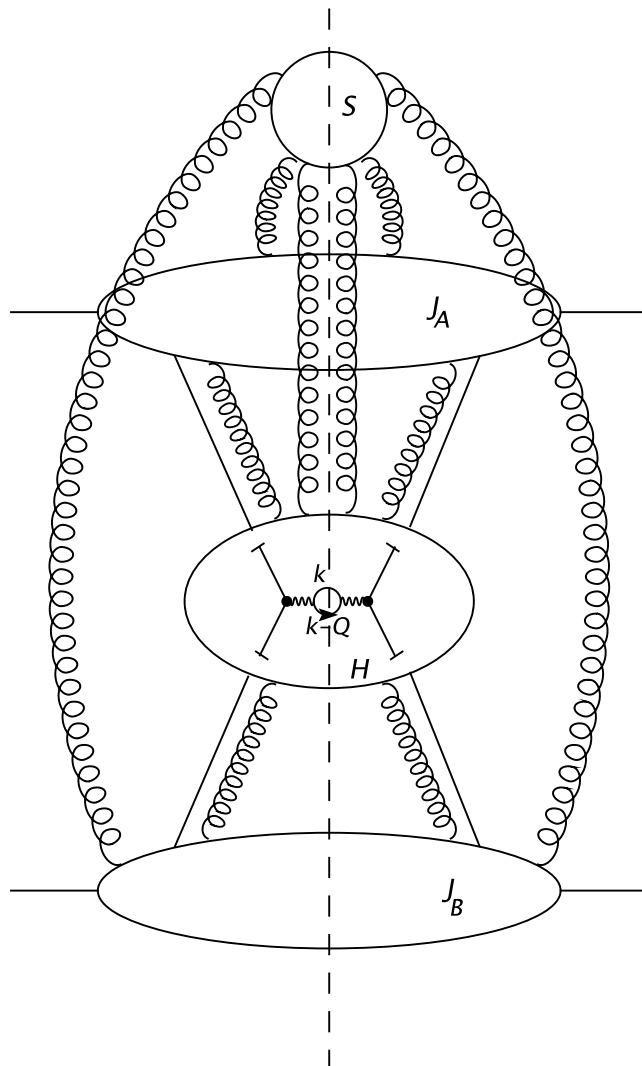
Figure 3.1: A general leading pinch singular surface for the Drell Yan process.

3.1 Cancellation of final state interactions

Consider the general leading region for a cut diagram G that contributes to the cross section for the Drell Yan process , shown in Fig. 3.1. In this section we will show that , as claimed above, all final-state interactions cancel in the fully inclusive cross section. This justifies the identification of the most general reduced diagrams for the Drell-Yan prodess, as discussed in Section 2.5 above.

Let E_α be the set of all states for a given time order α. Let $E_Q^{(\alpha)} \subset E_\alpha$ denote the set of states that include the Drell-Yan pair for that order. Time ordered perturbation is a systematic method to integrate all energy loop integrals. In time ordered perturbation theory we can write G as

$$
G \;=\; \int \prod_{\substack{\text{loops} \\ i}} \frac{d^3 l_i}{(2\pi)^3} \prod_{\substack{\text{lines} \\ j}} \frac{1}{2|\mathbf{k}_j|} N(l) \sum_{\substack{\text{time} \\ \text{orderings } \alpha}} \sum_{\substack{\text{states} \\ \xi \text{ of } E_Q^\alpha}} \left\{ \left[\prod_{\substack{\text{states} \\ \eta < \xi}} (\sqrt{s} - e_\eta + i\epsilon)^{-1} \right] \right.
$$

$$
\left. \times \delta(\sqrt{s} - e_\xi) \left[\prod_{\substack{\text{states} \\ \eta > \xi}} (\sqrt{s} - e_\eta - i\epsilon)^{-1} \right] \right\}, \tag{3.4}
$$

where e_η is the on-shell energy of the state η

$$
e_\eta = \sum_{\substack{\text{lines} \\ i \in \eta}} |\mathbf{k}_i| \,, \tag{3.5}
$$

and the factors in the numerator are denoted by $N(l)$. States $\eta < (>) \xi$ means the states η that are before (after) the state ξ in the time ordering α. Note that we will be able to make a clear distinction between the initial state and final state interactions in such a time ordered expression for both the amplitude and

the complex conjugate amplitude, due to the fact that the hard interaction takes place in a very short time of order $\sim 1/Q$.

Now consider the interactions that take place after the electromagnetic hard interaction vertex shown in Fig. 3.1. We will call these interactions final state interactions. Suppose there are m final state interactions, then for the $m+1$ final states we can write down a factor F, which has only the final states for each time ordering in Eq. (3.4) as[1]

$$F_m = \sum_{\substack{\text{final states} \\ \xi=1}}^{m+1} \left[\prod_{\eta=1}^{\xi-1} (\sqrt{s} - e_\eta + i\epsilon)^{-1} \right] \delta(\sqrt{s} - e_\xi) \left[\prod_{\eta=\xi+1}^{m+1} (\sqrt{s} - e_\eta - i\epsilon)^{-1} \right] . \tag{3.6}$$

To the delta function in this expression we now apply the distribution identity

$$(x + i\epsilon)^{-1} - (x - i\epsilon)^{-1} = -2\pi i \delta(x) , \tag{3.7}$$

and find

$$F_m = \frac{1}{-2\pi i} \left[\prod_{\eta=1}^{m+1} (\sqrt{s} - e_\eta + i\epsilon)^{-1} - \prod_{\eta=1}^{m+1} (\sqrt{s} - e_\eta - i\epsilon)^{-1} \right] . \tag{3.8}$$

We now insert Eq. (3.8) into Eq. (3.4). We are going to argue that in Eq. (3.4) one can always find an integration variable whose contour of integration is not pinched and can be deformed to a distance of order Q. Then if $m \geq 1$, that is if there are any soft final state interactions, F is going to be suppressed.

As shown in Ref. [41] such an integration variable is the lepton pair energy Q^0. Noting that all initial state denominators are independent of Q^0, we can

---

[1]As before the m final states are a subset of the total set of states E_α that include the Drell-Yan final state pair.

write the jth denominator of F as

$$D_j = d_j - Q^0 + i\epsilon \,, \tag{3.9}$$

with d_j independent of Q^0. We can deform the Q^0 integration contour for F of Eq. (3.8) up to a distance $\Delta Q \sim Q$ since for each of the terms in that equation all the poles for Q^0 are only on one side of the real axis. In this case the integration measure will get a factor of ΔQ and the integrand will get a factor of $1/(\Delta Q)^{m+1}$ resulting in a net suppression of $1/(\Delta Q)^m$. This is true whenever the integrand has at least two denominators. If both of the terms in F have only one denominator, that is for $m = 0$, in other words if there are no final state interactions, then the contour integral results in $F = 1$.

In summary, we see that after summing over all final states, which corresponds to the ξ sum in Eq. (3.6), the final state factor F that is a part of Eq. (3.4) can be replaced by a Kroneker delta: δ_{m0}. The only final state interactions that remain are therefore those that are part of the hard scattering. As a result of this final state cancellation, we can ignore those leading pinch sigularities which have soft gluons with momenta $q << \sqrt{s}$ that connect the incoming jets to the hard scattering part after the electromagnetic hard scattering vertex. This is because we have seen that after the sum over final states one can always find a suitable integration variable whose contour deformation results in the suppression of the singularities due to the above mentioned contributions. After the cancellation of final states, the most general leading pinch singular surface for the Drell Yan process is shown in Fig. 3.2. Final state interactions still affect the cross section but because they involve no leading

pinch singular surfaces, they can be computed in perturbation theory.

Before we continue with the factorization of collinear gluons, we would like to make one remark about the final state cancellation. As we will see, for the soft gluon factorization the following approximations will be crucial

$$
\begin{aligned}
2\,p_A \cdot q &\approx 2p_A^+ q^- \,, \\
2\,p_B \cdot q &\approx 2p_B^- q^+ \,,
\end{aligned}
\tag{3.10}
$$

where p_A and p_B are the momenta for the incoming A and B jets and q is the momentum of a soft gluon that couples to the jets. This approximation corresponds to the momentum space region where the transverse component of the soft gluon momentum is negligibly small. The region where the approximation given in Eq. (3.10) for the soft gluon momenta does not hold is called the Glauber region in Ref. [44]. Whenever the approximation in Eq. (3.10) holds, the soft gluon attaching the jets is insensitive to the transverse structure of the jets. Conversely, when Eq. (3.10) does not hold, the gluons probe the jet sub-structure. Therefore the Glauber regions potentially are a threat for the factorization. However, as we will discuss shortly with an explicit example, cancellation of final state interactions ensures that the Glauber regions either cancel all together or can be avoided by proper contour deformations [45, 46, 47, 48].

Let's look at the q^- integrals for the gluon correction diagrams in Fig. 3.3. For later use also, we define an active line as a line which attaches to the hard part and a spectator line as one which does not. We consider the region where the gluon attaching the active and spectator quark lines is soft, i.e. $q^+ << P_A^+$.
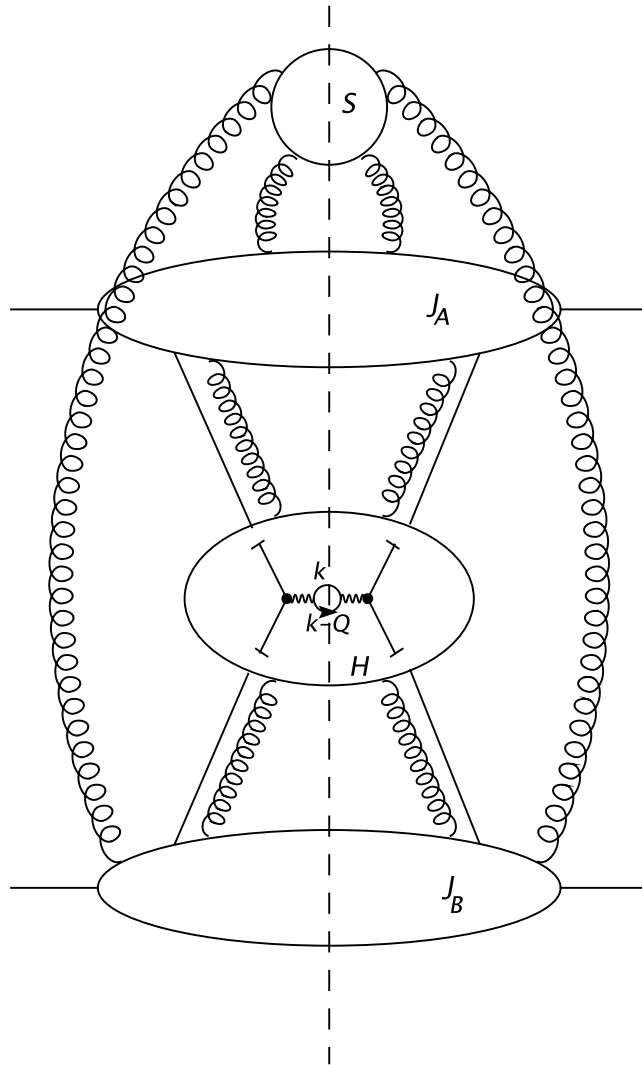
Figure 3.2: A general leading pinch singular surface for the Drell Yan process after final state cancellation.
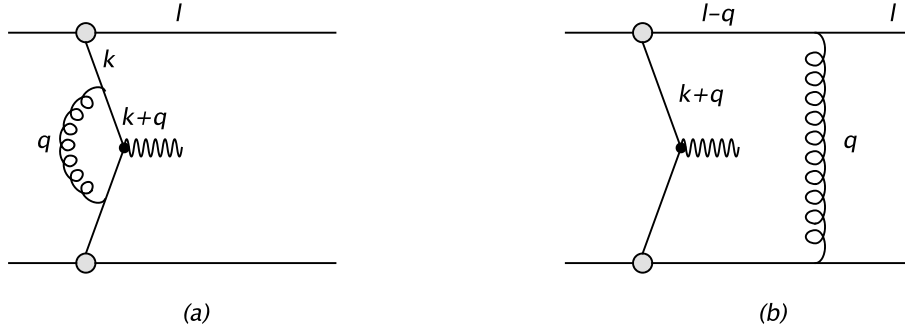
Figure 3.3: Gluon correction graphs where gluons attach to an active quark and a spectator quark in (a) and (b) respectively.

At the pinch surface $l^+ = (1 - x_A)P_A^+$, $0 < x_A < 1$. Up to common factors, the Feynman integrals can be written as

$$
\begin{aligned}
I_a &\approx \int \frac{1}{2q^+q^- - q_T^2 + i\epsilon} \frac{1}{2x_A P_A^+(k_A^- + q^-) - \rho^2 + i\epsilon} \phi_a(q^-)\, dq^- , \\
I_b &\approx \int \frac{1}{2q^+q^- - q_T^2 + i\epsilon} \frac{1}{2x_A P_A^+(k_A^- + q^-) - \rho^2 + i\epsilon} \\
&\qquad \times \frac{1}{2(1 - x_A)P_A^+(l^- - q^-) - \rho^2 + i\epsilon} \phi_b(q^-)\, dq^- , \qquad (3.11)
\end{aligned}
$$

where $\rho^2 = (k_{A,T} + q_T)^2$, and, where ϕ_a and ϕ_b are slowly varying functions of q^-. Let us take $q_T \sim M$, $M << Q$ any fixed momentum scale, and $P_A^+ \sim Q >> q^+$. We first study the case when

$$
|q^-| < M , \qquad |P_A^+ q^-| >> M^2 \sim \rho^2 . \qquad (3.12)
$$

In the center of mass frame of the incoming hadron A, the polarization vector that couples the gluon to the A-jet lies to a very good approximation in the minus direction, which can be understood with the power counting discussion of the previous chapter. In the region given by Eq. (3.12), the momentum

of this gluon also satisfies $|q^-| \sim M >> M^2/P_A^+$. Therefore we see that the polarization vector for the gluon is to a very good approximation proportional to its four momentum. This means that the gluon attaching to the incoming A-jet for this momentum region is a scalar-polarized and therefore an unphysical gluon. We will see that for those diagrams where unphysical gluons attach the jets, we can use the Ward identities that result from gauge invariance for simplifications. We shall see that using Ward identities, all scalar-polarized gluons factor from the A-jet.

Now let us consider the momentum space region where Eq. (3.12) does not hold. In particular this may happen when

$$|q^-| \sim M^2/P_A^+. \tag{3.13}$$

This region of momentum space is called the Glauber region [44], as we have briefly introduced before. The first thing to notice is that when Eq. (3.13) holds, both q^- and q_T must be taken into account in the A-jet. The leading polarization remains in the minus direction, however, the gluon is no longer effectively scalar-polarized. In this region, we can also no longer apply gauge invariance to simplify the contributions. We can see that the Glauber region, by using power counting methods of Chapter 2, contributes to both I_a and I_b of Eq. (3.11). Therefore one may very naturally ask if the Glauber regions spoil factorization. The short answer is no. Here we will briefly motivate why this is so, using the example given in Fig. 3.3. A more rigorous argument may be found in Refs. [41, 49] .

To illustrate the basic arguments for factorization, we analyze the pole
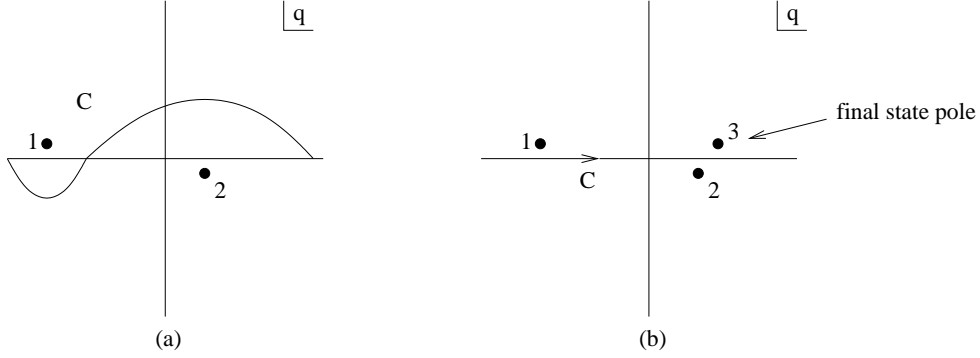
Figure 3.4: Poles for the diagrams in Fig. 3.3a. and b. in the q^- plane.

structures of the integrals I_a and I_b in the complex q^- plane. The poles for I_a are

$$
\begin{aligned}
q_1^- &= \frac{q_T^2}{2q^+} - \frac{i\epsilon}{2q^+}, \\
q_2^- &= -k_A^- + \frac{\rho^2}{2x_A P_A^+} - \frac{i\epsilon}{2x_A P_A^+}.
\end{aligned}
\tag{3.14}
$$

The poles for I_b are

$$
\begin{aligned}
q_1^- &= \frac{q_T^2}{2q^+} - \frac{i\epsilon}{2q^+}, \\
q_2^- &= -k_A^- + \frac{\rho^2}{2x_A P_A^+} - \frac{i\epsilon}{2x_A P_A^+}, \\
q_3^- &= l^- - \frac{\rho^2}{2(1-x_A)P_A^+} + \frac{i\epsilon}{2(1-x_A)P_A^+}.
\end{aligned}
\tag{3.15}
$$

For $-P_A^+ < q^+ < 0$, these poles in the q^- plane are shown in Fig. 3.4. One needs to observe that q_1^- and q_2^- for both I_a and I_b are separated by $\mathcal{O}(M)$ but q_2^- and q_3^- for I_b are separated by $\mathcal{O}(M^2/P_A^+)$.

We see that for the diagram in Fig. 3.3a the q^- contour is not pinched because the q_1^- and q_2^- poles are separated by $\mathcal{O}(M)$. Therefore we can deform the q^- contour away from the second pole in Fig. 3.4a as far as is necessary to

get out of the Glauber region of momentum space. This contour deformation is illustrated in Fig. 3.4a. However, this is not the case for the diagram in Fig. 3.3b where the soft gluon attaches to a spectator line. We can see from Fig. 3.4b that the q^- contour is pinched in between the second and the third poles in this figure which are both at the scale M^2/P_A^+. However as noted on the figure also, the third pole that pinches the q^- contour is a final state pole. As we have discussed earlier in this section, when we sum over all the possible final states of the same diagram, shown in Fig. 3.3b, this pole simply cancels. After this cancellation, the q^- contour is no longer pinched and can therefore be deformed away from the Glauber region. We see that, even though we can not use the gauge invariance arguments for the diagrams in the Glauber region, cancellation of final state poles saves the day for factorization. We would like to note that this example fairly easily generalizes to diagrams of higher order and such a generalization is discussed in Ref. [41].

3.2 Factorization for collinear lines

In the previous section we have seen that final state interactions cancel once we sum over the relevant final states of a given cut diagram. After this cancellation we are left with the leading pinch singular surfaces shown in Fig. 3.2. Also we have seen that the Glauber regions of momentum space where the transverse momenta of the soft gluons attaching the jets become important are taken care of by the same final state cancellation. In this section we will briefly discuss how the collinear gluons attaching the hard part in the covariant
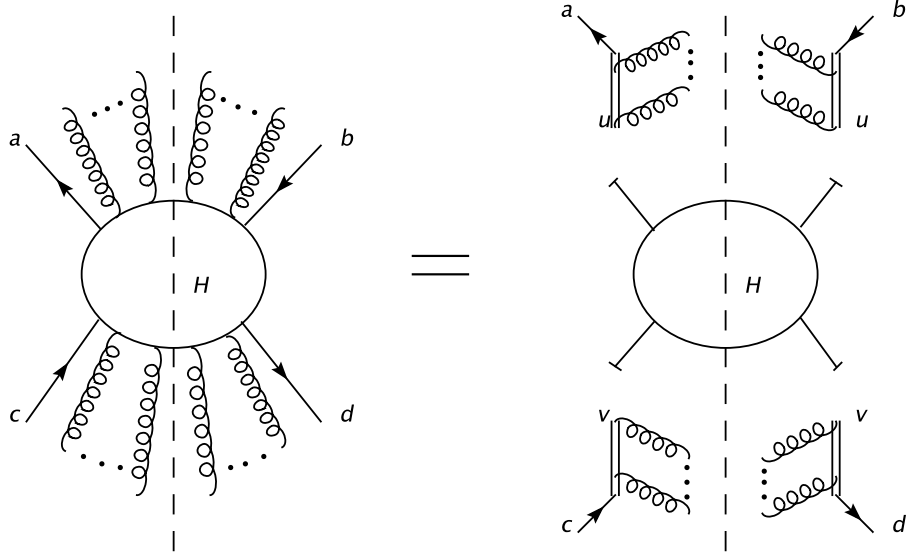
Figure 3.5: Diagramatic representation of the Ward identity for the longitudinally polarized gluons attaching the hard part.

Feynman gauge factor from the hard scattering. We will make use of the power counting rules we have derived earlier in Chapter 2.

We begin by defining projections of gluon momenta,

$$
\begin{aligned}
\hat{k}^\mu &= (k^+, 0, \mathbf{0}_T), \\
\tilde{k}^\mu &= (0, k^-, \mathbf{0}_T),
\end{aligned}
\tag{3.16}
$$

and light-like vectors in the plus and minus directions,

$$
\begin{aligned}
u^\mu &= \frac{1}{\sqrt{2}}(0, 1, \mathbf{0}_T), \\
v^\mu &= \frac{1}{\sqrt{2}}(1, 0, \mathbf{0}_T).
\end{aligned}
\tag{3.17}
$$

For the scalar polarized gluon propagators that attach the hard part we now

make the following collinear approximations [47]

$$g_{\alpha\beta} H^\beta \approx \frac{u_\alpha \hat{k}_\beta H^\beta}{u \cdot \hat{k} - i\epsilon} \, , \qquad (3.18)$$

if k^μ is collinear to the A-jet and

$$g_{\alpha\beta} H^\beta \approx \frac{v_\alpha \tilde{k}_\beta H^\beta}{v \cdot \tilde{k} - i\epsilon} \, , \qquad (3.19)$$

if k^μ is collinear to the B-jet. With the above approximations, the application of nonabelian Ward identities of Refs. [50, 51] is trivial and the result is given in Fig. 3.5. The double lines represent eikonal lines which are given by an eikonal line operator

$$\Phi_{v_i}^{[f_i]}(\sigma', \sigma) = P \exp \left[-ig \int_\sigma^{\sigma'} d\lambda \, v_i \cdot A^{[f_i]}(\lambda v_i) \right] \, , \qquad (3.20)$$

where v_i^μ is the four velocity for the eikonal line. P denotes path ordering. This is the same phase factor mentioned in the introduction of this chapter. The nonabelian Ward identities and the Feynman rules for eikonal lines are discussed in Appendix A, and a more complete proof is given in Refs. [41, 52]. The physical interpretation of the collinear longitudinally polarized gluons attaching the eikonal lines is that they can not resolve any structure of the hard part H, only that it involves large momenta moving in the opposite direction. This is why H is equivalent to an eikonal line moving in the opposite direction for a collinear unphysical gluon.

3.3   Soft gluon factorization and cancellation

In the previous sections we have discussed how final state interactions cancel after the sums over the cuts for individual cut diagrams are performed,
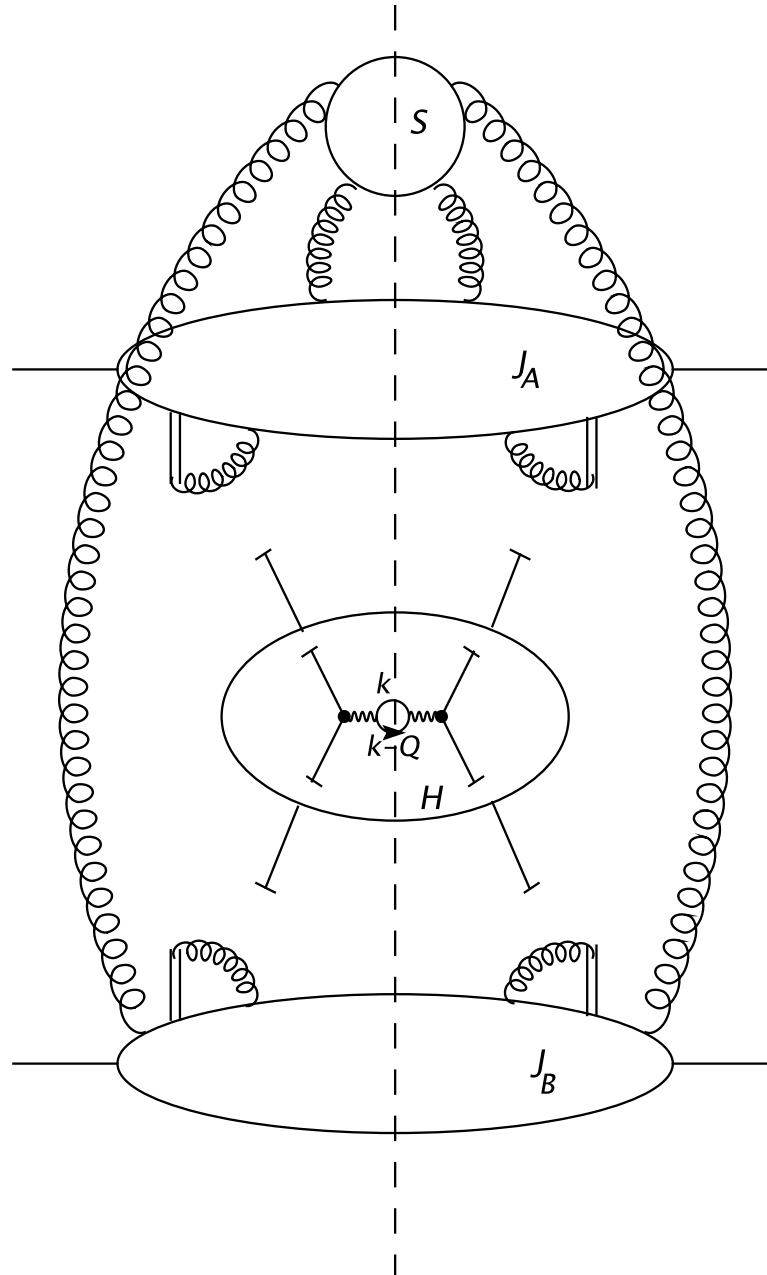
Figure 3.6: A general leading pinch singular surface for the Drell Yan process after final state cancellation and collinear gluon factorization.

and how the collinear gluons that attach the hard part factorize using gauge invariance. In this section we are going to show how soft gluons factorize and cancel.

3.3.1 Soft gluon factorization

We begin start our discussion by summarizing the results of the previous sections by writing down the expression for an arbitrary graph G that contributes to the Drell Yan cross section. The contribution from any leading pinch singular surface S can be written as

$$
\begin{aligned}
G_S &= \sum_C \int \frac{dk_A^+ \, dk_B^-}{2\pi \, 2\pi} \prod_l \int \frac{d^4 q_l}{(2\pi)^4} \prod_j \int \frac{d^4 \bar{q}_j}{(2\pi)^4} \, J_A^{(C)}(k_A^+, q_l^\alpha)^{\{\mu_1 \dots \mu_n\}} \\
&\quad \times S^{(C)}(q_l^\alpha, \bar{q}_j^\beta)_{\{\mu_1 \dots \nu_1 \dots\}} \, H^{(C)}(k_a^+, k_B^-) \, J_B^{(C)}(k_B^-, \bar{q}_j^\beta)^{\{\nu_1 \dots \nu_m\}}, \quad (3.21)
\end{aligned}
$$

which is represented in Fig. 3.6. The sum over C runs over possible cuts for the particular diagram. q_l and $\bar{q}_j$ are the momenta of soft gluons that attach to the A- and B-jets, respectively, as described in the figure. Notice that to represent a physical picture $k_A^+ = x_A Q$, $0 < x_A < 1$, and $k_B^- = x_B Q$, $0 < x_B < 1$. Eq. (3.21) has the same form as Eq. (3.2) except for the effects of soft gluons. Thus we must show that soft gluons that connect the jets cancel.

We now rewrite the sum over the cuts C in Eq. (3.21) as

$$
\begin{aligned}
G_S &= \int \frac{dk_A^+}{2\pi} \prod_l \int \frac{d^4 q_l}{(2\pi)^4} \sum_V \sum_{C_A \in V_A} \\
&\quad \times J_A^{(C_A)}(k_A^+, q_l^\alpha)^{\{\mu_1 \dots \mu_n\}} \sum_{C_R \in V_R} R^{(C_R)}(k_A^+, q_l^\alpha)_{\{\mu_1 \dots \mu_n\}}, \quad (3.22)
\end{aligned}
$$

where

$$R^{(C_R)}(k_A^+, q_l^\alpha)_{\{\mu_1 \ldots \mu_n\}} \;=\; \int \frac{dk_B^-}{2\pi} \prod_j \int \frac{d^4 \bar{q}_j}{(2\pi)^4} \, S^{(C_R)}(q_l^\alpha, \bar{q}_j^\beta)_{\{\mu_1 \ldots \nu_1 \ldots\}}$$
$$\times H^{(C_R)}(k_A^+, k_B^-) \, J_B^{(C_R)}(k_B^-, \bar{q}_j^\beta)^{\{\nu_1 \ldots \nu_m\}} \,. \quad (3.23)$$

Here we have reorganized the sum over cuts such that we first consider the vertices where soft gluons attach to J_A. V represents possible choices for which of these vertices are to the left or to the right of C. V_A and V_R represents the set of vertices in J_A and R respectively, consistent with the choice V. First, we sum over the choices of V and then we sum over different cuts of J_A and R seperately. Finally, we have represented everything that is not the A-jet as R.

We will study this expression using lightcone-ordered perturbation theory for the A-jet. We begin with the following approximation on Eq. (3.22). Since the A-jet consists of lines with large plus momentum components we will neglect the plus components of the soft gluon momenta q_l compared to the plus momentum components flowing on the lines of the A-jet. Also for the same reason that A-jet mostly consists of lines with large plus momenta, the contributions to the sums over the vector indices μ_i can be approximated by the values $\mu_i = +$. With these approximations, we can rewrite the factor $J_A^{(C)}$ in Eq. (3.22) as

$$J_A^{(C)}(k_A^+, q_l^\alpha)^{\{\mu_1 \ldots \mu_n\}} \approx J_A^{(C)}(k_A^+, \hat{q}_l^\alpha)^{\{+ \cdots +\}} \, v^{\mu_1} \cdots v^{\mu_n} \,, \quad (3.24)$$

where

$$\hat{q}^\alpha = (0, q_l^-, \mathbf{q_{l,T}}) \,, \quad (3.25)$$

and where v^μ is the light-like vector in the plus (A) direction defined above in Eq. (3.17). With these approximations, since we can neglect q_l^+ in the A-jet, we can take the factor $J_A^{(C)}$ outside the q_l^+ integrals and we can write

$$
\begin{aligned}
G_S \;=\; & \int \frac{dk_A^+}{2\pi} \prod_l \int \frac{dq_l^-\, d\mathbf{q_l}}{(2\pi)^3} \sum_V \sum_{C_A \in V_A} J_A^{(C_A)}(k_A^+, \hat{q}_l^\alpha)^{\{+\cdots+\}} \\
& \times \prod_l \int \frac{dq_l^+}{2\pi} \sum_{C_R \in V_R} R^{(C_R)}(k_A^+, q_l^\alpha)_{\{+\cdots+\}}\,.
\end{aligned}
\tag{3.26}
$$

We next construct x^+-ordered perturbation theory for the A-jet by evaluating the internal k^- integrals of $J_A^{(C_A)}$, keeping the plus and transverse components fixed [53, 54]. This will enable us to write down the explicit q_l^- dependence of J_A. After the evaluation of k^- integrals in J_A in the spirit of Refs. [53, 54] one can write it as a sum over the x^+-orderings T of its vertices as given in Ref. [42]

$$
J_A^{(C_A)} = \sum_T I_T'(q_l^\alpha)^* \otimes F_T^{(C_A)}(q_l^\alpha) \otimes I_T(q_l^\alpha)\,,
\tag{3.27}
$$

where I_T and $I_T'^*$ represent the initial state interactions to the left and to the right of the cut and F_T represents the final state interactions in J_A. The hard scattering takes place at $x^+ = 0$ and initial and final states are defined relative to the hard scattering. The convolution $\otimes$ is in the internal A-jet loop momenta integrations. Fig. 3.7 represents a generic x^+-ordering for J_A.

In much the same was as for time-ordered perturbation theory, Eq. (3.4),
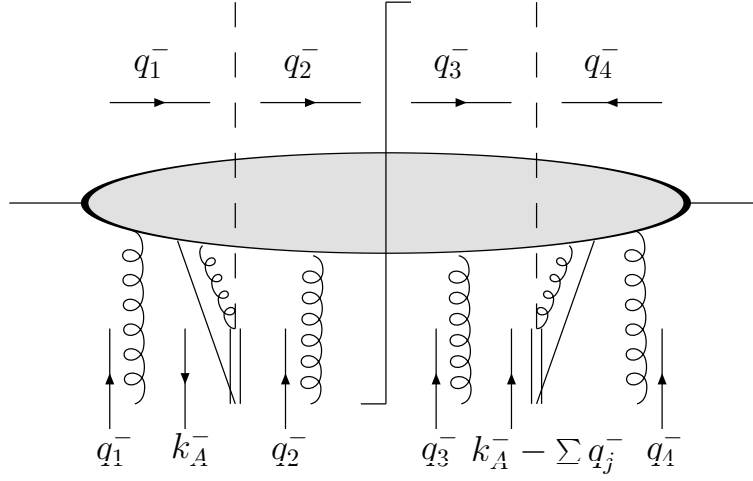
Figure 3.7: A diagram that illustrates the x^+-ordered perturbation theory for J_A with the flow of minus momenta. q's flow in along soft gluons and out along the collinear lines.

one can write these initial and final state factors as

$$
I_T(q_l^\alpha) = \prod_{\substack{\text{states } \xi \\ \xi < \text{H}}} \left[\sum_{\substack{\text{vertices } l \\ l < \xi}} (q_l^- + i\epsilon) - \sum_{\substack{\text{lines } j \\ j \in \xi}} \frac{\mathbf{k}_j^2}{2k_j^+} \right]^{-1},
$$

$$
I_T'(q_l^\alpha)^* = \prod_{\substack{\text{states } \xi \\ \text{H}' < \xi}} \left[-\sum_{\substack{\text{vertices } l \\ \xi < l}} (q_l^- + i\epsilon) - \sum_{\substack{\text{lines } j \\ j \in \xi}} \frac{\mathbf{k}_j^2}{2k_j^+} \right]^{-1}, \qquad (3.28)
$$

where the signs of the q_l^-'s correspond to the flow of momenta in Fig. 3.7.

$$F_T^{(C_A)}(q_l^\alpha) = \int_{-\infty}^{\infty} \frac{dk_A^-}{2\pi} \prod_{\substack{\text{states } \xi \\ C < \xi < H'}} \left[-k_A^- + \sum_{\substack{\text{vertices } l \\ l < \xi}} (q_l^- - i\epsilon) - \sum_{\substack{\text{lines } j \\ j \in \xi}} \frac{\mathbf{k}_j^2}{2k_j^+} \right]^{-1}$$

$$\times 2\pi\delta \left(-k_A^- + \sum_{\substack{\text{vertices } l \\ l < C}} q_l^- - \sum_{\substack{\text{lines } j \\ j \in C}} \frac{\mathbf{k}_j^2}{2k_j^+} \right)$$

$$\times \prod_{\substack{\text{states } \xi \\ H < \xi < C}} \left[-k_A^- + \sum_{\substack{\text{vertices } l \\ l < \xi}} (q_l^- + i\epsilon) - \sum_{\substack{\text{lines } j \\ j \in \xi}} \frac{\mathbf{k}_j^2}{2k_j^+} \right]^{-1}, \quad (3.29)$$

where k_A^- is the minus momentum that leaves the A-jet at hard vertex H and $k_A^- - \sum q_l^-$ is the minus momentum that flows back into the jet at hard vertex H'. Each term $k_j^2/2k_j^+$ is the on-shell minus momentum of line j, by analogy to the $e_i = |\vec{k}_i|$ in Eq.(3.4) and Eq. (3.5). Substituting Eq. (3.27) into Eq. (3.26) one gets

$$G_S = \int \frac{dk_A^+}{2\pi} \prod_l \int \frac{dq_l^- \, d\mathbf{q_l}}{(2\pi)^3} \sum_V \sum_{C_A \in V_A} \sum_T I_T'(q_l^\alpha)^* \otimes F_T^{(C_A)}(q_l^\alpha) \otimes I_T(q_l^\alpha)$$

$$\times \prod_l \int \frac{dq_l^+}{2\pi} \sum_{C_R \in V_R} R^{(C_R)}(k_A^+, q_l^\alpha) \quad (3.30)$$

where we have suppressed the indices. We now turn our attention to the sum $\sum_{C_R} R^{(C_R)}$.

3.3.2 Light-cone perturbation theory for $\bar{R}$

Before we return to the analysis of the A-jet, we would like to prove a very important intermediate result which we will explicitly use in the following
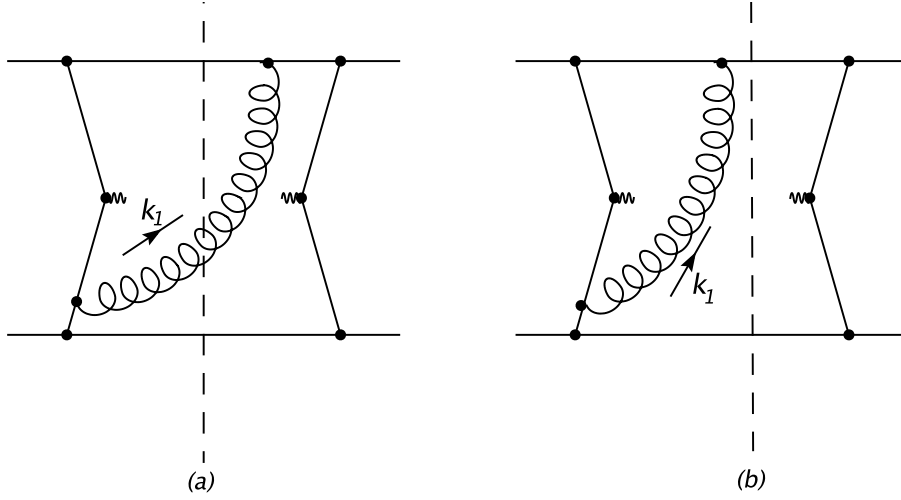
Figure 3.8: Two different cuts of the same x^--ordered graph.

steps of the analysis. We would like to prove that the quantity

$$\bar{R}(k_A^+, \hat{q}_l^\alpha; V) = \prod_l \int \frac{dq_l^+}{2\pi} \sum_{C_R \in V_R} R^{(C_R)}(k_A^+, q_l^\alpha) \tag{3.31}$$

is actually independent of V, which we defined to be the choice of which of the soft gluons attach the A-jet to the left of the cut C and which to the right. For this proof we need the x^-- ordered perturbation theory for $\bar{R}$ which is derived by performing all the internal plus loop integrals, while keeping the minus and transverse components fixed. Just as in the x^+-ordered light-cone perturbation theory for the A-jet, the result can be written as a sum over light-cone ordered perturbation theory diagrams [53, 54]

$$\bar{R}(k_A^+, \hat{q}_l^\alpha; V) = \sum_{C_R \in V_R} \sum_T I_T^{(R)\,\prime}(q_l^\alpha)^* \otimes F_T^{(C_R)}(q_l^\alpha) \otimes I_T^{(R)}(q_l^\alpha)\,, \tag{3.32}$$

A typical light cone ordered cut diagram is shown in Fig. 3.8, in which the vertices are ordered from left to right. At each vertex transverse and minus mo-

menta are conserved, and only those orderings in which minus momenta flows from right to left in the entire diagram contribute. The latter requirement limits the number of light cone ordered diagrams, and is a major simplification of this method. (The same result applies to plus momenta in the A-jet expression Eq. (3.26).)

For the analysis of infrared divergences, each of the factors in Eq. (3.32) can be considered to be a product of denominators, where each denominator represens one of the intermediate states specified by the ordering T. The denominator for state ξ is the "plus momentum deficit" of that state, by analogy to the "energy deficit" of states in time-ordered perturbation theory and the "minus-momentum deficit" of Eqs.(3.28)-(3.29): the difference between the plus momentum that has flowed into (or out of) the diagram to the left of the state and the sum of the on-shell plus momenta for the particles of that state. When the net plus momentum that has flowed into the diagram to the left of a given state matches the sum of on-shell plus momenta of the lines in that state, the denominator vanishes, and the state is referred to as on-shell.

All the factors described above correspond to any field theory, involving only scalars or full QCD. Choosing the Feynman gauge in QCD, however, all factors associated with particle spin appear as multiplicative polynomials in external and loop momenta. Although numerator factors play a crucial role in determining the strength of infrared singularities [33, 34], they do not directly enter the arguments given below. Ignoring for simplicity these numerator factors associated with particle spin, we can represent the sum individual

factors of Eq. (3.32) as

$$
I_T^{(R)}(k_l^\alpha) = \prod_{\substack{states\ \xi \\ \xi < H}} \left[-\sum_{\substack{lines\ j \\ j \in \xi}} \frac{\mathbf{k}_j^2}{2k_j^-} + i\epsilon \right]^{-1} ,
$$

$$
I_T^{(R)\ '*}(k_l^\alpha) = \prod_{\substack{states\ \xi \\ H' < \xi}} \left[-\sum_{\substack{lines\ j \\ j \in \xi}} \frac{\mathbf{k}_j^2}{2k_j^-} - i\epsilon \right]^{-1} , \qquad (3.33)
$$

$$
F_T^{(C_R)}(q_l^\alpha) = \int_{-\infty}^{\infty} \frac{dk_B^+}{2\pi} \prod_{\substack{states\ \xi \\ C < \xi < H'}} \left[k_B^+ - \sum_{\substack{lines\ j \\ j \in \xi}} \frac{\mathbf{k}_j^2}{2k_J^-} - i\epsilon \right]^{-1}
$$

$$
\times \quad 2\pi\delta \left(k_B^+ - \sum_{\substack{lines\ j \\ j \in C}} \frac{\mathbf{k}_j^2}{2k_j^-} \right) \prod_{\substack{states\ \xi \\ H < \xi < C}} \left[k_B^+ - \sum_{\substack{lines\ j \\ j \in \xi}} \frac{\mathbf{k}_j^2}{2k_j^-} + i\epsilon \right]^{-1} .
$$

$$(3.34)$$

Referring to Fig. 3.8 as an example, we can now see why it is nontrivial that $\bar{R}$ is independent of how the external lines of $R^{(C_R)}$ are attached to the A-jet. Consider, for example, the line labelled k_1, which is emitted from a vertex in the amplitude and is absorbed on a line in the A-jet in Fig. 3.8. The figure shows two possible cuts of the same graph, corresponding to different choices of V. Although each cut crosses J_A and R in a different way, and corresponds to a different final state, we will show that after the integration over k_1^+ the values of R for both cuts are the same if k_1^+ is neglected in J_A. As we have discussed above the approximation where we neglect k_1^+ in the A-jet is a good one.

Now for different choices V of soft connections to the A-jet the possible cuts C_R and possible time orderings T are different. Given two different choices

V, however, for each time ordering for the first value there is a time ordering for the second value that has exactly the same initial state factors $I_T^{(R)}$ and $I_T^{(R)\,\prime*}$. Therefore, the V dependence in $\bar{R}$ is only in the final state factor F. We are going to show that all such dependence cancels.

We now sum over the set of final state functions $F_T^{(C_R)}$ for some fixed ordering, T. Let us suppose there are $m \geq 1$ final states in this sum. Referring to Eq. (3.34), we can represent the sum as

$$\sum_{C=1}^{m} F_T^{(C_R)}(q_l^\alpha) = \sum_{C=1}^{m} \int_{-\infty}^{\infty} \frac{dk_B^+}{2\pi} \left\{ \prod_{i=C+1}^{m} \frac{1}{k_B^+ - D_i - i\epsilon} \times 2\pi\delta(k_B^+ - D_C) \right.$$
$$\left. \times \prod_{i=1}^{C-1} \frac{1}{k_B^+ - D_i + i\epsilon} \right\}, \tag{3.35}$$

where D_s represents the sum of on-shell plus momenta of state s. We next follow a familiar procedure, just as we have done while showing the cancellation of final state interactions, and apply to each mass-shell delta function in this expression the distribution identity of Eq. (3.7), $2\pi\delta(x) = i/(x+i\epsilon) - i/(x-i\epsilon)$. As in Eq.(3.8) above, all except two of the resulting terms cancel pairwise,

$$\sum_{C=1}^{m} \left\{ \prod_{i=C+1}^{m} \frac{1}{k_B^+ - D_i - i\epsilon} 2\pi\delta(k_B^+ - D_C) \prod_{i=1}^{C-1} \frac{1}{k_B^+ - D_i + i\epsilon} \right\}$$
$$= i \prod_{i=1}^{m} \frac{1}{k_B^+ - D_i + i\epsilon} - i \prod_{i=1}^{m} \frac{1}{k_B^+ - D_i + i\epsilon}. \tag{3.36}$$

Using this unitarity identity in (3.35), we perform the integral over k_B^+, and find

$$\sum_{C=1}^{m} F_T^{(C)}(q_l^\alpha) = \delta_{m1}, \tag{3.37}$$

which follows readily from Cauchy's theorem. When there are no final state interactions, then the integral $(2\pi)^{-1} \int dk_B^+$ gives a factor of i. However if there

are final state interactions so that $m > 1$, then the integral over k_B^+ of each term in Eq. (3.36) gives zero. Therefore the final state interactions cancel once we sum over the final state cuts, replacing F by unity. In particular, after the sum over cuts, the remnant final state factor is independent of V.

Since we have argued that all the V dependence of $\bar{R}$ of Eq. (3.32) is in the final state interactions F, which cancel after the sum over all possible cuts of R that are consistent with the choice V, we can write $\bar{R}$ as

$$
\begin{aligned}
\bar{R}(k_A^+, \hat{q}_l^\alpha; V) &= \sum_{C_R \in V_R} \sum_T I_T^{(R)'}(q_l^\alpha)^* \otimes I_T^{(R)}(q_l^\alpha) \\
&\equiv \bar{R}(k_A^+, \hat{q}_l^\alpha) \,,
\end{aligned}
\tag{3.38}
$$

where in the second line we have dropped the dependence on V. The sum over final states is then given entirely by light-cone ordered diagrams for which all interactions are initial state.

In summary, we have just shown that for an arbitrary cut diagram, the piece of the diagram that is not a part of the A-jet, which we labelled as R, is independent of the way soft gluons attach the A-jet. Having accomplished this, we are now ready to write G_S, the contribution from an arbitrary pinched singular surface of Eq. (3.30), as

$$
\begin{aligned}
G_S &= \int \frac{dk_A^+}{2\pi} \prod_l \int \frac{dq_l^- \, d\mathbf{q_l}}{(2\pi)^3} \left\{ \sum_V \sum_{C_A \in V_A} \sum_T I_T'(q_l^\alpha)^* \otimes F_T^{(C_A)}(q_l^\alpha) \otimes I_T(q_l^\alpha) \right\} \\
&\quad \times \bar{R}(k_A^+, \hat{q}_l^\alpha) \,,
\end{aligned}
\tag{3.39}
$$

where $\bar{R}$ is given by Eq. (3.38) and is independent of the sum over V. This will enable us to sum J_A over all of its cuts C_A freely. Using exactly the same

reasoning as before, we can now apply the unitarity identity of Eq. (3.7) to the final state factor of Eq. (3.29) in J_A to find

$$\sum_{C_A} J_A^{(C_A)} = \sum_{C_A} \sum_T I_T'(q_l^\alpha) \otimes I_T(q_l^\alpha) \,. \tag{3.40}$$

3.3.3 Factorization and cancellation of soft gluons

All these manupilations were absolutely crucial because now from Eq. (3.28) we see that the initial state factors in J_A therefore $\sum_{C_A} J_A$ has no poles in the upper half q_l^- plane and therefore is not pinched. This allows us to deform the q_l^- contours into the upper half plane until we encounter poles from $\bar{R}$ which are at $|q_l^-| \sim |\mathbf{q}_l|$. It was proved in Ref. [42] that on the deformed contour we can neglect the transverse components of the soft gluon momenta $\mathbf{q}_l$, and once this is done we can pull the q_l^- contours back to the real axis. These contour deformations are discussed in Ref. [42] in great detail.

The result up to corrections suppressed by a power of Q is

$$G_S = \int \frac{dk_A^+}{2\pi} \prod_l \int \frac{dq_l^-}{2\pi} \left\{ \sum_V \sum_{C_A \in V_A} J_A^{(C_A)}(k_A^+, \tilde{q}_l^\alpha) \right\} \prod_l \int \frac{d\mathbf{q}_l}{(2\pi)^2} \bar{R}(k_A^+, \hat{q}_l^\alpha) \,, \tag{3.41}$$

where J_A depends now on $\tilde{q}_l^\alpha$, which consists of only the minus components of q_l such that

$$\tilde{q}_l^\alpha = q_l^- \, u^\alpha \,, \tag{3.42}$$

with u defined earlier in Eq. (3.17). In other words, we have shown that we can ignore the transverse momentum components of the soft gluons attaching the A-jet in J_A. This is a generalization of the Grammer-Yennie approximation for

soft photons in QED of Ref. [55]. The physical interpretation is that the soft gluons that attach to the A-jet actually can not resolve the structure of the jet in the minus or transverse directions. We therefore expect that the effects of all soft gluons will be summarized by phase factors analogous to Eq. (3.20).

For the simplicity of the notation we have been ignoring the contracted vector indices on J_A and R, which are explicit in Eq. (3.22). We have argued before that the leading contribution comes from the $\mu_i = +$ components. We can rewrite the $+$ components of J_A as

$$J_A^{(C_A)}(k_A^+, \tilde{q}_l^\alpha)^{\{+\cdots+\}} = J_A^{(C_A)}(k_A^+, \tilde{q}_l^\alpha)^{\{\mu_1\cdots\mu_n\}} \prod_{i=1}^n \frac{\tilde{q}_{i,\mu_i}}{v \cdot q_i - i\epsilon}, \qquad (3.43)$$

where we have simply multiplied and divided J_A by a factor of q_i^- for each gluon. This can be done as long as there are no poles in the rest of the integrand at $q_i^- = 0$, or if there are such poles then the $i\epsilon$ prescription for J_A must be the same as the $i\epsilon$ prescription we used above for the ratio $q^-/(q^- - i\epsilon) = 1$. Here we have chosen a final state $i\epsilon$ prescription, namely we have the factor $\frac{q^-}{q^- - i\epsilon}$. This is because we only consider cases where the initial states, states before the hard interaction at $x^\mu = 0$, are color singlets and therefore do not interact with the soft gluons. It is only those states that are after the hard interaction, in other words the final states that interact with these soft gluons therefore the $i\epsilon$ prescription in J_A is a final state $i\epsilon$ prescription.

At this point the factorization of soft gluons is a matter of direct application of the nonabelian Ward identities of Appendix A. The result can be written as

$$J_A^{(C_A)}(k_A^+, \tilde{q}_l^\alpha)_{ab}^{\{+\}} = J_A^{(C_A)}(k_A^+)_{a'b'} E_{a'a}^{\{+\}}(v^\mu, \tilde{q}_L^\alpha) E_{b'b}^{\{+\}*}(v^\mu, \tilde{q}_R^\alpha), \qquad (3.44)$$
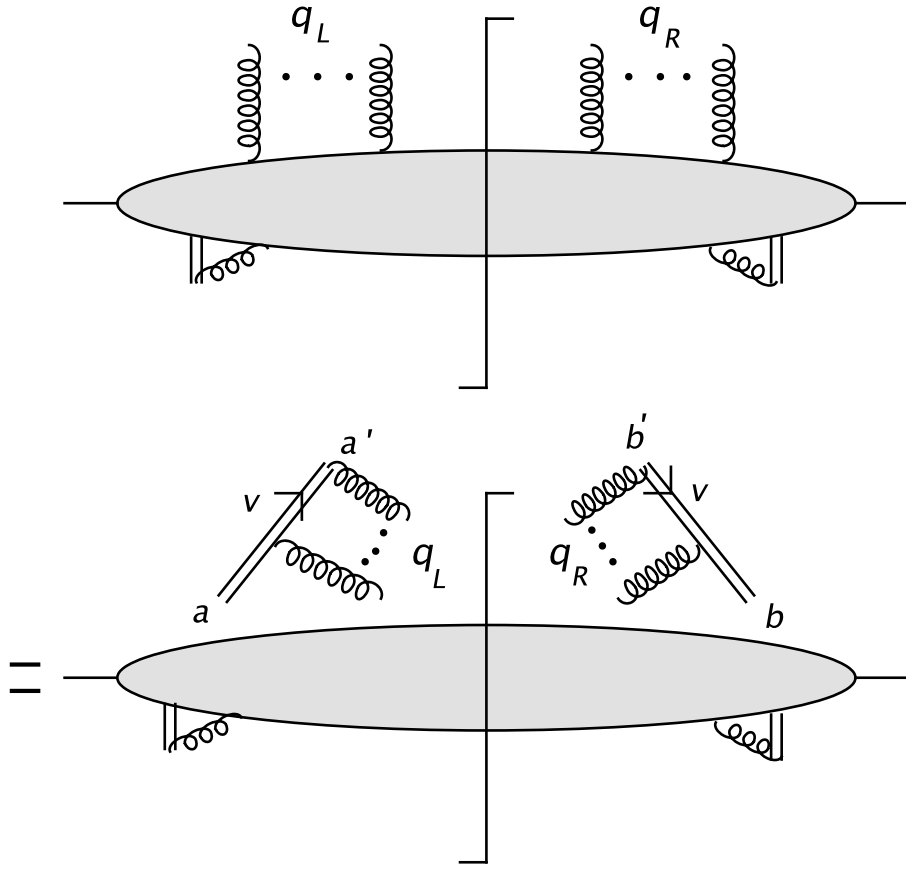
Figure 3.9: Graphical representation of Eq. (3.44) where soft lines are factored from the A-jet via nonabelian Ward identities.

where we have written the color indices explicitly and $\tilde{q}_L$ and $\tilde{q}_R$ attach the A-jet to the left and to the right of the cut. This equation is represented by Fig. 3.9 where E and E^* represents the two eikonal lines in the v^μ direction on the two sides of the cut. We can also see that the jet function J_A is diagonal in color space after the soft gluon factorization.

The same procedure for the B-jet results in a similar expression where the soft gluons factor from J_B. We can now apply our results to an arbitrary

leading pinch singular surface S to write down the contribution as

$$
\begin{aligned}
G_S \; = \; & \sum_C \int \frac{dk_A^+}{2\pi} \int \frac{dk_B^-}{2\pi} \frac{1}{3} Tr_{\text{color}} \, J_A^{(C)}(k_A^+) \, S_{c'cd'd}^{(C)} \, H_{c'cd'd}^{(C)}(k_A^+, k_B^-) \\
& \times \frac{1}{3} Tr_{\text{color}} \, J_B^{(C)}(k_B^-) \,,
\end{aligned}
\tag{3.45}
$$

where we have defined the soft function S as

$$
\begin{aligned}
S_{c'cd'd}^{(C)} \; = \; & \int \prod_l \frac{d^4 q_l}{(2\pi)^4} \prod_j \frac{d^4 \bar{q}_j}{(2\pi)^4} \, S^{(C)}(q_l^\alpha, \bar{q}_j^\beta) \, E_{ac'}^{(+)}(q_{l,L}) E_{ac}^{(+)}(q_{l,R}) \\
& \times E_{bd'}^{(-)}(\bar{q}_{j,L}) E_{bd}^{(-)}(\bar{q}_{j,R}) \,.
\end{aligned}
\tag{3.46}
$$

In this form the soft part, the hard part and the jets are completely factored and therefore each can seperately be summed over their individual cuts. Diagramatically the fully factorized form of the contribution of an arbitrary leading pinch singular surface S for the Drell Yan cross section is given by Fig. 3.10.

In the context of e^+e^- annihilation it was shown in Ref. [56] that $S_{c'cd'd} = \delta_{c'c}\delta_{d'd}$, which is the zeroth order contribution. The cancellation of soft gluons is due to the sum over final states and integration over loop energies. It is analogous to the cancellation of final state interactions due to unitarity. The same arguments can be applied to the soft function of the Drell Yan cross section to show that the higher order corrections cancel at leading order [41]. The final result for the leading contribution to G_S then can be written as

$$
G_S = \int \frac{dk_A^+}{2\pi} \frac{dk_B^-}{2\pi} \, J_{A,\text{soft}}(k_A^+) \, J_{B,\text{soft}}(k_B^-) \, H(k_A^+, k_B^-) \,.
\tag{3.47}
$$
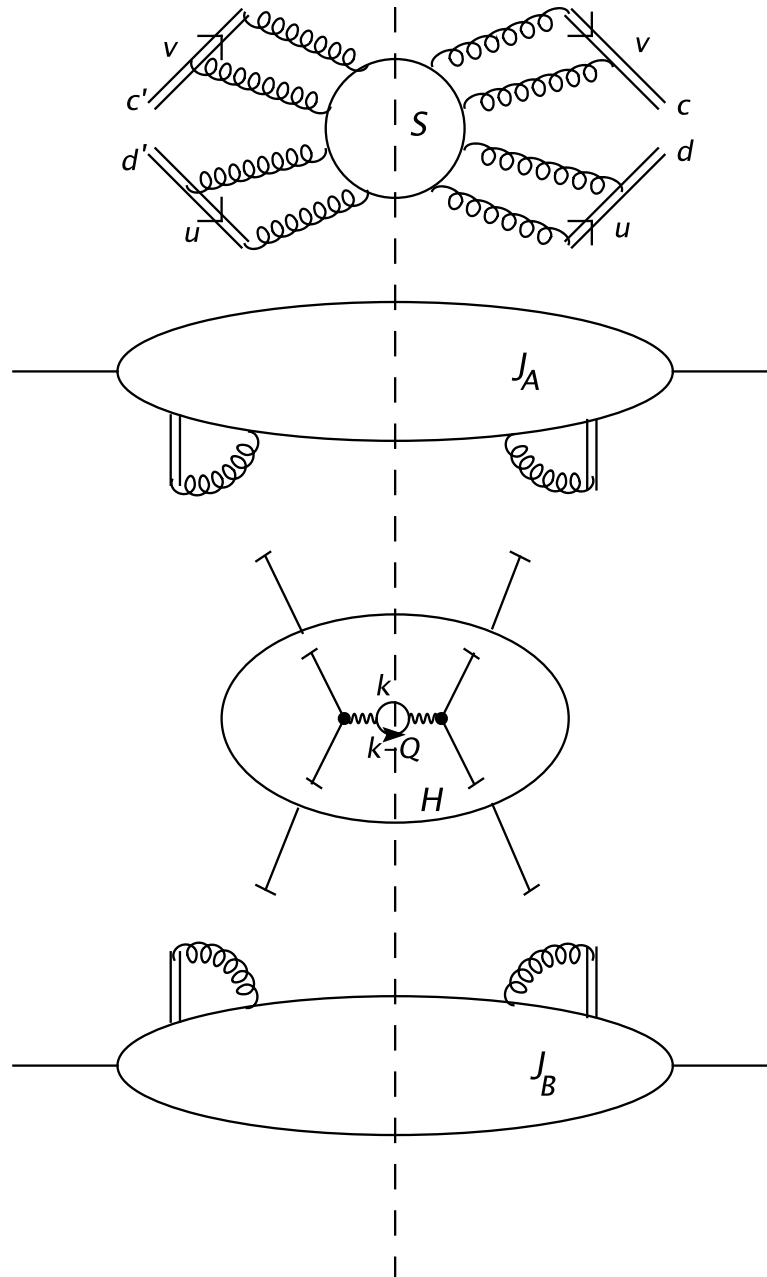
Figure 3.10: Graphical representation of Eq. (3.45) where the soft function, the hard function and the jet functions are fully factorized.

When Eq. (3.47) is summed over all graphs and over all leading pinch singular surfaces, one finds that the differential cross section takes the desired form of Eq. (3.2) [41]

$$\frac{d\sigma_{AB\to l\bar{l}+X}}{dQ^2\,dy} = \sum_{a,b} \int_0^1 \frac{d\xi_A}{\xi_A}\frac{d\xi_B}{\xi_B}\, f_{a/A}(\xi_A, Q^2)\, H_{ab}(x_A/\xi_A, x_B/\xi_B, Q^2) f_{b/B}(\xi_B, Q^2)\,.$$
(3.48)

The standard choice of parton distribution functions for quarks in hadrons, defined as the expectation value of certain operators in a hadronic state is given by [57]

$$f_{q/h}(\xi, \mu^2) = \frac{1}{4}\sum_\sigma \int_\infty^\infty \frac{dy^-}{2\pi} e^{-i\xi p^+ y^-}\, \langle h(p,\sigma)|\bar{q}(0^=, y^-, \mathbf{0}_T)\, n\cdot\gamma\, q(0)|h(p,\sigma)\rangle\,,$$
(3.49)

where n^μ is a light-like vector in the opposite direction to the incoming hadron with momentum p and spin σ. After one shows that the IR divergences cancel and the set of pinched singular surfaces reduces to a smaller set, what needs to be done for seperating out H in Eq. (3.2) is to define a set of nested subtractions in the spirit of Refs. [56, 58]. However, this analysis is outside the scope of this thesis.

3.4 Parton distribution functions and cross section predictions

So far we have discussed the steps of the proof of factorization for inclusive hadron-hadron scattering processes. The full factorized form of the

differential cross section is given in Eq. (3.2). As we have pointed out before, the parton distribution functions in this equation are universal, in other words process independent. This property of the parton distributions gives QCD its predictive power. Once determined by experiment, the same parton distribution functions can be used to predict cross sections for different processes and then these predictions can be tested by experiment. In this section, we will discuss how we determine the parton distribution functions by experiment and how we use this information to make cross section predictions in perturbative QCD. This discussion will also serve as a motivation for the study of $2 \rightarrow n$ partonic scattering amplitudes, which will be the main focus of the rest of this thesis.

Since the parton distribution functions are universal, we can use any process to determine them. We will use the DIS of an electron off a hadron. Tha hadronic tensor of the inclusive DIS is written in terms of two structure functions F_1 and F_2. One can write these structure functions in the following factorized forms [23]

$$
\begin{aligned}
F_2^{(h)}(x, Q^2) &= \sum_{\text{partons } a} \int_x^1 d\xi \, C_2^{(a)}\left(\frac{x}{\xi}, \frac{Q^2}{\mu^2}, \alpha_s(\mu^2)\right) f_{a/h}(\xi, \mu^2), \\
F_1^{(h)}(x, Q^2) &= \sum_{\text{partons } a} \int_x^1 \frac{d\xi}{\xi} \, C_1^{(a)}\left(\frac{x}{\xi}, \frac{Q^2}{\mu^2}, \alpha_s(\mu^2)\right) f_{a/h}(\xi, \mu^2), \ (3.50)
\end{aligned}
$$

where $f_{a/h}$ is the parton distribution function for parton a in hadron h with momentum fraction ξ. $C_i^{(h)}$ are the infrared safe coefficient functions for the full hadronic process. The first goal is to determine these coefficient functions in a given factorization scheme. We will explain what we mean by factorization scheme shortly. The strategy is as follows : first we consider the partonic

process. A similar factorization is valid for the partonic structure functions in terms of parton distribution functions for partons in partons and the same coefficient functions. We compare the perturbative expressions for the partonic structure functions and the parton-in-parton distribution functions to obtain the coefficient functions.

The one-loop parton-in-parton distribution functions using $\overline{\text{MS}}$ renormalization prescription are given by [23]

$$f_{a/f}^{(1)}(\xi, \epsilon) = \frac{\alpha_s}{2\pi} \left(\frac{-1}{\epsilon} + \gamma_E - \ln(4\pi) \right) P_{a/f}^{(1)}(\xi) , \qquad (3.51)$$

where $P_{a/f}^{(1)}$ is referred to as the one loop "evolution kernel". Since these distribution functions are computed using the $\overline{\text{MS}}$ renormalization prescription, they are reffered to as $\overline{\text{MS}}$ distributions. However, other choices of distribution functions can be defined by the following convolution

$$f_{a/h}^{(D)}(\xi, \mu^2) = \int_\xi^1 \frac{d\eta}{\eta} D_{ab} \left(\xi/\eta, \alpha_s(\mu^2) \right) f_{b/h}^{\overline{\text{MS}}}(\eta, \mu^2) , \qquad (3.52)$$

where D is any IR safe distribution. This is reffered to as the factorization scheme. One particularly interesting choice of D is such that it is equal to the full DIS coefficient function C_2, which is referred to as the DIS scheme. Having obtained the coefficient functions of Eq. (3.50), one can perform a DIS experiment to determine the second structure function F_2. Using this experimental result one can then extract out the parton distribution functions from Eq. (3.50).

The hard scattering function H_{ab} of Eq. (3.2) is calculable order-by-order in perturbation theory. The strategy to compute this function perturbatively

is as follows: we first consider the partonic process $a\,b \to l\bar{l} + X$. The next very nontrivial step is to assume factorization for the differential cross section for this partonic process as follows

$$\frac{d\sigma_{a\,b\to l\bar{l}+X}}{dQ^2\,dy} = \sum_{i,j} \int_0^1 \frac{d\xi_A}{\xi_A}\frac{d\xi_B}{\xi_B}\, f_{i/a}(\xi_A, Q^2)\, H_{ij}(x_A/\xi_A, x_B/\xi_B, Q^2) f_{j/b}(\xi_B, Q^2)\,,$$

(3.53)

where the parton distributions are for partons in partons and the hard scattering function is the same as the one for the full hadronic process. Even though such a factorization for partonic processes was considered in Ref. [59] we believe that a rigorous proof in the same spirit as we have presented following Refs. [41, 42] is still missing. A crucial drawback of the proof in Refs. [41, 42] is the explicit assumption that the incoming states are color neutral, therefore a generalization to incoming colored states is needed.

Once factorization of Eq. (3.53) is assumed, one can compute the partonic cross section and the parton in parton distribution functions order-by-order in perturbation theory and find the only unknowns, the hard scattering functions, H_{ab}, from that equation. Since the hard scattering function is the same for the partonic and the full hadronic cross sections, one can now use the universal parton distribution functions and the process dependent hard scattering function to make cross section predictions in perturbative QCD.

For the construction of the partonic cross section at a desired order in perturbation theory, one needs the $2 \to n$ partonic scattering amplitudes. Therefore we will study the virtual corrections to the $2 \to n$ partonic scattering amplitudes for the rest of this thesis. We will see that these virtual corrections

have in general infrared divergences which are given in terms of poles in powers of $1/\varepsilon$. Therefore the virtual corrections to the cross sections in general have such poles. However, it is guarranteed by the factorization theorems that these poles due to virtual corrections cancel against the poles due to real corrections to the partonic cross section we are computing at an arbitrary fixed order in perturbation theory.

However, this cancellation is often incomplete at certain kinematic boundaries of the phase space. In such situations, there are large logarithmic corrections to the cross section and it is very useful to *resum* these logarithmic corrections to all orders in perturbation theory to show the convergence of the perturbation expansion. In the case of hadronic collisions, in order to perform this resummation one needs a matrix of soft anomalous dimensions. As we shall see in the next chapter, this matrix is obtained by considering the vacuum expectation value of products of Wilson lines for each external parton. It will be the main objective of the rest of this thesis to calculate this matrix at two-loop level, which will eventually lead us to the resummation of next-to-next-to leading poles for the $2 \rightarrow n$ partonic scattering amplitudes.

Chapter 4

Resummation and Anomalous Dimensions for Resummed Amplitudes

The description of partonic hard scattering in quantum chromodynamics (QCD) is central to the analysis of final states at hadronic colliders. The calculation of cross sections for such processes requires a combination of virtual and real radiative corrections, organized according to underlying factorization theorems. This is the case for higher-order calculations to next- or next-to-next-to-leading order in α_s (NLO, NNLO, . . .). It holds as well as for resummed cross sections, in which selected corrections associated with soft and collinear gluon radiation are organized, at leading, next-to-leading or next-to-next-to-leading logarithms (LL, NLL, NNLL, . . .) to all orders in α_s.

In both fixed-order and resummed calculations the coherence properties of soft gluon radiation play an essential role. An anomalous dimension matrix for inclusive wide-angle soft gluon radiation was introduced in Refs. [60, 61], and computed to leading order for quark and gluon scattering processes in Ref. [62]. The one-loop matrix of soft anomalous dimensions has been applied to the

NLL threshold resummation of jet cross sections [63, 64] and of distributions of event-shape variables [65, 66] that are "global" in the sense of Ref. [67]. At two loops, the same matrix, combined with resummed form factors, was shown in Ref. [68] to control the single infrared poles of dimensionally-regularized partonic scattering amplitudes in $\varepsilon = 2 - D/2$. In this paper we will show how to compute this matrix directly at two loops, from a relatively limited set of diagrams in the eikonal approximation, using Wilson lines, giving as an explicit example quark-antiquark scattering.

The full analysis given below applies to any $2 \to n$ partonic amplitude in dimensional regularization. The two-loop soft anomalous dimension matrix allows the exponentiation of next-to-next-to-leading infrared poles, which appear in the combination $\alpha_s^n (1/\varepsilon)^{n-1}$ in the exponent, a level equivalent to next-to-next-to-leading logarithms. The resulting resummed amplitudes can be expanded out to the two-loop order, and the poles in ε can be compared to explicit two-loop scattering amplitudes, for example the basic $2 \to 2$ scattering processes [69, 70, 71, 72, 73, 74, 75, 76]. Those poles were expressed in terms of the color-space notation [77, 78] and the organization of two-loop singular terms presented in Ref. [79]. (Related work at one loop was performed in Refs. [80, 81].) We will verify that the expansion of the resummed amplitudes to two loops matches precisely the full infrared pole structure of the known two-loop scattering amplitudes, including the single poles in ε. Remarkably, we will find, as reported in Ref. [82], that the two-loop anomalous dimension matrix is related to the one-loop matrix by a constant, the same constant, K, appearing in the DGLAP splitting kernel, that relates the one and two-loop

anomalous dimensions for the Sudakov form factor. (The analogous matrix appears in the electroweak Sudakov corrections to four-fermion scattering, and has been extracted at two loops from the QCD four-quark scattering amplitude in Ref. [83].) The simplicity of this result will facilitate the development of practical resummed cross sections with color exchange at NNLL.

This paper is organized as follows. The next section reviews the collinear and infrared factorization of exclusive amplitudes. In that section, we provide a new explicit scale-setting choice for the soft function, which is necessary to define the scales of logarithms in the relevant anomalous dimensions. The third section describes the expansion of the jet functions to two loops. Here we describe a new "minimal" reorganization of the factorized amplitude, to facilitate the comparison to fixed-order calculations. In the fourth section, we describe in detail the one- and two-loop calculations necessary to determine the soft anomalous dimension matrix, for the specific case of quark-antiquark scattering. Here, we will employ the eikonal approximation, and the scale-setting choice for the soft function from Sec. 2. We show that diagrams attaching gluons to three different eikonal lines either vanish, or represent the exponentiation of the one-loop soft matrix. We close Sec. 4 by generalizing these calculations to arbitrary flavors for incoming partons and arbitrary flavors and numbers of outgoing partons. To do so, we present the color-mixing anomalous dimension matrix in the color-space notation of Ref. [77, 79]. Finally, in Sec. 5 we employ this notation, along with results of Sec. 4 for the soft anomalous dimensions and known two-loop elastic form factors for quarks and gluons, to give the explicit form of the two-loop single pole terms in ε,

for arbitrary $2 \rightarrow n$ partonic processes in QCD. We show that these pole terms agree with the single-pole "$\mathbf{H}^{(2)}$" terms found in NNLO $2 \rightarrow 2$ calculations [69, 75, 76, 84, 85] whose poles have been organized according to the formalism of Ref. [79]. Our results also agree with the proposal of Ref. [86] for the single poles for the case of $2 \rightarrow n$ gluon processes, which was based on the consistency of collinear factorization of amplitudes. We provide an appendix with explicit forms of Sudakov anomalous dimensions, and two appendices illustrating calculations of soft anomalous dimensions using eikonal methods. The final appendix details the computation of a particular commutator of color-space matrices, which is needed to compare our results with the explicit NNLO calculations.

4.1 Factorized amplitudes in dimensional regularization

Our considerations apply to $2 \rightarrow n$ scattering processes, denoted as "f",

$$\text{f}: \quad f_1(p_1, r_1) + f_2(p_2, r_2) \rightarrow f_3(p_3, r_3) + f_4(p_4, r_4) + \cdots + f_{n+2}(p_{n+2}, r_{n+2}).$$

$$(4.1)$$

The labels f_i refer to the flavor of the participating partons, each of momenta $\{p_i\}$ and color $\{r_i\}$. The amplitude for this process, $\mathcal{M}^{[\text{f}]}$, is a color tensor with indices associated with the external partons $\{r_i\} = \{r_1, r_2, \dots\}$. It is convenient to express these amplitudes in a basis of C independent color tensors,

$(c_I)_{\{r_i\}}$, so that [62, 79]

$$
\begin{aligned}
\mathcal{M}^{[\mathrm{f}]}_{\{r_i\}}\left(\beta_j, \frac{Q^2}{\mu^2}, \alpha_s(\mu^2), \varepsilon\right) &= \sum_{L=1}^{C} \mathcal{M}^{[\mathrm{f}]}_L\left(\beta_j, \frac{Q^2}{\mu^2}, \alpha_s(\mu^2), \varepsilon\right) (c_L)_{\{r_i\}} \\
&= |\mathcal{M}_{\mathrm{f}}\rangle,
\end{aligned}
\tag{4.2}
$$

where the ket may be thought of as a vector $\mathcal{M}^{[\mathrm{f}]}_L$ with C elements in the space of color tensors c_I. We will analyze these amplitudes at fixed momenta p_i for the participating partons, which we represent as

$$
p_i = Q\beta_i, \quad \beta_i^2 = 0,
\tag{4.3}
$$

where the β_i are four-velocities, and where Q is an overall momentum scale. For the purposes of this analysis, and to compare with existing NNLO calculations, we take all of the partons massless, as indicated. To be specific, we may take $\beta_1 \cdot \beta_2 = 1$ for the incoming partons in Eq. (4.1), which implies $Q^2 = s/2$, but this is not necessary.

In dimensional regularization ($D = 4 - 2\varepsilon$), on-shell amplitudes may be factorized into jet, soft and hard functions, which describe the dynamics of partons collinear with the external lines, soft exchanges between those partons, and the short-distance scattering process, respectively. This factorization follows from the general space-time structure of long-distance contributions to elastic processes [87]. A formal proof for the case $n = 2$ in QCD (quark-quark scattering) was presented long ago [60].

The general form of the factorized amplitude is

$$
\begin{aligned}
\mathcal{M}^{[\mathrm{f}]}_L\left(\beta_i, \frac{Q^2}{\mu^2}, \alpha_s(\mu^2), \varepsilon\right) &= J^{[\mathrm{f}]}\left(\frac{Q'^2}{\mu^2}, \alpha_s(\mu^2), \varepsilon\right) S^{[\mathrm{f}]}_{LI}\left(\beta_i, \frac{Q'^2}{\mu^2}, \frac{Q'^2}{Q^2}, \alpha_s(\mu^2), \varepsilon\right) \\
&\quad \times H^{[\mathrm{f}]}_I\left(\beta_i, \frac{Q^2}{\mu^2}, \frac{Q'^2}{Q^2}, \alpha_s(\mu^2)\right),
\end{aligned}
\tag{4.4}
$$

where μ is the renormalization scale. $J^{[f]}$ is the product of jet functions for each of the external partons, as above denoted collectively by [f], $S^{[f]}$ is the soft function, and $H^{[f]}$ is the short-distance function. For example, when the process is $1 + 2 \rightarrow 3 + 4$, the product of jet functions is

$$J^{[f]}\left(\frac{Q'^2}{\mu^2}, \alpha_s(\mu^2), \varepsilon\right) \equiv \prod_{i=1,2,3,4} J^{[i]}\left(\frac{Q'^2}{\mu^2}, \alpha_s(\mu^2), \varepsilon\right). \qquad (4.5)$$

Construction of the soft and jet functions requires the specification of at least one independent momentum scale, Q', which plays the role of a factorization scale. Such a scale, distinct from Q and μ, may be useful when one or more invariants obey strong ordering. Here, however, we shall consider "fixed-angle" scattering configurations, in which the parameter Q sets the scale for all invariants, up to numbers of order unity. With this in mind, we will simplify Eq. (4.4) somewhat, and pick $Q' = \mu$, that is, equal factorization and renormalization scales. Both the soft and jet functions then depend on $\alpha_s(\mu^2)$ only, and we will suppress their Q'^2 dependence, now expressing the same amplitude as

$$\mathcal{M}_L^{[f]}\left(\beta_i, \frac{Q^2}{\mu^2}, \alpha_s(\mu^2), \varepsilon\right) = J^{[f]}\left(\alpha_s(\mu^2), \varepsilon\right) S_{LI}^{[f]}\left(\beta_i, \frac{Q^2}{\mu^2}, \alpha_s(\mu^2), \varepsilon\right)$$
$$\times \ H_I^{[f]}\left(\beta_i, \frac{Q^2}{\mu^2}, \alpha_s(\mu^2)\right), \qquad (4.6)$$

that is, we suppress dependence on those variables that are set to unity by our choice of scales.

Clearly, any jet-soft-hard factorization of the sort described above is unique only up to finite factors in the various functions. There is an additional ambiguity between the jet and soft functions at the level of a single

infrared pole per loop in dimensional regularization. In the remainder of this section, we will provide specific definitions for the jet and soft functions that will enable us to define and resum them unambiguously, and which will be useful in our calculations below. We begin with the jet functions.

4.1.1 The jet functions and the Sudakov form factor

The factorization (4.4) holds for any exclusive amplitude, including the elastic, or Sudakov, form factor. A very natural definition of the jet functions is, therefore, the square root of the form factor [68]. Here, we will choose the case of the elastic scattering form factor with a color-singlet source, and spacelike momentum transfer. Reverting to the general case of jet momentum scale Q'^2, not necessarily equal to the renormalization scale, this is

$$J^{[i]}\left(\frac{Q'^2}{\mu^2}, \alpha_s(\mu^2), \varepsilon\right) = J^{[\bar{i}]}\left(\frac{Q'^2}{\mu^2}, \alpha_s(\mu^2), \varepsilon\right) = \left[\mathcal{M}^{[i\to i]}\left(\frac{Q'^2}{\mu^2}, \alpha_s(\mu^2), \varepsilon\right)\right]^{\frac{1}{2}}.$$

(4.7)

Below, we shall take μ as the $\overline{\text{MS}}$ renormalization scale, $\mu^2 = \mu_0^2 \exp[-\varepsilon(\gamma_E - \ln(4\pi))]$. With this choice, we may rely on the explicit form of the quark spacelike electromagnetic Sudakov form factor in $D = 4 - 2\varepsilon$ dimensions. A similar definition may be given for gluon jets in terms of matrix elements of conserved, singlet operators. In either case, the all-orders expression for the (square root of the) resummed form factor, organizing all pole terms, and implicitly specifying all finite terms of the jet defined as in Eq. (4.7),

is [88, 89, 90, 91]

$$J^{[i]}\left(\frac{Q'^2}{\mu^2}, \alpha_s(\mu^2), \varepsilon\right) = \exp\Bigg\{\frac{1}{4}\int_0^{Q'^2}\frac{d\xi^2}{\xi^2}\bigg[\mathcal{K}^{[i]}(\alpha_s(\mu^2), \varepsilon)$$
$$+ \mathcal{G}^{[i]}\left(-1, \bar{\alpha}_s\left(\frac{\mu^2}{\xi^2}, \alpha_s(\mu^2), \varepsilon\right), \varepsilon\right)$$
$$+ \frac{1}{2}\int_{\xi^2}^{\mu^2}\frac{d\tilde{\mu}^2}{\tilde{\mu}^2}\gamma_K^{[i]}\left(\bar{\alpha}_s\left(\frac{\mu^2}{\tilde{\mu}^2}, \alpha_s(\mu^2), \varepsilon\right)\right)\bigg]\Bigg\}, \quad (4.8)$$

where we use a notation for the running coupling that emphasizes its re-expansion in terms of the coupling at fixed scale μ. For our purposes below, we shall need only the "leading" form of the running coupling,

$$\bar{\alpha}_s\left(\frac{\mu^2}{\tilde{\mu}^2}, \alpha_s(\mu^2), \varepsilon\right) = \alpha_s(\mu^2)\left(\frac{\mu^2}{\tilde{\mu}^2}\right)^\varepsilon\sum_{n=0}^\infty\left[\frac{\beta_0}{4\pi\varepsilon}\left(\left(\frac{\mu^2}{\tilde{\mu}^2}\right)^\varepsilon - 1\right)\alpha_s(\mu^2)\right]^n,$$
$$(4.9)$$

with the one-loop coefficient

$$\beta_0 = \frac{11}{3}C_A - \frac{4}{3}T_F n_F. \quad (4.10)$$

In the expression for the jet functions above, the choice $Q'^2 = \mu^2$ can be imposed trivially. The functions $\mathcal{K}^{[i]}$, $\mathcal{G}^{[i]}$ and $\gamma_K^{[i]}$ are anomalous dimensions that can be determined by comparison to fixed-order calculations of the Sudakov form factors for quarks and gluons. These form factors are now known in QCD up to three loops [92, 93, 94, 95, 96, 97, 98]. Notice that the coupling in the argument of $\mathcal{K}^{[i]}$ is fixed at μ, so that the integral of this term alone is not well-defined at $\xi^2 = 0$ even for $D \neq 4$. This apparent divergence, however, is cancelled by contributions from the upper limit of the $\tilde{\mu}^2$ integral of the anomalous dimension $\gamma_K^{[i]}$, and relates the latter to $\mathcal{K}^{[i]}$ order-by-order in

perturbation theory. We will provide explicit expansions for these functions in Appendix B.

4.1.2 The soft function

We will broadly follow Ref. [62] in the definition of the soft function for partonic amplitudes, although we will modify certain details in the construction. The fundamental observation of Ref. [62] is that the soft function, describing color exchange between the jets, is independent of collinear dynamics, and may be constructed from an eikonal amplitude, that is, the vacuum expectation of products of ordered exponentials. For each external parton of flavor f_i, we introduce a nonabelian path-ordered phase operator,

$$\Phi_{v_i}^{[f_i]}(\sigma', \sigma) = P \exp \left[-ig \int_{\sigma}^{\sigma'} d\lambda \, v_i \cdot A^{[f_i]}(\lambda v_i) \right], \qquad (4.11)$$

where $v_i^\mu \sim \beta_i^\mu$ is a four-velocity. For specific calculations at two loops, it will be useful to choose these velocities to be slightly timelike,

$$0 < v_i^2 \ll 1. \qquad (4.12)$$

The "opposite moving" velocity $\bar{v}_i^\mu$ projects out the large component of v_i^μ. The gauge field $A^{[f_i]}$ is a matrix in the representation of parton i. In the construction of the soft function, we will eventually take all $v_i^2 \to 0$, or equivalently, $v_i^\mu \to \beta_i^\mu$. In perturbation theory, the operators $\Phi_{v_i}^{[f_i]}(\infty, 0)$ and $\Phi_{v_i}^{[f_i]}(0, -\infty)$ respectively generate outgoing and incoming eikonal lines in the v_i-directions. The eikonal sources couple to gluons at vertices in the color representation

of parton i. An essential feature of these diagrams is that they are invariant under rescalings of the velocities, $v_i \rightarrow \sigma v_i$.

We are now ready to construct eikonal multi-point amplitudes from products of ordered exponentials, tied together by the same color tensors, c_L that appear in the expansion of the partonic amplitudes, Eq. (4.4). For the $2 \rightarrow 2$ case, $1 + 2 \rightarrow 3 + 4$, this gives

$$W_I^{[\mathrm{f}]}{}_{\{r_k\}} = (c_L)_{\{r_k\}} W_{LI}^{[\mathrm{f}]}\left(\frac{v_i \cdot v_j}{\sqrt{v_i^2 v_j^2}}\right) = \sum_{\{d_i\}} \langle 0| \; \Phi_{v_4}^{[f_4]}(\infty,0)_{r_4,d_4} \; \Phi_{v_3}^{[f_3]}(\infty,0)_{r_3,d_3}$$
$$\times (c_I)_{d_4 d_3, d_2 d_1} \; \Phi_{v_1}^{[f_1]}(0,-\infty)_{d_1,r_1} \Phi_{v_2}^{[f_2]}(0,-\infty)_{d_2,r_2} |0\rangle \, .$$

$$(4.13)$$

Such a product is gauge invariant. The eikonal amplitude, or web function, W depends in general on both the invariants $v_i \cdot v_j$ and the invariant lengths v_i^2. The basic observation of Ref. [62] is that all potentially collinear divergent ratios factorize from dependence on wide-angle radiation for eikonal as well as partonic amplitudes. We can use this factorization to isolate the soft function systematically, using only calculations in the eikonal approximation.

Because of the factorization of collinear singularities, such dependence is universal, depending only on the number and flavors of the external jets. In particular, as observed above, form factors, with two external lines and trivial color flow, generate the same collinear dependence. Thus, all collinear dependence cancels in the ratio of our four-point eikonal amplitude W_I and the product of two eikonal form factors, just as in the ratio of the four-point partonic amplitudes to the corresponding form factors. We shall define S_{LI} by this ratio. Notice that information on color flow is not affected at all by the

eikonal jet functions, which like partonic jets, are diagonal in color. Thus, we define

$$S_{LI}^{[f]}\left(\frac{\beta_i \cdot \beta_j}{u_0}\right) = \lim_{v^2 \to 0} \frac{W_{LI}^{[f]}\left(\frac{v_i \cdot v_j}{v^2}\right)}{\prod_{i \in f}\left[W^{(i \to i)}\left(\frac{u_0}{v^2}\right)\right]^{1/2}}, \tag{4.14}$$

where as above the velocities β_i are the lightlike limits of the v_i. The denominators are eikonal versions of the elastic form factors, defined with incoming velocities v_i and outgoing $\bar{v}_i$, where $v_i^2 = \bar{v}_i^2 = v^2$ and $v_i \cdot \bar{v}_i = u_0$, with u_0 a constant of order unity, independent of i, namely

$$W^{(i \to i)}\left(\frac{u_0}{v^2}\right) = \langle 0| \, \Phi_{\bar{v}_i}^{[f_i]}(\infty, 0) \, \Phi_{v_i}^{[f_i]}(0, -\infty) \, |0\rangle. \tag{4.15}$$

This form factor generates the square of the collinear poles associated with the eikonal jet of flavor i in W_{LI}, and hence the soft function (4.14) is free of collinear divergences. We may thus take the lightlike limit for the velocities to define the soft function in the ratio.

Equation (4.14) allows us to compute the soft function, once we determine how to choose the variable u_0, so that we may match the eikonal calculation to the partonic amplitude. We can determine the correct choice as follows.

We first re-express Eq. (4.6) for the partonic amplitude, converting it into an expression for the soft function as a ratio analogous to Eq. (4.14),

$$S_{LI}^{[f]}\left(\beta_i, \frac{Q^2}{\mu^2}, \alpha_s(\mu^2), \varepsilon\right) H_I^{[f]}\left(\beta_i, \frac{Q^2}{\mu^2}, \alpha_s(\mu^2)\right) = \frac{\mathcal{M}_L^{[f]}\left(\beta_i, \frac{Q^2}{\mu^2}, \alpha_s(\mu^2), \varepsilon\right)}{J^{[f]}\left(\alpha_s(\mu^2), \varepsilon\right)}. \tag{4.16}$$

This simple result enables us to set the scale u_0 in the definition of the eikonal form factors of Eq. (4.14). In Eq. (4.16), S can depend on the velocities only

through the ratios $\beta_i \cdot \beta_j Q^2/\mu^2$. When S is calculated in this way from the ratio of partonic quantities, Q sets the scale of all momenta in the amplitude, and μ, the factorization scale in Eq. (4.6), may be reinterpreted as the momentum transfer in the form factors that define the jet functions. When calculated from the eikonal ratio, on the other hand, S depends only on the variables $\beta_i \cdot \beta_j/u_0$. To match the soft function computed in eikonal approximation with the partonic amplitude, we need only require

$$\frac{\beta_i \cdot \beta_j}{u_0} = \frac{Q^2 \beta_i \cdot \beta_j}{\mu^2} \qquad \rightarrow \qquad u_0 = \frac{\mu^2}{Q^2} \, . \tag{4.17}$$

This relation will be used in our explicit calculations later. We are now ready to provide an all-orders expression for the soft function, analogous to Eq. (4.8) for the jet functions.

4.1.3 Resumming the soft function

We will use the $\overline{\text{MS}}$ scheme for renormalization throughout. Before renormalization, all of the purely eikonal amplitudes discussed in the previous subsection give (only) scaleless integrals in perturbation theory. Such integrals vanish identically in dimensional regularization. In fact, these functions are only nontrivial because of renormalization, with every infrared pole resulting from the subtraction of a corresponding ultraviolet pole. This is the case whether or not W is collinear-regulated by introducing masses for its eikonal phases.

Thus, for both the web function W and the soft function S, we have

(suppressing indices)

$$W_{\text{bare}}^{[\text{f}]} = 1 = Z_{W_{\text{f}}}(\alpha_s(\mu), \varepsilon) \, W_{\text{ren}}^{[\text{f}]},$$

$$S_{\text{bare}}^{[\text{f}]} = 1 = Z_{S_{\text{f}}}(\alpha_s(\mu), \varepsilon) \, S_{\text{ren}}^{[\text{f}]}, \tag{4.18}$$

and similarly for the eikonal form factors in the ratio (4.14). Both S and W are therefore defined entirely by their anomalous dimension matrices,

$$\begin{aligned}
(\Gamma_A)_{IJ} &= \left(Z_A^{-1}\right)_{IK} \frac{d\,(Z_A)_{KJ}}{d\ln\mu} \\
&= \left(Z_A^{-1}\right)_{IK} \beta(g, \varepsilon) \frac{\partial\,(Z_A)_{KJ}}{\partial g}, \tag{4.19}
\end{aligned}$$

which are given in any minimal scheme by the residues $Z_{A,1}^{(k)}$, with $A = W_{\text{f}}$ or S_{f}, of single ultraviolet poles in $1/\varepsilon$, at kth order in the expansion

$$Z_A = 1 + \sum_{k=1}^{\infty} \left(\frac{\alpha_s}{\pi}\right)^k Z_A^{(k)}(\varepsilon) = \sum_{k=1}^{\infty} \left(\frac{\alpha_s}{\pi}\right)^k \sum_{n=1}^{k} Z_{A,n}^{(k)} \left(\frac{1}{\varepsilon}\right)^n. \tag{4.20}$$

Then, for example, from the one-loop bare integrals we find the one-loop anomalous dimension from the residues of the one-loop single ultraviolet poles,

$$\Gamma_A^{(1)} = -2\, Z_{A,1}^{(1)}, \tag{4.21}$$

where $\Gamma_A^{(n)}$ is the nth order coefficient of $(\alpha_s/\pi)^n$ in Γ_A. Similarly, to order $\mathcal{O}(\alpha_f^{\in})$, after one-loop renormalization we find the two-loop anomalous dimensions from the two-loop single poles,

$$\Gamma_A^{(2)} = -4\, Z_{A,1}^{(2)}. \tag{4.22}$$

From the definition of S, Eq. (4.14), the soft anomalous dimension matrix is found from the matrix for the corresponding eikonal amplitude by simply

subtracting the anomalous dimensions for the eikonal jets. We denote the latter by $\Gamma_2^{[i]}(u_0/v^2, \alpha_s)$, and write

$$\Gamma_{S_{\mathrm{f}},IJ}\left(\frac{\beta_i \cdot \beta_j}{u_0}, \alpha_s\right) = \lim_{v^2 \to 0}\left[\Gamma_{W_{\mathrm{f}},IJ}\left(\frac{v_i \cdot v_j}{v^2}, \alpha_s\right) - \delta_{IJ} \sum_{i \in \mathrm{f}} \Gamma_2^{[i]}\left(\frac{u_0}{v^2}, \alpha_s\right)\right].$$
(4.23)

In $\Gamma_{S_{\mathrm{f}}}$, all sensitivity to collinear dynamics, and therefore to the choice of v^2, is cancelled, and the coefficients depend only on the invariants $\beta_i \cdot \beta_j$.

The matrix renormalization group equation for the eikonal amplitude $S_{IK}^{[\mathrm{f}]}$ is then

$$\left(\mu\frac{\partial}{\partial \mu} + \beta(g, \varepsilon)\frac{\partial}{\partial g}\right)S_{IK}^{[\mathrm{f}]} = -\Gamma_{S_{\mathrm{f}},IJ}\left(\frac{\beta_i \cdot \beta_j Q^2}{\mu^2}, \alpha_s\right) S_{JK}^{[\mathrm{f}]},$$
(4.24)

from which we can solve directly for S as a path-ordered exponential,

$$\mathbf{S}_{\mathrm{f}}\left(\frac{\beta_i \cdot \beta_j}{u_0}, \alpha_s(\mu^2), \varepsilon\right) = \mathrm{P}\exp\left[-\frac{1}{2}\int_0^{\mu^2}\frac{d\tilde{\mu}^2}{\tilde{\mu}^2}\right.$$
$$\left.\times \mathbf{\Gamma}_{S_{\mathrm{f}}}\left(\frac{\beta_i \cdot \beta_j}{u_0}, \bar{\alpha}_s\left(\frac{\mu^2}{\tilde{\mu}^2}, \alpha_s(\mu^2), \varepsilon\right)\right)\right],$$
(4.25)

where boldface (with a subscript for flavor flow) indicates a matrix. In summary, the matrix of anomalous dimensions, and hence the soft matrix itself, can be computed order-by-order purely from eikonal diagrams.

4.2   The jet functions to two loops

In this section, we expand the jet functions in the factorized amplitude (4.6) to fixed (second) order in α_s, in a form that is convenient for comparison to explicit partonic calculations.

To determine the jet anomalous dimensions, as well as to use the re-summed forms of the jet and soft functions with fixed-order calculations, we re-expand the running coupling in terms of a coupling at fixed scale. It is important to do so consistently in dimensional regularization, using the explicit form for the running coupling, Eq. (4.9). It will also be convenient to use Eq. (4.8) as a starting-point to isolate the truly universal pole terms in the logarithm of the jet function, separating them from the finite terms. To this end, we introduce the notation

$$
\begin{aligned}
\ln J^{[i]}(\alpha_s(\mu^2), \varepsilon) &= \sum_{n=1}^{\infty} \left(\frac{\alpha_s(\mu^2)}{\pi} \right)^n \sum_{m=1}^{n+1} \frac{E_m^{[i]\,(n)}(\varepsilon)}{\varepsilon^m} + \sum_{n=1}^{\infty} \left(\frac{\alpha_s(\mu^2)}{\pi} \right)^n e^{[i]\,(n)}(\varepsilon) \\
&= E^{[i]}(\alpha_s(\mu^2), \varepsilon) + e^{[i]}(\alpha_s(\mu^2), \varepsilon) ,
\end{aligned}
\tag{4.26}
$$

in terms of the coupling $\alpha_s(\mu^2)$ at fixed scale μ. As in Eq. (4.6), we set the jet factorization scale $Q' = \mu$. The pure pole terms in Eq. (4.26) have been expanded at each order as

$$
E^{[i]\,(n)}(\varepsilon) \equiv \sum_{m=1}^{n+1} \frac{E_m^{[i]\,(n)}(\varepsilon)}{\varepsilon^m} ,
\tag{4.27}
$$

while the functions $e^{[i]\,(n)}(\varepsilon)$ absorb all terms that remain finite for $\varepsilon = 0$, order-by-order in α_s. The coefficients $E_m^{[i]\,(n)}$ and the functions $e^{[i]\,(n)}(\varepsilon)$ are determined, of course, by the expansions of the functions γ_K, $\mathcal{K}$ and $\mathcal{G}$, which depend in general on the definition (4.7) of the jet. This separation, however, eliminates the remaining arbitrariness in choosing the form factor by defining a "minimal" jet, consisting of the exponential of pole terms only,

$$
\mathcal{J}^{[i]}(\alpha_s(\mu^2), \varepsilon) \equiv \exp \left[E^{[i]}(\alpha_s, \varepsilon) \right] .
\tag{4.28}
$$

In this notation, we rewrite our basic factorization, Eq. (4.6), in "minimal" form as

$$\mathcal{M}_L^{[\mathrm{f}]}\left(\beta_i, \frac{Q^2}{\mu^2}, \alpha_s(\mu^2), \varepsilon\right) = \prod_{i\in\mathrm{f}} \mathcal{J}^{[i]}\left(\alpha_s(\mu^2), \varepsilon\right) S_{LI}^{[\mathrm{f}]}\left(\frac{\beta_i\cdot\beta_j Q^2}{\mu^2}, \alpha_s(\mu^2), \varepsilon\right)$$
$$\times \ \mathcal{H}_I^{[\mathrm{f}]}\left(\beta_i, \frac{Q^2}{\mu^2}, \alpha_s(\mu^2)\right), \qquad (4.29)$$

where we have absorbed the (color-diagonal) finite factors into the perturbative definition of the short-distance function

$$\mathcal{H}_I^{[\mathrm{f}]}\left(\beta_i, \frac{Q^2}{\mu^2}, \alpha_s(\mu^2), \varepsilon\right) = \exp\left[\sum_{i\in\mathrm{f}} e^{[i]}\left(\alpha_s(\mu^2), \varepsilon\right)\right] H_I^{[\mathrm{f}]}\left(\beta_i, \frac{Q^2}{\mu^2}, \alpha_s(\mu^2)\right).$$
$$(4.30)$$

We will also find it useful to write this expression in the color state notation of Eq. (4.2), as

$$|\mathcal{M}_\mathrm{f}\rangle = \prod_{i\in\mathrm{f}} \mathcal{J}^{[i]}\left(\alpha_s(\mu^2), \varepsilon\right) \mathbf{S}_\mathrm{f}\left(\frac{\beta_i\cdot\beta_j Q^2}{\mu^2}, \alpha_s(\mu^2), \varepsilon\right)|\mathcal{H}_\mathrm{f}\rangle, \quad (4.31)$$

where again the matrix structure of the soft function is denoted by boldface and where we treat $\mathcal{H}_I^{[\mathrm{f}]}$ in the notation of Eq. (4.2).

Before this refactorization, the logarithm of the full jet function $J^{[i]}$ at two loops is given by

$$\ln J^{[i]}(\alpha_s(\mu^2), \varepsilon) = \frac{1}{4}\left\{-\left(\frac{\alpha_s}{\pi}\right)\left(\frac{1}{2\varepsilon^2}\gamma_K^{[i]\,(1)} + \frac{1}{\varepsilon}\mathcal{G}^{[i]\,(1)}(\varepsilon)\right)\right.$$
$$\left. +\left(\frac{\alpha_s}{\pi}\right)^2\left[\frac{\beta_0}{8}\frac{1}{\varepsilon^2}\left(\frac{3}{4\varepsilon}\gamma_K^{[i]\,(1)} + \mathcal{G}^{[i]\,(1)}(\varepsilon)\right) - \frac{1}{2}\left(\frac{\gamma_K^{[i]\,(2)}}{4\varepsilon^2} + \frac{\mathcal{G}^{[i]\,(2)}(\varepsilon)}{\varepsilon}\right)\right] + \dots\right\}.$$
$$(4.32)$$

To determine the coefficients $E_m^{[i]\,(n)}$ in the minimal two-loop jet function, we only need to expand the functions $\mathcal{G}^{[i]\,(n)}(\varepsilon)$,

$$\mathcal{G}^{[i]\,(n)}(\varepsilon) = \mathcal{G}_0^{[i]\,(n)} + \varepsilon\,\mathcal{G}^{[i]\,(n)\prime}(0) + \dots . \tag{4.33}$$

Explicit forms for these anomalous dimensions can be found in Appendix B. In terms of these quantities, we readily find that the full single-pole terms in the logarithm of the jet function are given at one and two loops by

$$
\begin{aligned}
E_2^{[i]\,(1)} &= -\frac{1}{8}\,\gamma_K^{[i]\,(1)}\,, \\
E_1^{[i]\,(1)} &= -\frac{\mathcal{G}_0^{[i]\,(1)}}{4}\,, \\
E_3^{[i]\,(2)} &= \frac{3\beta_0}{128}\,\gamma_K^{[i]\,(1)}\,, \\
E_2^{[i]\,(2)} &= \frac{\beta_0}{32}\,\mathcal{G}_0^{[i]\,(1)} - \frac{1}{32}\,\gamma_K^{[i]\,(2)}\,, \\
E_1^{[i]\,(2)} &= -\frac{\mathcal{G}_0^{[i]\,(2)}}{8} + \frac{\beta_0\,\mathcal{G}^{[i]\,(1)\prime}(0)}{32}\,, \\
E_1^{[q]\,(2)} &= -\frac{3}{8}C_F^2\left[\frac{1}{16} - \frac{1}{2}\zeta(2) + \zeta(3)\right] - \frac{1}{16}C_A C_F\left[\frac{961}{216} + \frac{11}{4}\zeta(2) - \frac{13}{2}\zeta(3)\right] \\
&\quad + \frac{1}{16}\,C_F T_F n_F\left[\frac{65}{54} + \zeta(2)\right]\,, \\
E_1^{[g]\,(2)} &= \frac{1}{32}C_A^2\left[-\frac{346}{27} + \frac{11}{6}\zeta_2 + \zeta_3\right] + \frac{1}{16}C_A T_F n_F\left[\frac{64}{27} - \frac{\zeta_2}{3}\right] + \frac{1}{16}C_F T_F n_F\,,
\end{aligned}
$$
$$\tag{4.34}$$

where for $E_1^{[i]\,(2)}$ we give the explicit expressions for the quark and gluon cases. Notice that the full single pole term includes a contribution from the running of the finite term at one loop, which appears as an $\mathcal{O}(\varepsilon)$ contribution in $\mathcal{G}^{[i]\,(1)}$.
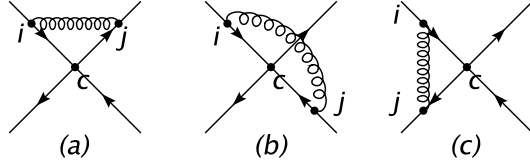
Figure 4.1: One-loop diagrams that contribute to $\Gamma^{(1)}_{S_{\mathrm{f}}}$

4.3 Eikonal amplitudes at one and two loops

We begin this section with a calculation of the soft anomalous dimension matrix for quark-antiquark elastic scattering at one and two loops, in terms of a specific color basis [62], and then discuss the representation of the matrix in the color generator notation of [77, 79]. We will see that the basic result of our calculation, the proportionality of the one- and two-loop matrices, applies to a much wider class of processes.

4.3.1 $2 \rightarrow 2$ eikonal diagrams at one loop

Here we will present the calculation for one loop corrections to W, Eq. (4.13), for quark-antiquark scattering, and by using Eq. (4.21) we will derive the corresponding one-loop soft anomalous dimension matrix. Representative one-loop diagrams are shown in Fig. 4.1. One can write the amplitude for any diagram D as

$$M_D = F_D \times C_{D,I} \,, \tag{4.35}$$

where F_D is the corresponding Feynman integral in dimensional regularization and $C_{D,I}$ is the color tensor. We will refer to F_D as the velocity factor below, because it absorbs all dependence on kinematic variables. To uniquely define

the normalizations of the velocity factors, and hence the color tensors, we define them to equal the corresponding integrals for the scattering of eikonal lines that couple to the exchanged gluons via color-independent "abelian" vertices. In particular, we absorb into the velocity factors the (-1) associated with a gluon coupled to an eikonal line in the anti-quark representation. Note that this separation of color and velocity factors is possible even if the eikonal lines are in the adjoint representation. This method will facilitate our eventual comparison to results expressed in the formalism of Ref. [79].

Consider the left-hand diagram in Fig. 4.1, which we will call a "t-channel diagram", referring to the pair of eikonal lines to which the gluon is connected. We will follow Refs. [99, 100], and express the velocity factor as an integral in configuration space. For an arbitrary one-gluon correction to a phase operator of the form of Eq. (4.13), such a correction is given by

$$F_t = (ig\mu^\varepsilon)^2 \int_{\mathcal{C}_i} dx_\mu \int_{\mathcal{C}_j} dy_\nu \, D^{\mu\nu}(x - y), \tag{4.36}$$

where integration is performed over the positions of gluons on the paths of the Wilson lines, $\mathcal{C}_i$ and $\mathcal{C}_j$. For the lines in Eq. (4.13) these paths are specified by

$$\mathcal{C}_i = v_i\,\beta, \qquad \mathcal{C}_j = v_j\,\alpha, \tag{4.37}$$

where α and β run from $-\infty$ to 0 (0 to ∞) for an incoming (outgoing) path. For the t-channel diagram shown in Fig. 4.1(a), for example, where $t = (p_1 - p_3)^2 = (p_2 - p_4)^2$, we may have $\{i, j\} = \{1, 3\}$ or $\{2, 4\}$.

In Feynman gauge the coordinate-space gluon propagator, in dimensional

regularization with $D = 4 - 2\varepsilon$, is given by [100]

$$
\begin{aligned}
D_{\mu\nu}(x) &= g_{\mu\nu} D(x) \\
&= g_{\mu\nu} \frac{\Gamma(1-\varepsilon)}{4\pi^{2-\varepsilon}} \frac{1}{(x^2 - i\epsilon)^{1-\varepsilon}} .
\end{aligned}
\tag{4.38}
$$

Using this expression in Eq. (4.36), we have

$$
\begin{aligned}
F_t &= (ig\mu^\epsilon)^2 \int_0^\infty d\alpha \int_{-\infty}^0 d\beta \, v_i^\mu D_{\mu\nu}(v_j\alpha - v_i\beta) v_j^\nu \\
&= (ig\mu^\varepsilon)^2 (v_i \cdot v_j) \frac{\Gamma(1-\varepsilon)}{4\pi^{2-\varepsilon}} \int_0^\infty d\alpha \int_0^\infty d\beta \frac{1}{[(v_j\alpha + v_i\beta)^2 - i\epsilon]^{1-\varepsilon}} .
\end{aligned}
\tag{4.39}
$$

As observed above, all such integrals vanish in dimensional regularization, since they are scaleless. The contribution of each such velocity-dependent integral is given by its counterterm, equal to its infrared pole and hence to the negative of its ultraviolet (UV) pole. Of course, F_t may be evaluated as a momentum-space integral with equivalent results.

In order to isolate the (single) UV pole in Eq. (4.39), we apply an infrared cut-off for the integral by introducing a small parameter λ with units of mass. This can be effected simply by inserting $\theta(1/\lambda - \alpha)$ in Eq. (4.39). The α and β integrals are then easily related to a single integral in terms of $z = \frac{\alpha}{(\alpha+\beta)}$ (see Eq. (C.3) in Appendix C). We find

$$
F_t = -\left(\frac{\alpha_s}{\pi}\right) \left(\frac{\pi\mu^2}{\lambda^2}\right)^\varepsilon \Gamma(1-\varepsilon) \frac{1}{2\varepsilon} \int_0^1 dz \frac{v_i \cdot v_j}{([v_j z + v_i(1-z)]^2)^{1-\varepsilon}} .
\tag{4.40}
$$

The single UV pole term in this expression is given by [99, 100]

$$
F_t^{s.p.}(v_i, v_j) = -\left(\frac{\alpha_s}{\pi}\right) \frac{1}{2\varepsilon} \gamma_{ij} \coth \gamma_{ij} ,
\tag{4.41}
$$

where

$$\cosh \gamma_{ij} \equiv \frac{v_i \cdot v_j}{\sqrt{v_i^2 v_j^2}} \,. \tag{4.42}$$

Because there is only a single, overall infrared divergence in F_t, any such cut-off will give the same ultraviolet pole.

In the high-energy limit $(\gamma_{ij} \gg 1)$, we have

$$F_t^{s.p.}(v_i, v_j) = - \left(\frac{\alpha_s}{\pi}\right) \frac{1}{2\varepsilon} \gamma_{ij} \,. \tag{4.43}$$

For $\{i, j\} = \{1, 3\}$ and $\{i, j\} = \{2, 4\}$ the answers are identical, in this $2 \to 2$ process. In the high-energy limit we define

$$\gamma_{13} = \gamma_{24} = T \,, \qquad \gamma_{14} = \gamma_{23} = U \,, \qquad \gamma_{12} = \gamma_{34} = S \,, \tag{4.44}$$

where

$$
\begin{aligned}
T &= \ln\left(\frac{2v_1 \cdot v_3}{v^2}\right) = \ln\left(\frac{2v_2 \cdot v_4}{v^2}\right) \,, \\
U &= \ln\left(\frac{2v_1 \cdot v_4}{v^2}\right) = \ln\left(\frac{2v_2 \cdot v_3}{v^2}\right) \,, \\
S &= \ln\left(\frac{-2v_1 \cdot v_2}{v^2}\right) = \ln\left(\frac{-2v_3 \cdot v_4}{v^2}\right) \,, \tag{4.45}
\end{aligned}
$$

with $v_i^2 \equiv v^2$ for all i. The velocity factors for u- and s-channel diagrams are found by taking into account the extra minus sign associated with coupling to an eikonal line in the antiquark representation, as well as that from crossing substitutions, which change the sign of $\coth \gamma_{ij}$ from unity to -1 in the high-energy limit,

$$
\begin{aligned}
F_u(v_i, v_j) &= -F_t(v_i, v_j) \,, \\
F_s(v_i, v_j) &= F_t(v_i, -v_j) \,. \tag{4.46}
\end{aligned}
$$
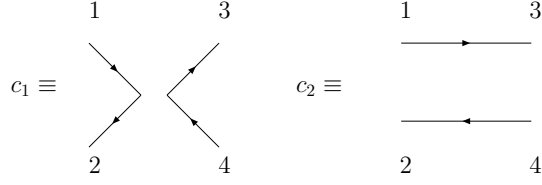
Figure 4.2: Color basis $\{c_1, c_2\}$ for four-quark process

Here, $\{i, j\} = \{1, 4\}$ and $\{2, 3\}$ for the u-channel diagrams, and $\{i, j\} = \{1, 2\}$ and $\{3, 4\}$ for the s-channel diagrams. The function F_s has the same overall sign as F_t because it differs both by an antiquark connection and by crossing, while F_u has the opposite sign.

In summary, the single poles for the velocity factors for the diagrams in Fig. 4.1 are given by

$$
\begin{aligned}
F_t^{s.p.} &= -\left(\frac{\alpha_s}{\pi}\right)\frac{1}{2\varepsilon}T\,, \\
F_u^{s.p.} &= \left(\frac{\alpha_s}{\pi}\right)\frac{1}{2\varepsilon}U\,, \\
F_s^{s.p.} &= -\left(\frac{\alpha_s}{\pi}\right)\frac{1}{2\varepsilon}S\,.
\end{aligned}
\tag{4.47}
$$

To construct the counterterms, of course, we must also compute the corresponding color tensors for each diagram.

We will use $C_i^{[a]}$ to denote the color tensor for the t-channel diagram in Fig. 4.1, with color tensor c_i, $i = 1, 2$ at short distances. For the latter we choose the basis tensors shown in Fig. 4.2. The coefficients of the color tensors absorb all overall factors not included in the velocity factors of Eq. (4.47).

One can calculate these color tensors from the basic identity for the gen-

erators of SU(N_c),

$$\sum_a (T^a)_{r_2 r_1} (T^a)_{r_3 r_4} = \frac{1}{2} \delta_{r_2 r_4} \delta_{r_3 r_1} - \frac{1}{2N_c} \delta_{r_2 r_1} \delta_{r_3 r_4} \,. \tag{4.48}$$

In the color basis given in Fig. 4.2, the color tensors of the t-channel diagrams are given by

$$
\begin{aligned}
C_1^{[t]} &= -\frac{1}{2N_c} c_1 + \frac{1}{2} c_2 \,, \\
C_2^{[t]} &= \frac{N_c^2 - 1}{2N_c} c_2 = C_F \, c_2 \,.
\end{aligned}
\tag{4.49}
$$

We will employ a similar notation below for other one-loop and for two-loop diagrams. Color tensors for the u and s channel diagrams are computed in a similar way with the results

$$
\begin{aligned}
C_1^{[u]} &= -\frac{1}{2N_c} c_1 + \frac{1}{2} c_2 \,, \\
C_2^{[u]} &= \frac{1}{2} c_1 - \frac{1}{2N_c} c_2 \,,
\end{aligned}
\tag{4.50}
$$

and

$$
\begin{aligned}
C_1^{[s]} &= C_F \, c_1 \,, \\
C_2^{[s]} &= \frac{1}{2} c_1 - \frac{1}{2N_c} c_2 \,.
\end{aligned}
\tag{4.51}
$$

We summarize these relations in matrix form by

$$C_I^{[a]} = \sum_{J=1,2} c_J \, d_{JI}^{[a]} \,, \tag{4.52}$$

where the matrix element $d_{JI}^{[a]}$ specifies the mixing from color tensor c_I to tensor c_J by the exchange of a gluon in channel $a = t, u, s$. An important identity that we will use below is

$$d_{JI}^{[t]} + d_{JI}^{[s]} - d_{JI}^{[u]} = C_F \, \delta_{JI} \,, \tag{4.53}$$

which we easily verify from the relations above. Note that this equality holds in an arbitrary representation. [1]

The contribution of each diagram to the matrix counterterm $Z_{W_f}^{(1)}$ is now found by the product of the corresponding color factor times the pole part of the velocity factors,

$$\left(Z_{W_f}^{(1)}\right)_{JI} = 2 \sum_{a=s,t,u} d_{JI}^{[a]} \frac{F_a^{s.p.}}{\alpha_s/\pi},$$

(4.54)

in terms of the single-pole terms of Eq. (4.47) and the color factors read off from Eqs. (4.49)–(4.51). Given the counterterm matrix, we can evaluate $\mathbf{\Gamma}_{W_f}^{(1)}$ by using Eq. (4.21) with the result

$$\mathbf{\Gamma}_{W_f}^{(1)} = \begin{pmatrix} \frac{1}{N_c}(U-T) + 2\,C_F\,S & (S-U) \\ & \\ & \\ (T-U) & \frac{1}{N_c}(U-S) + 2\,C_F\,T \end{pmatrix}.$$

(4.55)

Exactly the same calculation gives $\Gamma_2^{[i]}$, the anomalous dimension for the eikonal jet function, defined as the square root of the eikonal singlet form factor, Eq. (4.15). In Eq. (4.43), we simply let $\cosh \gamma_{ij} \to u_0/v^2 = \mu^2/(Q^2 v^2)$ (using Eq. (4.17)), in the limit $v^2 \to 0$. The one-loop result for parton i is then given by

$$\Gamma_2^{[i]\,(1)}\left(\frac{u_0}{v^2}\right) = \frac{1}{2}\,C_i\,\ln\left(\frac{\mu^2}{Q^2 v^2}\right),$$

(4.56)

---

[1]Equation (4.53) is equivalent in this case to the well-known identity $\sum_i \mathbf{T}_i = 0$ in the color generator notation that we will review below.

with $C_i = C_F$ for quarks and C_A for gluons. By using this expression and the definition for Γ_{S_f}, Eq. (4.23), we find

$$
\mathbf{\Gamma}_{S_f}^{(1)} = \begin{pmatrix} \frac{1}{N_c}\left(\mathcal{U} - \mathcal{T}\right) + 2\,C_F\,\mathcal{S} & \left(\mathcal{S} - \mathcal{U}\right) \\ & \\ & \\ \left(\mathcal{T} - \mathcal{U}\right) & \frac{1}{N_c}\left(\mathcal{U} - \mathcal{S}\right) + 2\,C_F\,\mathcal{T} \end{pmatrix}, \tag{4.57}
$$

where

$$
\mathcal{T} \equiv \ln\left(\frac{-t}{\mu^2}\right), \qquad \mathcal{U} \equiv \ln\left(\frac{-u}{\mu^2}\right), \qquad \mathcal{S} \equiv \ln\left(\frac{-s}{\mu^2}\right). \tag{4.58}
$$

After performing the subtraction of the jet functions, we set $v_i \to \beta_i$, and then use Eqs. (4.3) and (4.17) to recast the result in terms of the usual Mandelstam variables, t, u and s. We notice that, as anticipated, all collinear logarithms, and hence sensitivity to our choice of collinear regulation, are absent in the soft anomalous dimension matrix, $\mathbf{\Gamma}_{S_f}^{(1)}$.

4.3.2 $\quad 2 \to 2$ eikonal diagrams at two loops

Figure 4.3 shows the classes of topologically inequivalent diagrams that contribute to $\Gamma_{S_f}^{(2)}$, when combined with their one-loop counterterm diagrams. One obtains the full set from all different combinations of external legs with these topologies. It is easy to see that the number of graphs for each inequivalent set is $N_a = 6$, $N_b = 6$, $N_c = 6$, $N_d = 12$, $N_e = 12$, $N_f = 12$, $N_g = 4$, $N_h = 24$ and $N_i = 3$, which in total gives 85 two-loop diagrams. As in the
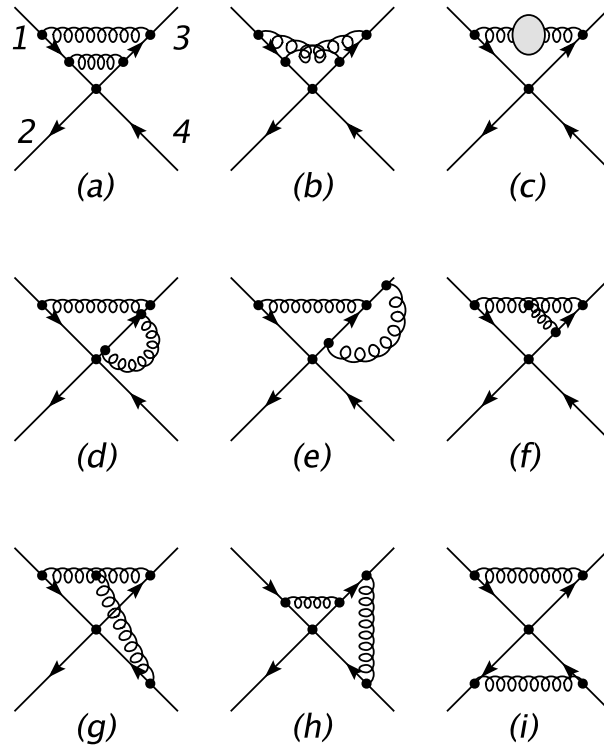
Figure 4.3: Two-loop diagrams that contribute to $\Gamma^{(2)}_{W_{\mathrm{f}}}$

one-loop case, we find anomalous dimensions from the combinations of velocity factors and color tensors.

Consider first diagram (i), which is the only two-loop topology involving all four eikonal lines. Diagram (i) does not have a surviving single UV pole when we add its one-loop counterterms.

Regarding the remaining cases, we consider first those diagrams involving two eikonal lines only, which we refer to as "2E" diagrams. Next, we will show that diagram (g) vanishes, which we consider a very important result. Finally, we will calculate all the contributions from the surviving "3E" diagram type (h). In this case, we will find that the diagrams, although non-vanishing,

reduce to the product of one-loop diagrams, and thus do not contribute to the two-loop anomalous dimensions.

The 2E diagrams and $\Gamma_i^{(2)}$

In the 2E diagrams, (a), (b), (c), (d), (e) and (f), the gluons connect to only two of the four eikonal lines in W. These same diagrams also contribute to the two-loop cusp anomalous dimension, $\Gamma_2^{[i]\,(2)}$, and their single UV poles are well known [100]. We review their velocity factors here, because they are needed for the two-loop anomalous dimension matrix. Additional details are given in Appendix D.

The color factors of the 2E diagrams are proportional to the color-mixing matrix elements for single t-channel gluon exchange, $d_{JI}^{[t]}$, defined in Eq. (4.52). This is manifestly the case for the individual diagrams (c), (d), (e) and (f). For the sum of diagrams (a) and (b), it relies on the result [99, 100] that the single-pole terms in the velocity factors of these two diagrams are the negatives of each other. The net color factor for the (a) and (b) single poles is then proportional to the commutator of two generators, which allows it to be expressed in terms of the one-loop color factor, as $C_A\, d_{JI}^{[t]}$. We can thus present the contributions of all the 2E diagrams in terms of the $d_{JI}^{[a]}$, with $a = s, t, u$.

In terms of the factors $d_{JI}^{[t]}$, the two-loop counterterms[2] for the diagrams

---

[2]These results, of course, require that we combine these diagrams with the corresponding one-loop counterterms for their divergent subdiagrams. Notice that diagram (b) in Fig. 4.3 does not have a one-loop counterterm since it does not have a divergent subdiagram.

(a), (b), (c) and (f) in the high-energy limit are, analogously to the one-loop velocity factors, Eq. (4.47),

$$\left(Z_{W_{\mathrm{f}}}^{(a+b)}\right)_{JI} = -\left(\frac{\alpha_s}{\pi}\right)^2 d_{JI}^{[t]} \frac{C_A}{2} \frac{1}{2\varepsilon} \left[\frac{T^3}{6} + \frac{\zeta(2)}{2} T - \frac{\zeta(3)}{2}\right],$$

$$\left(Z_{W_{\mathrm{f}}}^{(c)}\right)_{JI} = -\left(\frac{\alpha_s}{\pi}\right)^2 d_{JI}^{[t]} \frac{1}{2} \frac{1}{2\varepsilon} \left(\frac{31}{36}C_A - \frac{5}{9}T_F n_F\right) T, \qquad (4.59)$$

and

$$\left(Z_{W_{\mathrm{f}}}^{(f)}\right)_{JI} = -\left(\frac{\alpha_s}{\pi}\right)^2 d_{JI}^{[t]} \frac{C_A}{2} \frac{1}{4\varepsilon} \left\{ \left[-\frac{T^3}{6} + (1 - \zeta(2))\, T\right] \right.$$
$$\left. + \left[\frac{T^2}{2} - T + \zeta(2)\right] \right\}, \qquad (4.60)$$

with T the logarithm of $2v_1 \cdot v_3/v^2$, as in Eq. (4.45). In Eq. (4.60), the second term in square brackets gives the result of those numerator terms that are proportional to v_3^2 before the integration. (See Appendix D.) The entire T-dependence of these terms cancels against the contributions from diagrams (d) and (e), which are also proportional to v_3^2 before integration and are given individually by

$$\left(Z_{W_{\mathrm{f}}}^{(d)}\right)_{JI} = -\left(\frac{\alpha_s}{\pi}\right)^2 d_{JI}^{[t]} C_F \frac{1}{4\varepsilon} \left[-\frac{T^2}{2} + T - \frac{\zeta(2)}{2}\right],$$

$$\left(Z_{W_{\mathrm{f}}}^{(e)}\right)_{JI} = \left(\frac{\alpha_s}{\pi}\right)^2 d_{JI}^{[t]} \left(C_F - \frac{C_A}{2}\right) \frac{1}{4\varepsilon} \left[-\frac{T^2}{2} + T - \frac{\zeta(2)}{2}\right]. \quad (4.61)$$

The combined t-channel contribution from the six diagrams (a), (b), (c), (d), (e) and (f) to the soft anomalous dimension matrix is found by adding

Eqs. (4.59)–(4.61)[3],

$$
\begin{aligned}
\left(Z_{W_{\mathrm{f}}}^{[t]} \right)_{JI} &\equiv 2 \left(Z_{W_{\mathrm{f}}}^{(a+b)} + Z_{W_{\mathrm{f}}}^{(c)} + 2 \left[Z_{W_{\mathrm{f}}}^{(d)} + Z_{W_{\mathrm{f}}}^{(e)} + Z_{W_{\mathrm{f}}}^{(f)} \right] \right)_{JI} \\
&= -\frac{1}{2\varepsilon} \left(\frac{\alpha_s}{\pi} \right)^2 d_{JI}^{[t]} \left\{ \left[C_A \left(\frac{67}{36} - \frac{\zeta(2)}{2} \right) - \frac{5}{9} T_F n_F \right] \ln \left(\frac{2 v_1 \cdot v_3}{v^2} \right) \right. \\
&\qquad \left. + \frac{C_A}{2} \left(\zeta(2) - \zeta(3) \right) \right\} \\
&= \left(\frac{\alpha_s}{\pi} \right)^2 d_{JI}^{[t]} \left\{ \frac{K}{2} \frac{F_t^{s.p.}}{(\alpha_s/\pi)} - \frac{C_A}{4\varepsilon} \left(\zeta(2) - \zeta(3) \right) \right\} , \qquad (4.62)
\end{aligned}
$$

where the second line recalls a standard notation [101] for the quantity K,

$$
K \equiv C_A \left(\frac{67}{18} - \zeta(2) \right) - \frac{10}{9} T_F n_F . \qquad (4.63)
$$

The result (4.62) includes a factor of two for the other t-channel exchange, between lines 2 and 4.

Analogous considerations, of course, apply to diagrams with pairs of s- and u-channel 2E diagrams. Together with the t-channel diagrams, they contribute to the two-loop anomalous dimension matrix for W according to Eq. (4.22),

$$
\begin{aligned}
\mathbf{\Gamma}_{W_{\mathrm{f}}}^{(2E)(2)} &= \frac{K}{2} \sum_{i=s,t,u} d_{JI}^{[i]} \left(\frac{-2\varepsilon F_i^{s.p.}}{(\alpha_s/\pi)} \right) + \delta_{JI} C_A C_i \left(\zeta(2) - \zeta(3) \right) \\
&= \frac{K}{2} \mathbf{\Gamma}_{W_{\mathrm{f}}}^{(1)} + \delta_{JI} C_A C_i \left(\zeta(2) - \zeta(3) \right) , \qquad (4.64)
\end{aligned}
$$

where we have used the identity (4.53), and where $\mathbf{\Gamma}_{W_{\mathrm{f}}}^{(1)}$ is the same one-loop anomalous dimension given in Eq. (4.55).

---

[3]Note that one needs to multiply Eqs. (4.60) and (4.61) by 2 because for these diagrams there are two ways of attaching the gluons to the eikonal lines.

In a precisely similar manner we find for the two-loop form factor (cusp) anomalous dimension for partonic representation i,

$$\Gamma_2^{[i]\,(2)}\left(\frac{u_0}{v^2}\right) = \frac{C_i}{4}\left[K\ln\left(\frac{\mu^2}{Q^2 v^2}\right) + C_A\left(\zeta(2) - \zeta(3)\right)\right].\qquad(4.65)$$

As at one loop, we combine Eqs. (4.64) and (4.65) in Eq. (4.23), in order to find the contribution of the 2E diagrams to the two-loop soft anomalous dimensions for scattering.

It is now clear that the two-loop soft anomalous dimension matrix inherits from the 2E diagrams a factor of K times the one-loop anomalous dimension matrix. The result is,

$$\boldsymbol{\Gamma}_{S_{\mathrm{f}}}^{(2E)\,(2)} = \frac{K}{2}\,\boldsymbol{\Gamma}_{S_{\mathrm{f}}}^{(1)},\qquad(4.66)$$

with $\boldsymbol{\Gamma}_{S_{\mathrm{f}}}^{(1)}$ the same one-loop anomalous dimension given in Eq. (4.57). All velocity-independent terms in the $Z_{W_{\mathrm{f}}}^{(2E)}$ that are not in $\boldsymbol{\Gamma}_{S_{\mathrm{f}}}^{(1)}$ cancel in Eq. (4.23) against the corresponding finite terms from the eikonal form factors in the two-loop soft anomalous dimension, along with all collinear-singular dependence. This is important, because the constant terms depend in general on the eikonal approximation and our choice of collinear regularization. At the same time, we have now used all the collinear-singular dependence in the Sudakov anomalous dimensions, Eq. (4.65), to cancel the $\ln v^2$-dependence of the 2E diagrams of W. The 3E diagrams, represented by (g) and (h) in Fig. 4.3, have no remaining subtractions. The combination of these classes of diagrams must therefore be free of collinear singularities at the two-loop level.

Vanishing of three-gluon diagram with three eikonal lines

Now let's show that diagram (g) in Fig. 4.3 vanishes. Up to overall factors which play no role, the velocity Feynman integral for a generic three-gluon diagram can be written as

$$
\begin{aligned}
F(v_A, v_B, v_C) &= \int d^D k_1 d^D k_2 \, \frac{1}{v_B \cdot k_1 + i\epsilon} \frac{1}{v_A \cdot k_2 + i\epsilon} \frac{1}{v_C \cdot (k_1 + k_2) + i\epsilon} \\
&\times \frac{1}{k_1^2 + i\epsilon} \frac{1}{k_2^2 + i\epsilon} \frac{1}{(k_1 + k_2)^2 + i\epsilon} \times \Big[v_A \cdot v_B \, v_C \cdot (k_1 - k_2) \\
&+ v_A \cdot v_C \, v_B \cdot (k_1 + 2k_2) + v_B \cdot v_C \, v_A \cdot (-2k_1 - k_2) \Big],
\end{aligned}
$$

$$(4.67)$$

where the term in square brackets is the three-gluon vertex momentum factor. Here v_A, v_B and v_C are three different eikonal velocities. We take lightlike $v_A^2 = v_B^2 = 0$. We can then expand any momentum p^μ as

$$
p^\mu = \frac{v_A^\mu}{v_A \cdot v_B} v_B \cdot p + \frac{v_B^\mu}{v_A \cdot v_B} v_A \cdot p + p_T^\mu,
$$

$$(4.68)$$

with p_T^μ the transverse components, satisfying $v_A \cdot p_T = v_B \cdot p_T = 0$.

For use in the integral we introduce the variables:

$$
\xi_i = \frac{v_A \cdot v_C}{v_A \cdot v_B} v_B \cdot k_i, \qquad\qquad \eta_i = \frac{v_B \cdot v_C}{v_A \cdot v_B} v_A \cdot k_i.
$$

$$(4.69)$$

We introduce these variables into the integral by using v_A and v_B to define light-cone coordinates,

$$
\begin{aligned}
dk_i^+ dk_i^- &= \frac{1}{v_A \cdot v_B} d(v_B \cdot k_i) \, d(v_A \cdot k_i) \\
&= \frac{v_A \cdot v_B}{(v_A \cdot v_C)(v_B \cdot v_C)} d\xi_i d\eta_i,
\end{aligned}
$$

$$(4.70)$$

so that

$$k_i^2 = 2\frac{(v_A \cdot k_i)(v_B \cdot k_i)}{v_A \cdot v_B} - k_{i,T}^2 = 2\frac{v_A \cdot v_B}{(v_A \cdot v_C)(v_B \cdot v_C)}\xi_i\eta_i - k_{i,T}^2. \quad (4.71)$$

When we change variables in F to the ξ's and η's, we find

$$
\begin{aligned}
F(v_A, v_B, v_C) &= \frac{v_A \cdot v_B}{(v_A \cdot v_C)(v_B \cdot v_C)}\int\prod_{i=1}^{2} d\xi_i \, d\eta_i \, d^{D-2}k_{i,T} \\
&\times \frac{1}{2\frac{v_A\cdot v_B}{(v_A\cdot v_C)(v_B\cdot v_C)}\xi_i\eta_i - k_{i,T}^2 + i\epsilon} \\
&\times \frac{1}{2\frac{v_A\cdot v_B}{(v_A\cdot v_C)(v_B\cdot v_C)}(\xi_1 + \xi_2)(\eta_1 + \eta_2) - (k_{1,T} + k_{2,T})^2 + i\epsilon} \\
&\times \frac{1}{\xi_1 + i\epsilon}\frac{1}{\eta_2 + i\epsilon}\frac{1}{\xi_1 + \xi_2 + \eta_1 + \eta_2 - v_{C,T}\cdot(k_1 + k_2)_T + i\epsilon} \\
&\times \Big[\xi_1 - \xi_2 + \eta_1 - \eta_2 - v_{C,T}\cdot(k_1 - k_2)_T + \xi_1 + 2\xi_2 - 2\eta_1 - \eta_2\Big] \\
&= 0.
\end{aligned}
\qquad (4.72)
$$

The integral vanishes because the numerator is antisymmetric under $\xi_1 \leftrightarrow \eta_2$, $\xi_2 \leftrightarrow \eta_1$ and $k_{1,T} \leftrightarrow k_{2,T}$, while the product of the denominators is symmetric. Notice that group factors play no part in this argument. This result is therefore very general and applies to any $2 \to n$ process with lightlike velocities.

Exponentiation of the remaining 3E diagrams

The only remaining class of diagrams is illustrated by diagram (h) in Fig. 4.3. Along with its companions found by permuting the eikonal lines, we can refer to these as "3E" diagrams, since they are the only nonvanishing diagrams with gluons connected to three eikonal lines. There are 24 such 3E diagrams, 8 of them with s and t channel gluon exchanges, 8 of them with s
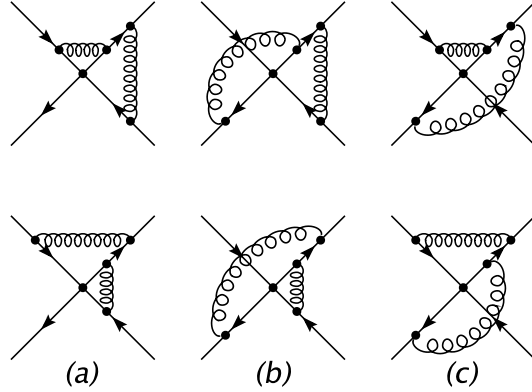
Figure 4.4: a-c) Pairs of 3E diagrams.

and u channel gluons, and finally 8 of them with t and u channel gluons. They come in pairs as shown in Fig. 4.4.

We now show that the analysis of the previous subsection regarding the three-gluon diagrams leads to a very interesting result for the remaining 3E diagrams as well. In this case, the diagrams do not vanish, but reduce to products of one-loop diagrams[4]. They therefore provide no contribution to the two-loop anomalous dimension matrix.

Each such 3E diagram contains one eikonal line with two gluons attached to it, which we label as v_C. The two lines having one gluon attached are labelled v_A and v_B. We will consider a pair of 3E diagrams that are related simply by exchanging the order in which the two gluons attach to v_C, as in Fig. 4.4(a) for example. The two diagrams have differing color and momentum

---

[4]The reduction of a different class of multi-loop eikonal diagrams, namely the 2E diagrams of ladder type, to powers of one-loop diagrams, was previously observed in Ref. [102] to hold to all loop orders.

structures, but we can rewrite their sum as the sum of one term with symmetric color and momentum integrals, plus a second term with antisymmetric color and momentum integrals. In the spirit of the discussion above, we suppress the color matrices held in common and write

$$\mathcal{F}_{ab}(v_A, v_B, v_C) \equiv \mathcal{F}_{ab}^{(\mathrm{sym})}(v_A, v_B, v_C) + \mathcal{F}_{ab}^{(\mathrm{antisym})}(v_A, v_B, v_C), \qquad (4.73)$$

where the subscripts a and b refer to the color generators on the v_C-eikonal, contracted with generators on the v_A or v_B line, respectively. Consider first the antisymmetric term, which is given by

$$\begin{aligned}
\mathcal{F}_{ab}^{(\mathrm{antisym})}(v_A, v_B, v_C) &= \frac{1}{2}\,(T_b\,T_a - T_a\,T_b) \\
&\times \int d^D k_1 d^D k_2\, \frac{1}{v_B \cdot k_1 + i\epsilon}\,\frac{1}{v_A \cdot k_2 + i\epsilon}\,\frac{1}{k_1^2 + i\epsilon}\,\frac{1}{k_2^2 + i\epsilon} \\
&\times \frac{1}{v_C \cdot (k_1 + k_2) + i\epsilon}\left[\frac{1}{v_C \cdot k_1 + i\epsilon} - \frac{1}{v_C \cdot k_2 + i\epsilon}\right].
\end{aligned}$$
$$(4.74)$$

(In the color-generator notation described in section 4.3.4 below, the color operator associated with this antisymmetric term takes the form $[\mathbf{T}_B{\cdot}\mathbf{T}_C\,,\,\mathbf{T}_C{\cdot}\mathbf{T}_A]$.) The same change of variables, Eq. (4.69), leads to an expression that is again manifestly antisymmetric under the relabelling $\xi_{1,2} \leftrightarrow \eta_{2,1}$, $k_{1,T} \leftrightarrow k_{2,T}$,

$$\begin{aligned}
\mathcal{F}_{ab}^{(\mathrm{antisym})}(v_A, v_B, v_C) &= \frac{1}{2}\,(T_b\,T_a - T_a\,T_b) \\
&\times \frac{1}{(v_A \cdot v_C)(v_B \cdot v_C)} \int \prod_{i=1}^{2} d\xi_i\, d\eta_i\, d^{D-2}k_{i,T}\ \frac{1}{2\frac{v_A \cdot v_B}{(v_A \cdot v_C)(v_B \cdot v_C)}\xi_i \eta_i - k_{i,T}^2 + i\epsilon} \\
&\times \frac{1}{\xi_1 + i\epsilon}\,\frac{1}{\eta_2 + i\epsilon}\,\frac{1}{\xi_1 + \eta_1 - v_{C,T} \cdot k_{1,T} + i\epsilon}\,\frac{1}{\xi_2 + \eta_2 - v_{C,T} \cdot k_{2,T} + i\epsilon} \\
&\times \frac{\xi_2 - \xi_1 + \eta_2 - \eta_1 - v_{C,T} \cdot (k_2 - k_1)_T}{\xi_1 + \xi_2 + \eta_1 + \eta_2 - v_{C,T} \cdot (k_1 + k_2)_T + i\epsilon} \\
&= 0.
\end{aligned}$$
$$(4.75)$$

The entire color-antisymmetric part of the infrared region thus vanishes whenever the eikonal approximation is valid, and the cancellation is exact for the eikonal amplitudes we consider here.

Turning to the symmetric term, we need only use the eikonal identity $1/[x(x+y)] + 1/[y(x+y)] = 1/(xy)$ to rewrite it as the product of the two lowest-order single-gluon exchange diagrams,

$$
\begin{aligned}
\mathcal{F}_{ab}^{(\mathrm{sym})}(v_A, v_B, v_C) \;=\; & \frac{1}{2}\, (T_b\, T_a + T_a\, T_b) \\
& \times \int d^D k_1 \frac{1}{v_B \cdot k_1 + i\epsilon}\, \frac{1}{v_C \cdot k_1 + i\epsilon}\, \frac{1}{k_1^2 + i\epsilon} \\
& \times \int d^D k_2 \frac{1}{v_A \cdot k_2 + i\epsilon}\, \frac{1}{v_C \cdot k_2 + i\epsilon}\, \frac{1}{k_2^2 + i\epsilon}\,. \quad (4.76)
\end{aligned}
$$

(In the color-generator notation described in section 4.3.4, the color operator associated with this symmetric term takes the form $\{\mathbf{T}_B\!\cdot\!\mathbf{T}_C\,,\ \mathbf{T}_C\!\cdot\!\mathbf{T}_A\}$.) These diagrams have the correct color and kinematic structure to represent the two-loop terms in the exponentiation of the color matrix of one-loop infrared poles. They are precisely cancelled in the two-loop soft function by the corresponding products of one-loop counterterms.

We conclude that *the entire two-loop anomalous dimension is due to the 2E diagrams and is given by Eq. (4.66)*, in which we may remove the superscript $(2E)$, to obtain

$$
\mathbf{\Gamma}_{S_{\mathrm{f}}}^{(2)} = \frac{K}{2}\, \mathbf{\Gamma}_{S_{\mathrm{f}}}^{(1)}\,. \tag{4.77}
$$

We have thus determined that the two-loop anomalous dimension color-mixing matrix is related to the one-loop matrix by the same factor that relates the

one- and two-loop Sudakov anomalous dimensions, $A(\alpha_s)$. Evidently, the next-to-next-to-leading poles in amplitudes with color exchange are generated by the same exponentiation of "webs" as for the elastic form factor [103, 104, 105, 106, 107]. Additionally, we note that in the "bremsstrahlung" or CMW scheme [108], this contribution, along with the corresponding term in the cusp anomalous dimension, is absorbed into a redefinition of the strong coupling, which effectively boosts the strength of parton showering.

4.3.3 Expansion of the soft function

To relate the soft anomalous dimension to fixed-order calculations, we expand the resummed soft function, given as a path-ordered exponential in Eq. (4.25), to order $\mathcal{O}(\alpha_f^{\in})$. The result is

$$
\begin{aligned}
\mathbf{S}_{\mathrm{f}}\left(\frac{Q^2}{\mu^2}=1,\alpha_s(Q^2),\epsilon\right) &= 1+\frac{1}{2\varepsilon}\left(\frac{\alpha_s}{\pi}\right)\mathbf{\Gamma}_{S_{\mathrm{f}}}^{(1)}+\frac{1}{8\varepsilon^2}\left(\frac{\alpha_s}{\pi}\right)^2\left(\mathbf{\Gamma}_{S_{\mathrm{f}}}^{(1)}\right)^2 \\
&\quad -\frac{\beta_0}{16\varepsilon^2}\left(\frac{\alpha_s}{\pi}\right)^2\mathbf{\Gamma}_{S_{\mathrm{f}}}^{(1)}+\frac{1}{4\varepsilon}\left(\frac{\alpha_s}{\pi}\right)^2\mathbf{\Gamma}_{S_{\mathrm{f}}}^{(2)} \\
&= 1+\frac{1}{2\varepsilon}\left(\frac{\alpha_s}{\pi}\right)\mathbf{\Gamma}_{S_{\mathrm{f}}}^{(1)}+\frac{1}{8\varepsilon^2}\left(\frac{\alpha_s}{\pi}\right)^2\left(\mathbf{\Gamma}_{S_{\mathrm{f}}}^{(1)}\right)^2 \\
&\quad -\frac{\beta_0}{16\varepsilon^2}\left(\frac{\alpha_s}{\pi}\right)^2\mathbf{\Gamma}_{S_{\mathrm{f}}}^{(1)}+\frac{1}{8\varepsilon}\left(\frac{\alpha_s}{\pi}\right)^2 K\,\mathbf{\Gamma}_{S_{\mathrm{f}}}^{(1)},
\end{aligned}
\tag{4.78}
$$

where in the second equality we have used Eq. (4.77) for the two-loop anomalous dimension matrix. Combining this result with the second-order minimal jet function, Eq. (4.32), in the formula for the factorized amplitude, Eq. (4.29), we will derive a result to compare directly with the pole structure of explicit two-loop calculations.

4.3.4 Iterative color-matrix form

Given the one- and two-loop anomalous dimension soft matrices (4.57) and (4.77), and the expansion of the quark jet function, as in Eq. (4.32), we can use the factorized amplitude, Eq. (4.29), to calculate all infrared and collinear poles at order α_s^2 for quark-antiquark scattering. The result will be a set of coefficients of the specific basis tensors in color space that we have chosen, Fig. 4.2. In this basis, we can perform threshold resummation for jet and other cross sections.

To compare to explicit calculations at the two-loop level, however, and to generalize to higher numbers of external partons, it is convenient to make contact with a somewhat different notation, in which the color interactions of soft gluons is represented by a color matrix $\mathbf{T}_i^a$ for the insertion of a gluon on external line i, with $\mathbf{T}_i^a$ a generator in the color representation of that parton i, whose color-matrix (rather than generator) indices are summed against those of the lower-order amplitude that is "dressed" by this soft gluon. In the notation of Eq. (4.2) above for the color content of an amplitude, the action of the generators may be made explicit as the action of a vector, with indices in the adjoint representation; for example for $i = 1$,

$$\left[\mathbf{T}_1^a \,|\mathcal{M}_{\mathrm{f}}\rangle\right]_{d_1, r_2\ldots} \equiv \mathcal{M}_L^{[\mathrm{f}]}\left(\beta_j, \frac{Q^2}{\mu^2}, \alpha_s(\mu^2), \varepsilon\right) \, \delta_i \, (T^a)_{d_1 r_1} \, (c_L)_{\{r_1, r_2\ldots\}} \, , \quad (4.79)$$

where $\delta_i = \pm 1$ absorbs minus signs associated with antiparticles and crossing. In the convention of Ref. [79], $\delta_i = 1$ when i is an eikonal line representing an outgoing quark or gluon, or incoming antiquark; $\delta_i = -1$ for an incoming quark or gluon, or outgoing antiquark. Defined in this way, the vector color generator

matrices obey the fundamental relation $\sum_i \mathbf{T}_i = 0$, which is an expression of gauge invariance. The $\mathbf{T}_i$s are conventionally normalized to $\mathbf{T}_i \cdot \mathbf{T}_i = C_i$, with $i = q, g$.

A gluon exchanged between two parton lines i and j produces the product $\mathbf{T}_i \cdot \mathbf{T}_j$, which acts on an amplitude in a fashion precisely similar to Eq. (4.79). This notation allows for a convenient iterative expression for color exchange due to soft gluon exchange, without requiring an explicit choice for the color basis.

The color-space notation above may be applied to the computation of the soft function as well as to the amplitude itself. Consider the soft function at a single loop, determined by the one-loop soft anomalous dimension. As we have seen, the latter is built up from the contributions of soft gluon exchanges between pairs of eikonal lines. From each exchange, the contribution to the anomalous dimension is found from Eq. (4.21), where the one-loop single-pole term in Z_{S_f} equals the one-loop UV pole term computed from the corresponding diagram.

Each diagrammatic contribution, then, is proportional to a product $\mathbf{T}_i \cdot \mathbf{T}_j$ acting on the lower-order amplitude, multiplied by the result of the eikonal integral. Referring to Fig. 4.1, the relevant single-pole coefficients are given in Eq. (4.47). The action of $\mathbf{\Gamma}_{S_\mathrm{f}}^{(1)}$ on the color tensor is the sum of all such terms, with a subtraction for the jet anomalous dimensions; this subtraction is proportional to the identity matrix in color space, as in Eq. (4.23). This

gives

$$
\begin{aligned}
\mathbf{\Gamma}_{S_{\mathrm{f}}}^{(1)}\left(\frac{s_{ij}}{\mu^2}\right)|\mathcal{M}_{\mathrm{f}}\rangle &= \left[\frac{1}{2}\sum_{i\in\mathrm{f}}\sum_{j\neq i\in\mathrm{f}}(\delta_i\mathbf{T}_i\cdot\delta_j\mathbf{T}_j)\left(\frac{-2\varepsilon\, F_{s_{ij}}^{s.p.}}{(\alpha_s/\pi)}\right)\right. \\
&\qquad\left. -\sum_{i\in\mathrm{f}}\Gamma_2^{[i]\,(1)}\left(\frac{u_0}{v^2}\right)\right]|\mathcal{M}_{\mathrm{f}}\rangle \\
&= \left[-\frac{1}{2}\sum_{i\in\mathrm{f}}\sum_{j\neq i}\mathbf{T}_i\cdot\mathbf{T}_j\,\ln\left(\frac{-s_{ij}}{Q^2 v^2}\right)\right. \\
&\qquad\left. -\frac{1}{2}\sum_{i\in\mathrm{f}}C_i\,\ln\left(\frac{\mu^2}{Q^2 v^2}\right)\right]|\mathcal{M}_{\mathrm{f}}\rangle \\
&= \frac{1}{2}\sum_{i\in\mathrm{f}}\sum_{j\neq i}\mathbf{T}_i\cdot\mathbf{T}_j\,\ln\left(\frac{\mu^2}{-s_{ij}}\right)|\mathcal{M}_{\mathrm{f}}\rangle, \qquad (4.80)
\end{aligned}
$$

where $s_{ij} = (p_i + p_j)^2$, with all momenta defined to flow into (or out of) the amplitude. For the four-parton case above, $s_{12} = s$, $s_{13} = t$, and so forth. The overall $1/2$ compensates for double counting in the sum. To derive the final result, we have used the explicit forms of the δ_is described above, as well as the identities $\sum_i\mathbf{T}_i = 0$ and $\mathbf{T}_i\cdot\mathbf{T}_i = C_i$ (in the quark-scattering case, all $C_i = C_F$). In this notation the color identities enforce the cancellation of the collinear-sensitive $\ln(1/v^2)$ terms.

Identical considerations apply to the two-loop case. The nonvanishing anomalous dimension matrix is again a sum of diagrammatic contributions, corresponding to gluon exchange processes involving two eikonal lines only. As we have seen, these contributions have the same color-generator structure, $\mathbf{T}_i\cdot\mathbf{T}_j$, found at one loop. The 3E diagrams have a more complicated color structure, but they do not contribute to the two-loop soft anomalous dimension matrix.

To be more specific, we saw that diagram (h) in Fig. 4.3 can be organized into antisymmetric and symmetric color structures, which can be represented as commutators and anti-commutators of one-loop color structures, of the form $[\mathbf{T}_i \cdot \mathbf{T}_j, \, \mathbf{T}_j \cdot \mathbf{T}_k]$ and $\{\mathbf{T}_i \cdot \mathbf{T}_j, \, \mathbf{T}_j \cdot \mathbf{T}_k\}$. Note that the antisymmetric quantity can be written as,

$$[\mathbf{T}_i \cdot \mathbf{T}_j, \mathbf{T}_j \cdot \mathbf{T}_k] = \mathbf{T}_i^a \, [\mathbf{T}_j^a, \mathbf{T}_j^b] \, \mathbf{T}_k^b = -i \, f^{abc} \, \mathbf{T}_i^a \, \mathbf{T}_j^b \mathbf{T}_k^c \, . \qquad (4.81)$$

As the final form shows, it is totally antisymmetric under permutations of the three eikonal lines. This is also the form of the color factor for the other type of 3E diagram, the three-gluon diagram (g) in Fig. 4.3.

As emphasized above, the velocity factors multiplying both commutator and anti-commutator structures vanish. (In the case of the anti-commutator, the vanishing occurs after adding the one-loop counterterms.) Nevertheless, we display the commutator in Eq. (4.81), because it has occurred in the literature before. We will encounter such terms below in our analysis of explicit two-loop calculations, and show how they are consistent with the specific solution for the soft anomalous dimension, Eq. (4.78), in which this combination of color generators does not appear.

4.3.5   Generalizations

The analysis given above applies far beyond the $2 \to 2$ quark-antiquark scattering amplitude. When the soft anomalous dimension is expressed in terms of color generators, as in Eq. (4.80) at one loop, and using this equation and Eq. (4.77) to do so at two loops, the result is slightly less explicit than,

say, Eq. (4.57), but it is much more general. When we generalize from quark and antiquark to gluon lines, and when we add more partons in the final state, the only change in our considerations above is to change the color generators $\mathbf{T}_i$, and sum over more variables i and j. The eikonal momentum integrals that give rise to the coefficients of the generators are the same for any choice of parton pairs or triplets.

In these terms, the two-loop results organized in Eqs. (4.80) and (4.77) are not limited to quark-antiquark scattering, but apply to the scattering of any flavor combination. Furthermore, these relations are by no means limited to $2 \to 2$ scattering, and apply to any $2 \to n$ process, as in multi-jet production. These results, therefore, are a step toward threshold and related resummations in hadronic scattering [62, 65] at the level of next-to-next-to-leading logarithm.

At present, however, for the purposes of resummation we must still rely upon the explicit form of the matrix as in Eq. (4.25) to generate the amplitude at arbitrary orders. Anticipating further applications, it will be useful to investigate flexible choices of color basis, perhaps based on the trace notation described, for example, in Ref. [109] (this point was noted in Ref. [65]). We reserve these considerations for future work.

4.4 Single poles at NNLO

In this section, we combine the expansions of the jet and soft functions in the "minimal" factorized amplitude, Eqs. (4.29) and (4.31), and give an explicit expression for infrared poles to two loops, including single poles. We

go on to compare these "postdictions" of the two-loop single pole terms to the results of explicit calculations, and verify that they agree. Traditionally, these results have been presented in a form proposed some time before by Catani [79], and we will briefly review this formalism and relate it to the two-loop expansion of our resummed expressions.

4.4.1 Two-loop poles from the factorized amplitude

Here, as above, we adopt the notation $f(\alpha_s) = \sum_n (\alpha_s/\pi)^n f^{(n)}$. In this notation, we can express the Born and one-loop amplitudes for process f in terms of the factorized jet, soft and hard functions of Eq. (4.31) as

$$\left| \mathcal{M}_{\mathrm{f}}^{(0)} \right\rangle = \left| \mathcal{H}_{\mathrm{f}}^{(0)} \right\rangle \tag{4.82}$$

$$\left| \mathcal{M}_{\mathrm{f}}^{(1)} \right\rangle = \left(\sum_{i \in \mathrm{f}} E^{[i](1)} + \mathbf{S}_{\mathrm{f}}^{(1)} \right) \left| \mathcal{M}_{\mathrm{f}}^{(0)} \right\rangle + \left| \mathcal{H}_{\mathrm{f}}^{(1)} \right\rangle$$

$$= \left(-\frac{1}{4} \sum_{i \in \mathrm{f}} \left(\frac{1}{2\varepsilon^2} \gamma_K^{[i](1)} + \frac{1}{\varepsilon} \mathcal{G}_0^{[i](1)} \right) + \frac{1}{2\varepsilon} \mathbf{\Gamma}_{S_{\mathrm{f}}}^{(1)} \right) \left| \mathcal{M}_{\mathrm{f}}^{(0)} \right\rangle + \left| \mathcal{H}_{\mathrm{f}}^{(1)} \right\rangle , \tag{4.83}$$

where for the jet functions we have used the minimal form (4.28). In the second equality for $|\mathcal{M}_{\mathrm{f}}^{(1)}\rangle$, we have used explicit expressions for the jet functions and the soft matrix, the latter from Eq. (4.78). Using these results, we find for the two-loop amplitude

$$\left| \mathcal{M}_{\mathrm{f}}^{(2)} \right\rangle = \left[\frac{1}{2} \left(\sum_{i \in \mathrm{f}} E^{[i](1)} + \mathbf{S}_{\mathrm{f}}^{(1)} \right)^2 + \sum_{i \in \mathrm{f}} E^{[i](2)} + \mathbf{S}_{\mathrm{f}}^{(2)} - \frac{1}{2} \left(\mathbf{S}_{\mathrm{f}}^{(1)} \right)^2 \right] \left| \mathcal{M}_{\mathrm{f}}^{(0)} \right\rangle$$

$$+ \left(\sum_{i \in \mathrm{f}} E^{[i](1)} + \mathbf{S}_{\mathrm{f}}^{(1)} \right) \left| \mathcal{H}_{\mathrm{f}}^{(1)} \right\rangle + \left| \mathcal{H}_{\mathrm{f}}^{(2)} \right\rangle . \tag{4.84}$$

Now both the $E^{[i](n)}$ and the $\mathbf{S}_{\text{f}}^{(n)}$ are given by sums of pure poles in ε. As a result, their squares and products all begin at $1/\varepsilon^2$. At two loops, then, the single-pole terms that multiply the Born amplitude $|\mathcal{M}_{\text{f}}^{(0)}\rangle$ in Eq. (4.84) are given entirely by the single poles in $E^{[i](2)}$ and $\mathbf{S}_{\text{f}}^{(2)}$. From Eq. (4.28) for the jets, and Eq. (4.78) for the soft matrix, these poles are found from the coefficients of the soft and jet anomalous dimensions,

$$
\begin{aligned}
\left|\mathcal{M}_{\text{f}}^{(2)}\right\rangle &= \left[\frac{1}{2}\left(\sum_{i\in\text{f}} E^{[i](1)} + \frac{1}{2\varepsilon}\boldsymbol{\Gamma}_{S_{\text{f}}}^{(1)}\right)^2 + \sum_{i\in\text{f}}\sum_{j=2}^{3} E_j^{[i](2)} - \frac{\beta_0}{16\varepsilon^2}\boldsymbol{\Gamma}_{S_{\text{f}}}^{(1)}\right]\left|\mathcal{M}_{\text{f}}^{(0)}\right\rangle \\
&\quad + \left[\sum_{i\in\text{f}} E_1^{[i](2)} + \frac{1}{4\varepsilon}\boldsymbol{\Gamma}_{S_{\text{f}}}^{(2)}\right]\left|\mathcal{M}_{\text{f}}^{(0)}\right\rangle \\
&\quad + \left(\sum_{i\in\text{f}} E^{[i](1)} + \frac{1}{2\varepsilon}\boldsymbol{\Gamma}_{S_{\text{f}}}^{(1)}\right)\left|\mathcal{H}_{\text{f}}^{(1)}\right\rangle + \left|\mathcal{H}_{\text{f}}^{(2)}\right\rangle,
\end{aligned}
\tag{4.85}
$$

where we have separated the double- and higher-order pole terms from single-pole terms that multiply the Born amplitude, followed by single poles times the one-loop hard scattering, and finally the two-loop hard scattering.

From Eq. (4.34), the two-loop single-pole terms that multiply the Born amplitude $|\mathcal{M}_{\text{f}}^{(0)}\rangle$ in Eq. (4.85) are given by

$$
\begin{aligned}
\left[\sum_{i\in\text{f}} E_1^{[i](2)} + \frac{1}{4\varepsilon}\boldsymbol{\Gamma}_{S_{\text{f}}}^{(2)}\right]\left|\mathcal{M}_{\text{f}}^{(0)}\right\rangle &= \frac{1}{\varepsilon}\left[-\frac{\mathcal{G}_0^{[i](2)}}{8}\right. \\
&\qquad \left. +\frac{\beta_0\,\mathcal{G}^{[i](1)\prime}(0)}{32} + \frac{K}{8}\boldsymbol{\Gamma}_{S_{\text{f}}}^{(1)}\right]\left|\mathcal{M}_{\text{f}}^{(0)}\right\rangle,
\end{aligned}
\tag{4.86}
$$

where we recall the notation of Eq. (4.33) for the coefficients $\mathcal{G}^{[i](n)}(\varepsilon)$. Given that the one- and two-loop $\mathcal{G}^{[i](n)}$ have been known for a long time, and that we have just calculated the two-loop soft anomalous dimension matrix, this

expression provides an explicit form for the intrinsic two-loop single poles in dimensionally regulated amplitudes.

Note that a redefinition of $\mathbf{S}_{\mathrm{f}}^{(1)}$ to include a non-pole term would both change the definition of $|\mathcal{H}_{\mathrm{f}}^{(1)}\rangle$ at one loop in Eq. (4.83), and introduce single-pole terms into the $(E^{[i](1)} + \mathbf{S}_{\mathrm{f}}^{(1)})^2$ contribution to the two-loop expression Eq. (4.84). As we shall see below, the Born-times-single-pole terms remain invariant under this shift only if the shift commutes with the $\mathbf{\Gamma}_{S_{\mathrm{f}}}^{(1)}$. We therefore need all of the expansion (4.85), in order to make contact with the results of explicit two-loop calculations at the single-pole level.

4.4.2 One- and two-loop amplitudes in Catani's notation

To compare to existing calculations, we now review the notation of Ref. [79], in which they are normally presented. We first observe that in this notation, amplitudes are organized in powers of $(\alpha_s/2\pi)$, rather than (α_s/π). We will distinguish this trivial difference below by a prime in the color states, as $|\mathcal{M}_{\mathrm{f}}'^{(n)}\rangle = 2^n|\mathcal{M}_{\mathrm{f}}^{(n)}\rangle$.

In this formalism, the single- and double-pole structure of one-loop amplitudes is expressed in terms of the color generator operators introduced above,

$$\mathbf{I}_{\mathrm{f}}^{(1)}(\varepsilon) = \frac{1}{2} \frac{e^{-\varepsilon\psi(1)}}{\Gamma(1-\varepsilon)} \sum_{i\in\mathrm{f}} \sum_{j\neq i} (\mathbf{T}_i \cdot \mathbf{T}_j) \left[\frac{1}{\varepsilon^2} + \frac{\gamma_i}{\mathbf{T}_i^2} \frac{1}{\varepsilon} \right] \left(\frac{\mu^2}{-s_{ij}} \right)^{\varepsilon}, \quad (4.87)$$

with $\psi(1) = -\gamma_E$ the logarithmic derivative of the Gamma function. Here $\gamma_g = \beta_0/2$ and $\mathbf{T}_g^2 = C_A$ for gluons ($i = g$), and $\gamma_i/\mathbf{T}_i^2 = 3/2$ for $i = q$

or $\bar{q}$. The poles of the one-loop amplitude in color-state notation are then represented as

$$\left|\mathcal{M}_{\mathrm{f}}^{\prime(1)}\right\rangle = \mathbf{I}_{\mathrm{f}}^{(1)}(\varepsilon) \left|\mathcal{M}_{\mathrm{f}}^{\prime(0)}\right\rangle + \left|\mathcal{M}_{\mathrm{f}}^{\prime(1)\mathrm{fin}}\right\rangle .$$

(4.88)

The explicit relation to the resummation formalism at one loop is found by expanding $\mathbf{I}_{\mathrm{f}}^{(1)}$ in powers of ε,

$$
\begin{aligned}
\mathbf{I}_{\mathrm{f}}^{(1)} \left|\mathcal{M}_{\mathrm{f}}^{\prime(0)}\right\rangle &= \left[2 \sum_{i\in\mathrm{f}} E^{[i](1)}(\varepsilon) + \frac{1}{\varepsilon}\mathbf{\Gamma}_{S_{\mathrm{f}}}^{(1)} + \frac{\zeta(2)}{4} \sum_{i\in\mathrm{f}} \mathbf{T}_i^2 \right. \\
&\left. + \frac{1}{2}\sum_{j\neq i}(\mathbf{T}_i\cdot\mathbf{T}_j)\left(\frac{1}{2}\ln^2\left(\frac{\mu^2}{-s_{ij}}\right) + \frac{\gamma_i}{\mathbf{T}_i^2}\ln\left(\frac{\mu^2}{-s_{ij}}\right)\right) + \mathcal{O}(\varepsilon)\right] \left|\mathcal{M}_{\mathrm{f}}^{\prime(0)}\right\rangle \\
&\equiv \left[2\sum_{i\in\mathrm{f}} E^{[i](1)}(\varepsilon) + \frac{1}{\varepsilon}\mathbf{\Gamma}_{S_{\mathrm{f}}}^{(1)} + \mathbf{I}_{\mathrm{f}}^{(1)\mathrm{fin}} \right] \left|\mathcal{M}_{\mathrm{f}}^{\prime(0)}\right\rangle .
\end{aligned}
$$

(4.89)

Taking into account the overall factor of two from the expansion in $\alpha_s/2\pi$, the pole terms in Eq. (4.88) are thus identical to those in Eq. (4.83). The matrix $\mathbf{I}_{\mathrm{f}}^{(1)}$ generates as well explicit μ-dependent finite contributions contained in $\mathbf{I}_{\mathrm{f}}^{(1)\mathrm{fin}}$, which in the "minimal" factorization are absorbed into the one-loop hard function $|\mathcal{H}_{\mathrm{f}}\rangle$. The one-loop infrared finite amplitudes are related by

$$\left|\mathcal{H}_{\mathrm{f}}^{\prime(1)}\right\rangle = \left|\mathcal{M}_{\mathrm{f}}^{\prime(1)\mathrm{fin}}\right\rangle + \mathbf{I}_{\mathrm{f}}^{(1)\mathrm{fin}} \left|\mathcal{M}_{\mathrm{f}}^{\prime(0)}\right\rangle .$$

(4.90)

This is an example of a finite shift of the sort mentioned above, which redefines the finite function at one loop.

At two loops, Ref. [79] predicted the fourth- through second order poles in terms of the generators $\mathbf{I}_{\mathrm{f}}^{(1)}$, and absorbed the then-unknown single pole

contributions in terms of a color operator $\mathbf{H}_{\mathrm{f}}^{(2)}$,

$$
\begin{aligned}
\mathbf{I}_{\mathrm{f}}^{(2)}(\varepsilon) \;=\; & -\frac{1}{2}\,\mathbf{I}_{\mathrm{f}}^{(1)}(\varepsilon)\left(\mathbf{I}_{\mathrm{f}}^{(1)}(\varepsilon)+\frac{\beta_0}{\varepsilon}\right) \\
& +\frac{\mathrm{e}^{\varepsilon\psi(1)}\Gamma(1-2\varepsilon)}{\Gamma(1-\varepsilon)}\left(\frac{\beta_0}{2\varepsilon}+K\right)\mathbf{I}_{\mathrm{f}}^{(1)}(2\varepsilon)+\mathbf{H}_{\mathrm{f}}^{(2)}(\varepsilon)\,. \quad (4.91)
\end{aligned}
$$

The two-loop amplitude is then organized as

$$
\left|\mathcal{M}_{\mathrm{f}}^{\prime(2)}\right\rangle = \mathbf{I}_{\mathrm{f}}^{(2)}(\varepsilon)\left|\mathcal{M}_{\mathrm{f}}^{\prime(0)}\right\rangle + \mathbf{I}_{\mathrm{f}}^{(1)}(\varepsilon)\left|\mathcal{M}_{\mathrm{f}}^{\prime(1)}\right\rangle + \left|\mathcal{M}_{\mathrm{f}}^{\prime(2)\mathrm{fin}}\right\rangle\,. \quad (4.92)
$$

In the intervening years, the color generators $\mathbf{H}_{\mathrm{f}}^{(2)}$ have been determined by matching to the single-pole structure of explicit two-loop QCD scattering amplitude calculations, for example $gg \to gg$, $q\bar{q} \to gg$, $q\bar{q} \to q\bar{q}$, and $e^+e^- \to q\bar{q}g$ [69, 70, 71, 75, 76, 84, 85, 86]. Here we follow Ref. [86] and write

$$
\mathbf{H}_{\mathrm{f}}^{(2)}(\varepsilon) = \frac{1}{4\varepsilon}\left\{\sum_{i\in\mathrm{f}} H_i^{(2)} + \hat{\mathbf{H}}_{\mathrm{f}}^{(2)}\right\} + \mathcal{O}(\varepsilon)\,, \quad (4.93)
$$

where we split the single-pole factor into a color-diagonal term, which can be represented as a sum of constants $H_i^{(2)}$ for each external parton i, and a matrix $\hat{\mathbf{H}}_{\mathrm{f}}^{(2)}$ that includes all color mixing. This matrix can be written as [69, 70, 71, 75, 76, 84, 85, 86]

$$
\hat{\mathbf{H}}_{\mathrm{f}}^{(2)} = i\sum_{(i,j,k)} f_{a_1 a_2 a_3}\,\mathbf{T}_i^{a_1}\,\mathbf{T}_j^{a_2}\,\mathbf{T}_k^{a_3}\,\ln\left(\frac{-s_{ij}}{-s_{jk}}\right)\ln\left(\frac{-s_{jk}}{-s_{ki}}\right)\ln\left(\frac{-s_{ki}}{-s_{ij}}\right)\,, \quad (4.94)
$$

where the sum is over distinguishable but unordered triplets of external lines (i,j,k). We note the similarity to the color structure from the 3E diagrams, Eq. (4.81). We emphasize that this form has been obtained directly only for processes with at most four partonic legs. In Ref. [86] it was also shown to be consistent with the proper collinear behavior of the $2 \to n$ gluon amplitudes.

It is these expressions that we will compare to the two-loop expansion of the factorized amplitude, Eqs. (4.85) and (4.86). Rather than provide explicit expressions at this point for the constants $H_i^{(2)}$ from [86], we will derive below expressions relating the constants $H_i^{(2)}$ to the jet anomalous dimensions (in $\overline{\text{MS}}$ scheme). Here we will find useful an identity found in Ref. [110]. The matrix $\hat{\mathbf{H}}_{\text{f}}^{(2)}$ in Eq. (4.94) will emerge from our results for the two-loop soft anomalous dimension matrix, plus the effects of a one-loop finite color-mixing term. We now turn to this exercise.

4.4.3 $\mathbf{H}^{(2)}$ from the anomalous dimensions

Inserting the definition of $\mathbf{I}_{\text{f}}^{(2)}$, Eq. (4.91), into Eq. (4.92) and expanding to the accuracy of ε^0, we readily find

$$
\begin{aligned}
\left|\mathcal{M}_{\text{f}}'^{(2)}\right\rangle &= \frac{1}{2}\left(\mathbf{I}_{\text{f}}^{(1)}(\varepsilon)\right)^2 \left|\mathcal{M}_{\text{f}}'^{(0)}\right\rangle \\
&+ \left[\frac{\beta_0}{2\varepsilon}\left(\mathbf{I}_{\text{f}}^{(1)}(2\varepsilon) - \mathbf{I}_{\text{f}}^{(1)}(\varepsilon)\right) + \left(K + \frac{3\varepsilon\zeta(2)}{4}\beta_0\right)\mathbf{I}_{\text{f}}^{(1)}(2\varepsilon)\right. \\
&\qquad\qquad \left. + \mathbf{H}_{\text{f}}^{(2)}(\varepsilon) + \mathcal{O}(\varepsilon^0)\right] \left|\mathcal{M}_{\text{f}}'^{(0)}\right\rangle \\
&+ \mathbf{I}_{\text{f}}^{(1)}(\varepsilon)\left|\mathcal{M}_{\text{f}}'^{(1)\text{fin}}\right\rangle + \left|\mathcal{M}_{\text{f}}'^{(2)\text{fin}}\right\rangle .
\end{aligned}
\tag{4.95}
$$

We will relate this expression to the single-pole result from the factorized amplitude, Eqs. (4.85) and (4.86).

The single-pole terms in Eq. (4.95) that multiply the Born amplitude come from two sources: the $(\mathbf{I}_{\text{f}}^{(1)})^2$ operator on the first line, and the terms in the square brackets on the second line, which also include finite corrections indicated by $+\mathcal{O}(\varepsilon^0)$.

To make contact with the expansion of the resummed amplitude, Eq. (4.85), we first separate the poles in each of the $\mathbf{I}_{\mathrm{f}}^{(1)}$ terms, according to Eq. (4.89),

$$
\begin{aligned}
\left|\mathcal{M}_{\mathrm{f}}^{\prime(2)}\right\rangle &= \left[\frac{1}{2}\left(2\sum_{i\in\mathrm{f}} E^{[i](1)}(\varepsilon) + \frac{1}{\varepsilon}\mathbf{\Gamma}_{S_{\mathrm{f}}}^{(1)} \right)^2 \right. \\
&\qquad \left. +2\left(\sum_{i\in\mathrm{f}} E^{[i](1)}(\varepsilon) \right) \mathbf{I}_{\mathrm{f}}^{(1)\mathrm{fin}} \right] \left|\mathcal{M}_{\mathrm{f}}^{\prime(0)}\right\rangle \\
&+\frac{1}{2}\left[\left(\mathbf{I}_{\mathrm{f}}^{(1)\mathrm{fin}}\frac{1}{\varepsilon}\mathbf{\Gamma}_{S_{\mathrm{f}}}^{(1)} + \frac{1}{\varepsilon}\mathbf{\Gamma}_{S_{\mathrm{f}}}^{(1)}\mathbf{I}_{\mathrm{f}}^{(1)\mathrm{fin}} \right) + \left(\mathbf{I}_{\mathrm{f}}^{(1)\mathrm{fin}} \right)^2 \right]\left|\mathcal{M}_{\mathrm{f}}^{\prime(0)}\right\rangle \\
&+\left[\frac{\beta_0}{2\varepsilon}\left(2\sum_{i\in\mathrm{f}} E^{[i](1)}(2\varepsilon) - 2\sum_{i\in\mathrm{f}} E^{[i](1)}(\varepsilon) - \frac{1}{2\varepsilon}\mathbf{\Gamma}_{S_{\mathrm{f}}}^{(1)} \right) \right. \\
&\qquad +\frac{3\zeta(2)\beta_0}{8\varepsilon}\sum_{i\in\mathrm{f}} E_2^{[i](1)} + K\left(2\sum_{i\in\mathrm{f}} E^{[i](1)}(2\varepsilon) + \frac{1}{2\varepsilon}\mathbf{\Gamma}_{S_{\mathrm{f}}}^{(1)} \right) \\
&\qquad \left. +\mathbf{H}_{\mathrm{f}}^{(2)}(\varepsilon) + \mathbf{I}_{\mathrm{f}}^{(2)\mathrm{fin}} \right]\left|\mathcal{M}_{\mathrm{f}}^{\prime(0)}\right\rangle \\
&+\left[2\sum_{i\in\mathrm{f}} E^{[i](1)}(\varepsilon) + \frac{1}{\varepsilon}\mathbf{\Gamma}_{S_{\mathrm{f}}}^{(1)} + \mathbf{I}_{\mathrm{f}}^{(1)\mathrm{fin}} \right]\left|\mathcal{M}_{\mathrm{f}}^{\prime(1)\mathrm{fin}}\right\rangle + \left|\mathcal{M}_{\mathrm{f}}^{\prime(2)\mathrm{fin}}\right\rangle ,
\end{aligned}
$$

$$(4.96)$$

where in $\mathbf{I}_{\mathrm{f}}^{(2)\mathrm{fin}}$ we isolate the finite terms from $\mathbf{I}_{\mathrm{f}}^{(2)}$ that multiply the Born amplitude. Comparison with Eq. (4.85) requires further that we commute the soft anomalous dimension matrices with poles to the left of the finite amplitudes, and that we also re-express $\left|\mathcal{M}^{\prime(1)\mathrm{fin}}\right\rangle$ in terms of $\left|\mathcal{H}^{\prime(1)}\right\rangle$ using Eq. (4.90). The first step, in particular, leads to an additional commutator

contribution at the level of the single poles times the Born amplitude,

$$
\begin{aligned}
|\mathcal{M}_{\mathrm{f}}'^{(2)}\rangle \;=\; & \frac{1}{2}\left(2\sum_{i\in\mathrm{f}}E^{[i](1)}(\varepsilon)+\frac{1}{\varepsilon}\mathbf{\Gamma}_{S_{\mathrm{f}}}^{(1)}\right)^{2}|\mathcal{M}_{\mathrm{f}}'^{(0)}\rangle \\
& +\left[\frac{\beta_{0}}{2\varepsilon}\left(2\sum_{i\in\mathrm{f}}E^{[i](1)}(2\varepsilon)-2\sum_{i\in\mathrm{f}}E^{[i](1)}(\varepsilon)-\frac{1}{2\varepsilon}\mathbf{\Gamma}_{S_{\mathrm{f}}}^{(1)}\right)\right.\\
& \left.\qquad\quad +K\sum_{i\in\mathrm{f}}\frac{E_{2}^{[i](1)}}{2\varepsilon^{2}}\right]|\mathcal{M}_{\mathrm{f}}'^{(0)}\rangle \\
& +\left[\frac{3\zeta(2)\beta_{0}}{8\varepsilon}\sum_{i\in\mathrm{f}}E_{2}^{[i](1)}+K\left(\sum_{i\in\mathrm{f}}\frac{E_{1}^{[i](1)}}{\varepsilon}+\frac{1}{2\varepsilon}\mathbf{\Gamma}_{S_{\mathrm{f}}}^{(1)}\right)\right.\\
& \left.\qquad\quad +\frac{1}{2\varepsilon}\left[\mathbf{I}_{\mathrm{f}}^{(1)\mathrm{fin}},\mathbf{\Gamma}_{S_{\mathrm{f}}}^{(1)}\right]+\mathbf{H}_{\mathrm{f}}^{(2)}(\varepsilon)\right]|\mathcal{M}_{\mathrm{f}}'^{(0)}\rangle \\
& +\left[2\sum_{i\in\mathrm{f}}E^{[i](1)}(\varepsilon)+\frac{1}{\varepsilon}\mathbf{\Gamma}_{S_{\mathrm{f}}}^{(1)}\right]|\mathcal{H}_{\mathrm{f}}'^{(1)}\rangle\;+\;|\mathcal{H}_{\mathrm{f}}'^{(2)}\rangle\,. \qquad (4.97)
\end{aligned}
$$

Here we have organized the expression just as in Eq. (4.85), starting with the square of one-loop pole terms, two-loop second- and third-order poles, and then first-order poles, all times the Born amplitude, followed by poles times the one-loop hard amplitude and the finally the two-loop hard part,

$$
|\mathcal{H}'^{(2)}\rangle \equiv \left(\mathbf{I}_{\mathrm{f}}^{(2)\mathrm{fin}}-\frac{1}{2}\left(\mathbf{I}_{\mathrm{f}}^{(1)\mathrm{fin}}\right)^{2}\right)|\mathcal{M}_{\mathrm{f}}'^{(0)}\rangle+\mathbf{I}_{\mathrm{f}}^{(1)\mathrm{fin}}|\mathcal{H}_{\mathrm{f}}'^{(1)}\rangle+|\mathcal{M}_{\mathrm{f}}'^{(2)\mathrm{fin}}\rangle\,. (4.98)
$$

We are now ready to compare this expression to the two-loop single pole terms of Eq. (4.86). Higher-order poles can easily be checked in a similar manner [68].

Consider first the matrix parts of Eqs. (4.86) and (4.97). Recalling the factor of 4 associated with changing from the coefficient of $(\alpha_{s}/\pi)^{2}$ to $(\alpha_{s}/2\pi)^{2}$, we see that the $K\,\mathbf{\Gamma}_{S_{\mathrm{f}}}^{(1)}$ term is identical in the two expressions. Consistency then requires the remarkable result that the commutator of $\mathbf{I}_{\mathrm{f}}^{(1)\mathrm{fin}}$ in Eq. (4.89) with the one-loop soft anomalous dimension in Eq. (4.80) precisely cancel the

two-loop $\hat{\mathbf{H}}_{\mathrm{f}}^{(2)}$ function as defined in Eq. (4.94),

$$\left[\mathbf{I}_{\mathrm{f}}^{(1)\mathrm{fin}}, \mathbf{\Gamma}_{S_{\mathrm{f}}}^{(1)} \right] = -\frac{1}{2}\,\hat{\mathbf{H}}_{\mathrm{f}}^{(2)}\,. \tag{4.99}$$

In fact, a compact calculation, given in Appendix E, shows that Eq. (4.99) indeed holds for the explicit matrix $\hat{\mathbf{H}}_{\mathrm{f}}^{(2)}$ given in Eq. (4.94), for arbitrary $2 \to 2$ processes, and also for $2 \to n$ processes where all particles are identical. For those processes with five or more partons for which the quantities $\gamma_i/\mathbf{T}_i^2$ are not all identical, the commutator is more complicated, as can be seen by inspecting Eq. (4.89), and as discussed in Appendix E. Because we know the anomalous dimension matrix for all these processes, however, Eq. (4.99) can be turned around and taken as a definition of the corresponding matrices $\hat{\mathbf{H}}_{\mathrm{f}}^{(2)}$. Recently, the soft anomalous dimension matrix $\Gamma_{S_{\mathrm{f}}}^{(2)}$ for $2 \to 2$ processes was computed [83] by making use of just this connection to $\hat{\mathbf{H}}_{\mathrm{f}}^{(2)}$, along with the explicit results for $\hat{\mathbf{H}}_{\mathrm{f}}^{(2)}$ for quark-quark scattering [69].

The remaining, color-diagonal, single-pole terms in Eq. (4.97) are found using the values of the one-loop quantities $E^{[i](1)}$ given in Eq. (4.34), and the form of $\mathbf{H}_{\mathrm{f}}^{(2)}$ in given in Eq. (4.93). Then the single-poles times Born amplitudes of Eq. (4.97) are given by

$$\begin{aligned}
\left|\mathcal{M}_{\mathrm{f}}^{\prime(2)}\right\rangle_{\text{single pole} \times \text{Born}} &= \frac{1}{\varepsilon} \sum_{i\in\mathrm{f}} \left[\frac{H_i^{(2)}}{4} - \frac{3\zeta(2)\beta_0}{32}\,C_i - \frac{K\,\mathcal{G}_0^{[i]\,(1)}}{4} \right] \left|\mathcal{M}_{\mathrm{f}}^{\prime(0)}\right\rangle \\
&\quad + \frac{K}{2\varepsilon}\,\mathbf{\Gamma}_{S_{\mathrm{f}}}^{(1)} \left|\mathcal{M}_{\mathrm{f}}^{\prime(0)}\right\rangle,
\end{aligned}$$

$$\tag{4.100}$$

where we have suppressed dependence that contributes only at the level ε^0. The comparison of Eq. (4.100) with the expansion from the resummed ampli-

tude, Eq. (4.86), is now trivial. We simply appeal to the striking identity noted explicitly by Ravindran, Smith and van Neerven [110], which in our notation is written as

$$\frac{H_i^{(2)}}{4} - \frac{3\zeta(2)\beta_0}{32}\,C_i - \frac{K\,\mathcal{G}_0^{[i]\,(1)}}{4} \;=\; 4E_1^{[i]\,(2)}, \qquad (4.101)$$

where $E_1^{[i]\,(2)}$ is given in Eq. (4.34). In Ref. [110] this expression was observed to imply a close relationship between the $H_i^{(2)}$ constants and the form factors. We now see that, aside from color mixing, all the single-pole terms are identical to those in the form factors. Indeed, the precise terms relating the $H_i^{(2)}$ to the single-pole residues of the elastic form factor are present simply to cancel a set of "extra" single-pole terms generated from the expansion of $\mathbf{I}_{\mathrm{f}}^{(1)}$ in the two-loop amplitude. As in the case of the color-mixing anomalous dimensions, we can also consider Eq. (4.101) as a *definition* of the constants $H_i^{(2)}$.

In summary, we have shown that the full single-pole structure of the two-loop amplitudes can be reconstructed from the same anomalous dimensions that determine the next-to-next-to-leading poles of the factorized jet and soft functions at all orders in pertubation theory. This relation, and the explicit forms of the anomalous dimensions, hold for partonic scattering amplitudes with arbitrary numbers of external lines.

4.5 Conclusions

We have extended the factorization and resummation formalisms for exclusive amplitudes in QCD to next-to-next-to-leading poles in these ampli-

tudes. The same anomalous dimension matrices, calculated here directly for the first time at two loops, control a variety of resummed cross sections at NNLL. These calculations generalize the determination of the Sudakov anomalous dimensions to nontrivial color mixing.

We verified the formalism and anomalous dimensions by showing that they allow us to reproduce the very nontrivial color and momentum structure of single infrared poles at next-to-next-to-leading order for $2 \to 2$ processes in the literature.

The calculation of the NNLO soft anomalous dimensions opens the door to threshold resummation at next-to-next-to-leading logarithm for multijet cross sections [63, 65, 66]. Perhaps our most striking result is the discovery that the two-loop soft anomalous dimension matrix is obtained from the one-loop matrix simply by multiplying by $K\alpha_s/(2\pi)$, where K is the constant given in Eq. (4.63). This is exactly the same property obeyed by the scalar Sudakov or "cusp" anomalous dimension. Aside from its intrinsic interest, this relation will make possible next-to-next-to-leading logarithmic resummation formulas in a closed form, since it will be possible to diagonalize the two-loop anomalous dimension matrix independently of the running of the coupling [103, 104, 105, 106, 107, 108], using the same color eigenvectors found at one loop [63, 65, 66, 111, 112, 113, 114].

Our analysis applies not only to $2 \to n$ processes relevant to hadronic colliders. In addition, it applies to the inelastic scattering of a parton by a color-singlet source, as in deep-inelastic scattering, and to the creation of arbitrary numbers of partons from a color-singlet source in leptonic annihilation.

It will clearly also be of interest to extend this analysis to massive external lines.

Appendix A

Nonabelian Ward Identity and Eikonal Feynman Rules

In order to show the factorization of nonphysical gluons from both the hard part and from the A- and B-jets we have used the following Ward identity [50, 51]

$$\langle M|\kappa\, \partial_\mu\, A^{\mu,a}(x)|N\rangle = 0\,, \tag{A.1}$$

where $A^{\mu,a}(x)$ is the nonabelian gauge field carrying color a and M and N are physical states. This Ward identity is the simple statement that the sum of all possible attachments of a longitudinally polarized gluon to a physical observable vanishes. Eq. (A.1) is diagramatically represented by Fig. A.1a. where if we bring the right hand side of the figure to the left we would have all possible attachments of the unphysical gluon to the hard function denoted by the blob in the figure.

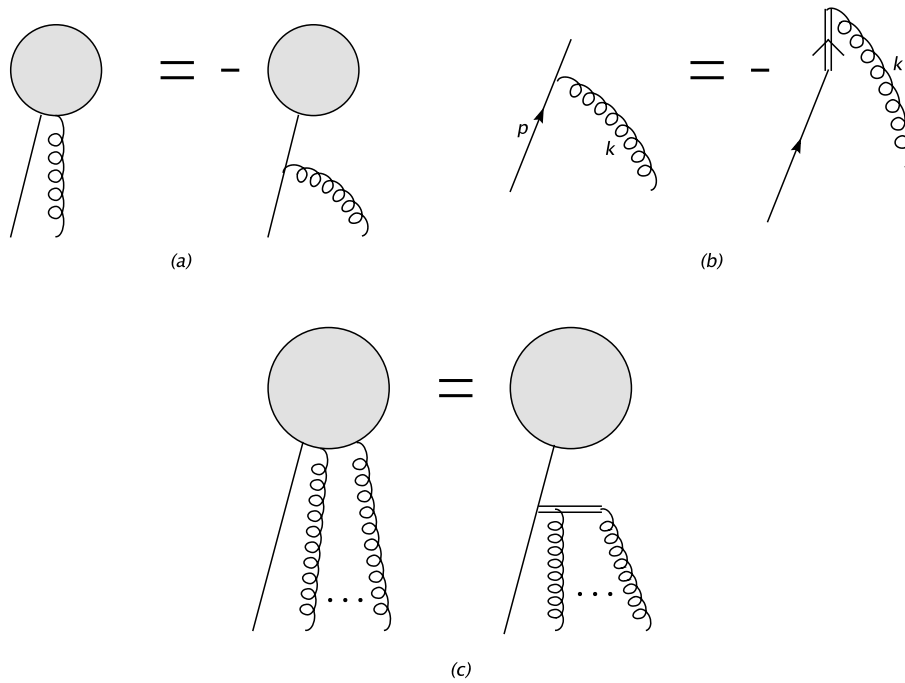Fig A.1b. is the eikonal identity for a longitudinally polarized gluon at-

Figure A.1: a) Diagramatic representation of the Ward identity of Eq. (A.1). b) Eikonal identity for a longitudinally polarized gluon attaching a fermion line. Double line represents a Wilson line. c) Repeated application of the eikonal identity of Fig. b) to Fig. a)

taching a fermion line, which can be written as

$$\bar{u}(p)\, g_s\, T^a\, \gamma^\mu\, \frac{1}{\not{p}+\not{k}}\, k_\mu = \bar{u}(p)\, g_s\, T^a\, \frac{\not{p}+\not{k}-\not{p}}{\not{p}+\not{k}} \;\; = \;\; \bar{u}(p)\, g_s\, T^a$$

$$= \;\; -\bar{u}(p)\, g_s\, T^a\, \frac{\beta^\mu k_\mu}{-\beta \cdot k}\,, \tag{A.2}$$

where k is the momentum for the longitudinally polarized gluon and p is the external momentum. In the first line of the equation after the second equal sign we have used the Dirac's equation for a fermion, $\bar{u}(p)(\not{p}-m)=0$, and in the second line we have multiplied and divided the expression by the factor $\beta \cdot k$ where β^μ is the four velocity for the fermion. As we see below in Eq. (A.3) this is nothing but the eikonal propagator which is represented by the double line in Fig. A.1b. The eikonal line is given by the path ordered exponential given by Eq. (3.20) which can be expanded as
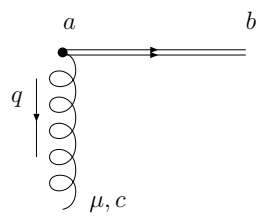
$$\Phi^{(f)}_\beta(0,\eta) \;\; \equiv \;\; \mathrm{Pexp}\left[\mathrm{i}\, g_s \int_0^\eta \mathrm{d}\xi \beta \cdot \mathrm{A}^{(f)}(\xi\,\beta^\mu) \right]$$

$$= \;\; 1 + \mathrm{P} \sum_{m=1}^{\infty} \prod_{i=1}^{m} \int \frac{\mathrm{d}^n k_i}{(2\pi)^n}\, g_s\, \beta \cdot \mathrm{A}^{(f)}(k_i^\mu) \frac{1}{\beta \cdot \sum_{j=1}^{i} k_j + \mathrm{i}\epsilon}\,, \tag{A.3}$$
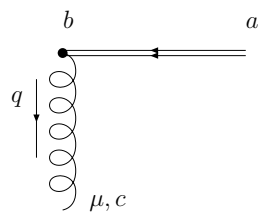
using
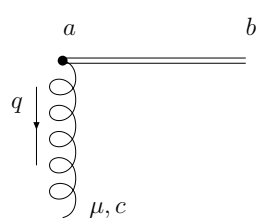
$$\int_{-\infty}^{\infty} dx\, \mathrm{e}^{\mathrm{i}\,k\,x}\, \theta(x) = \frac{\mathrm{i}}{k+\mathrm{i}\epsilon}\,. \tag{A.4}$$

The eikonal Feynman rules are obtained by the expansion given in Eq. (A.3) and are shown in Fig. A.2.

The nonabelian diagramatic Ward identity shown in Fig. A.1c. is then nothing but repeated application of the eikonal identity of Fig. A.1b. to Fig. A.1a.

$$= (-ig_s)(T_F^c)_{ba}(+v^\mu) \times \frac{i}{-v \cdot q + i\varepsilon}$$

$$= (-ig_s)(T_F^c)_{ba}(-v^\mu) \times \frac{i}{-v \cdot q + i\varepsilon}$$

$$= (-g_s)(f^{bac})(+v^\mu) \times \frac{i}{-v \cdot q + i\varepsilon}$$

Figure A.2: Eikonal feynman rules.

Appendix B

Anomalous dimensions

In this appendix, we provide the low-order anomalous dimensions entering the jet function, as defined in Eqs. (4.7) and (4.32). We give the nth-order coefficients $\gamma_K^{[i]\,(n)}$, $\mathcal{K}^{[i]\,(n)}$ and $\mathcal{G}^{[i]\,(n)}$ in an expansion in powers of $\alpha_s(\mu^2)/\pi$,

$$
\begin{aligned}
\gamma_K^{[i]\,(1)} &= 2C_i \,, \\
\gamma_K^{[i]\,(2)} &= C_i K = C_i \left[C_A \left(\frac{67}{18} - \zeta(2) \right) - \frac{10}{9} T_F n_F \right] \,, \\
\mathcal{K}^{[i]\,(1)} &= \frac{1}{2\varepsilon} \gamma_K^{[i]\,(1)} \,, \\
\mathcal{K}^{[i]\,(2)} &= \frac{1}{4\varepsilon} \gamma_K^{[i]\,(2)} - \frac{\beta_0}{16\varepsilon^2} \gamma_K^{[i]\,(1)} \,, \\
\mathcal{G}^{[q]\,(1)} &= \frac{3}{2} C_F + \varepsilon \frac{C_F}{2} \left(8 - \zeta(2) \right) + \mathcal{O}(\varepsilon^2) \,, \\
\mathcal{G}_0^{[q]\,(2)} &= 3C_F^2 \left[\frac{1}{16} - \frac{1}{2}\zeta(2) + \zeta(3) \right] + \frac{1}{4} C_A C_F \left[\frac{2545}{108} + \frac{11}{3}\zeta(2) - 13\zeta(3) \right] \\
&\quad - C_F T_F n_F \left[\frac{209}{108} + \frac{1}{3}\zeta(2) \right] \,, \\
\mathcal{G}^{[g]\,(1)} &= \frac{\beta_0}{2} - \varepsilon \frac{C_A}{2} \zeta(2) + \mathcal{O}(\varepsilon^2) \,, \\
\mathcal{G}_0^{[g]\,(2)} &= C_A^2 \left[\frac{10}{27} - \frac{11}{12}\zeta(2) - \frac{1}{4}\zeta(3) \right] + C_A T_F n_F \left[\frac{13}{27} + \frac{1}{3}\zeta(2) \right] + \frac{1}{2} C_F T_F n_F \\
&\quad + \frac{\beta_1}{4} \,, \tag{B.1}
\end{aligned}
$$

where $C_q = C_F$, $C_g = C_A$, and

$$\beta_1 = \frac{34}{3}C_A^2 - 4C_F T_F n_F - \frac{20}{3}C_A T_F n_F \, . \tag{B.2}$$

The results for $\mathcal{G}^{[i]\,(n)}$ were obtained from Ref. [97], which also contains results through three loops. We shift the gluonic expressions by terms proportional to β-function coefficients, which take into account the effects of the renormalizing the operator $G_{\mu\nu}^a G^{a\,\mu\nu}$, as explained in Ref. [110]. Because we only quote results through two-loop order, some of the results for $\mathcal{G}^{[i]\,(n)}$ could also have been extracted from the two-loop quark electromagnetic form factor [92] and from the $gg \to$ Higgs boson amplitude [96].

Appendix C

One-loop velocity factors

C.1 Basic integrals

Consider the one-loop t-channel diagram shown in Fig. 4.1(a). The velocity factor is given by

$$
\begin{aligned}
F_t &= (ig\mu^\varepsilon)^2 \, (v_1 \cdot v_3) \int_0^\infty d\alpha \int_0^\infty d\beta \, D(v_3\alpha + v_1\beta) \\
&= (ig\mu^\varepsilon)^2 \, \frac{1}{4\pi^{2-\varepsilon}}\Gamma(1-\varepsilon) \, (v_1 \cdot v_3) \int_0^\infty d\alpha \int_0^\infty d\beta \, \frac{1}{[(v_3\alpha + v_1\beta)^2]^{1-\varepsilon}} \, .
\end{aligned}
$$
(C.1)

We will use the following change of variables

$$
\alpha + \beta \equiv \eta \, , \qquad \alpha \equiv z\,\eta \, ,
$$
(C.2)

with Jacobian η. For IR regularization we impose $\alpha < \frac{1}{\lambda} \iff \eta < \frac{1}{\lambda z}$. [1] Also note that $0 < z < 1$. In terms of the new variables we have

$$
\begin{aligned}
F_t &= (ig\mu^\varepsilon)^2 \frac{1}{4\pi^{2-\varepsilon}} \Gamma(1-\varepsilon)\,(v_1 \cdot v_3) \int_0^1 dz \int_0^{\frac{1}{\lambda z}} d\eta\, \eta^{2\varepsilon-1} \\
&\quad \times \frac{1}{[(v_3\, z + v_1\, (1-z))^2]^{1-\varepsilon}} \\
&= (ig\mu^\varepsilon)^2 \frac{1}{4\pi^{2-\varepsilon}} \Gamma(1-\varepsilon)\,(v_1 \cdot v_3) \frac{1}{2\varepsilon} \frac{1}{\lambda^{2\varepsilon}} \int_0^\infty dz'\, \frac{1}{[(v_3 + v_1\, z')^2]^{1-\varepsilon}}\,,
\end{aligned}
$$

$$\tag{C.3}$$

with $z' \equiv \frac{1}{z} - 1$. From the expansion of the above expression, the single-pole term and the finite part of the one-loop diagram are given by

$$
\begin{aligned}
F_t &= -\left(\frac{\alpha_s}{\pi}\right)(v_1 \cdot v_3)\left\{ \frac{1}{2\varepsilon}\, I_1(v_1, v_3) + \frac{1}{2}\, I_m(v_1, v_3) \right. \\
&\quad \left. + \frac{1}{2}\left[\ln\left(\frac{\mu^2}{\lambda^2}\right) + \ln(\pi\, e^{\gamma_e})\right] I_1(v_1, v_3) \right\},
\end{aligned}
$$

$$\tag{C.4}$$

where we have defined the following integrals

$$
\begin{aligned}
I_1(v_1, v_3) &\equiv \int_0^1 dz \frac{1}{(v_3\, z + v_1\, \bar{z})^2} = \int_0^\infty dz' \frac{1}{(v_3 + v_1\, z')^2}\,, \\
I_m(v_1, v_3) &\equiv \int_0^\infty dz'\, \frac{\ln(v_3 + v_1\, z')^2}{(v_3 + v_1\, z')^2}\,,
\end{aligned}
$$

$$\tag{C.5}$$

with $\bar{z} \equiv 1 - z$.

---

[1] For these one-loop diagrams there is one overall IR divergence since all the collinear singularities factorize. Therefore it is sufficient to restrict only one of the gluon attachments.

C.2 Evaluation of I_1 and I_m

We are evaluating eikonal diagrams derived from external Wilson lines. By looking at the usual momentum-space expressions for the amplitudes one can easily see that all these diagrams are scale independent in the eikonal velocities v_i. With this property in mind we can simplify the evaluations of the integrals by choosing $v_i^2 = 1$ without loss of generality.

In order to evaluate $I_1(v_1, v_3)$ we use the following change of variable [99]

$$e^{2\psi} \equiv \frac{\sqrt{v_3^2} z + \sqrt{v_1^2} \bar{z} e^{\gamma_{13}}}{\sqrt{v_3^2} z + \sqrt{v_1^2} \bar{z} e^{-\gamma_{13}}} , \tag{C.6}$$

which gives

$$\frac{d\psi}{dz} = -\frac{1}{2} \frac{\sqrt{v_1^2 v_3^2}(e^{\gamma_{13}} - e^{-\gamma_{13}})}{(v_3 z + v_1 \bar{z})^2} . \tag{C.7}$$

From this change of variable it is very easy to see that

$$\int_0^{\gamma_{13}} d\psi = \sqrt{v_1^2 v_3^2} \sinh \gamma_{13} \int_0^1 dz \frac{1}{(v_3 z + v_1 \bar{z})^2} . \tag{C.8}$$

Therefore we get

$$I_1(v_1, v_3) = \frac{1}{\sqrt{v_1^2 v_3^2} \sinh \gamma_{13}} \gamma_{13} . \tag{C.9}$$

Note that

$$I_1(v_1, -v_3) = \frac{1}{\sqrt{v_1^2 v_3^2} \sinh \gamma_{13}} (i\pi - \gamma_{13}) , \tag{C.10}$$

by analytic continuation.

With $v_i^2 = 1$, I_m can be written as

$$
\begin{aligned}
I_m(v_1, v_3) &= \int_0^\infty dy \frac{1}{(y + e^{-\gamma_{13}})(y + e^{\gamma_{13}})} \ln\left[(y + e^{-\gamma_{13}})(y + e^{\gamma_{13}})\right] \\
&= \frac{1}{2\sinh\gamma_{13}} \int_0^\infty dy \left\{ \frac{\ln\left[(y + e^{-\gamma_{13}})(y + e^{\gamma_{13}})\right]}{y + e^{-\gamma_{13}}} \right. \\
&\qquad\qquad \left. - \frac{\ln\left[(y + e^{-\gamma_{13}})(y + e^{\gamma_{13}})\right]}{y + e^{\gamma_{13}}} \right\} \\
&= \frac{1}{2\sinh\gamma_{13}} \int_0^\infty dy \left\{ \frac{\ln(y + e^{-\gamma_{13}})}{y + e^{-\gamma_{13}}} + \frac{\ln(y + e^{\gamma_{13}})}{y + e^{-\gamma_{13}}} \right. \\
&\qquad\qquad \left. - \frac{\ln(y + e^{-\gamma_{13}})}{y + e^{\gamma_{13}}} - \frac{\ln(y + e^{\gamma_{13}})}{y + e^{\gamma_{13}}} \right\} . \quad \text{(C.11)}
\end{aligned}
$$

It is easy to verify that the first and last terms in the right-hand side of the final expression cancel, for example by changing variables to $u = y + e^{-\gamma_{13}}$ in the first term and $u = y + e^{\gamma_{13}}$ in the last. This leaves us with

$$
I_m(v_1, v_3) = \frac{1}{2\sinh\gamma_{13}} \int_0^\infty dy \left\{ \frac{\ln(y + e^{\gamma_{13}})}{y + e^{-\gamma_{13}}} - \frac{\ln(y + e^{-\gamma_{13}})}{y + e^{\gamma_{13}}} \right\} . \quad \text{(C.12)}
$$

In the high-energy limit $\gamma \gg 1$, where $e^\gamma \gg e^{-\gamma}$, one easily finds

$$
\begin{aligned}
I_m(v_1, v_3) &= \frac{1}{2\sinh\gamma_{13}} \left[-\mathrm{Li}_2(-e^{2\gamma_{13}}) + \mathrm{Li}_2(1) + \mathcal{O}(]^{-\gamma_{\infty\ni}}) \right] \\
&= \frac{1}{\sinh\gamma_{13}} \left[\frac{\pi^2}{6} + \gamma_{13}^2 + \mathcal{O}(]^{-\gamma_{\infty\ni}}) \right] . \quad \text{(C.13)}
\end{aligned}
$$

Following the same steps one also gets

$$
I_m(v_1, -v_3) = -\frac{1}{\sinh\gamma_{13}} \left[\frac{\pi^2}{6} + \gamma_{13}^2 + \mathcal{O}(]^{-\gamma_{\infty\ni}}) \right] . \quad \text{(C.14)}
$$

Appendix D

Velocity factors for 2E diagrams

We begin our analysis of the 2E diagrams with the diagram that has a three-gluon vertex, Fig. 4.3(f). We follow Refs. [115, 116, 99] and write the three-gluon vertex as

$$V_{\mu\nu\rho}(k, l, -k - l) = \bar{V}_{\mu\nu\rho}(k, l) + D_{\mu\nu\rho}(k, l) \,, \qquad (\text{D.1})$$

where

$$\begin{aligned} \bar{V}_{\mu\nu\rho}(k, l) &= (2l + k)_\mu g_{\nu\rho} + 2k_\rho g_{\mu\nu} - 2k_\nu g_{\mu\rho} \,, \\ D_{\mu\nu\rho}(k, l) &= -l_\nu g_{\mu\rho} - (k + l)_\rho g_{\mu\nu} \,, \end{aligned} \qquad (\text{D.2})$$

and where k and l are the loop momenta. Indices ν and ρ attach to the v_3 line. The diagram resulting from $\bar{V}_{\mu\nu\rho}$ is proportional to v_3^2 before integration. We also note that the contributions of diagrams of Fig. 4.3(d) and Fig. 4.3(e) are entirely proportional to v_3^2 before integration, since a single gluon propagator attaches twice to the same eikonal line. These v_3^2 contributions turn out to cancel each other in the high-energy limit. We give the result for the $\bar{V}_{\mu\nu\rho}$ contribution below.

The contribution resulting from the $D_{\mu\nu\rho}$ piece for the diagram of Fig. 4.3(f) is given by,

$$
W_{2E,3g-D}(v_1, v_3) = -(g\mu^\varepsilon)^4 \, d_{JI}^{[t]} \frac{C_A}{2} \int \frac{d^D k}{(2\pi)^D} \frac{d^D l}{(2\pi)^D} \frac{1}{k^2} \frac{1}{l^2} \frac{1}{(k+l)^2}
$$
$$
\times \left[\frac{2\, v_3 \cdot v_1}{(v_1 \cdot k)(v_3 \cdot k)} + \frac{v_3 \cdot v_1}{(v_1 \cdot k)(v_3 \cdot l)} \right] ,
$$

$$(D.3)$$

where we have suppressed factors of $i\epsilon$ in the denominators. One can evaluate the above expression in either momentum or configuration space. We will not review the derivation of the following result [99],

$$
W_{2E,3g-D}^{s.p.} = \left(\frac{\alpha_s}{\pi} \right)^2 d_{JI}^{[t]} \frac{C_A}{2} \left\{ \gamma_{13} \coth \gamma_{13} \left(-\frac{1}{4\varepsilon} + \frac{1}{16\varepsilon}\zeta(2) \right) + \frac{1}{8\varepsilon} I_2(\gamma_{13}) \right\} ,
$$

$$(D.4)$$

where

$$
I_2(\gamma_{13}) \equiv \sinh 2\gamma_{13} \int_0^{\gamma_{13}} d\psi \frac{\psi \coth \psi}{\sinh^2 \gamma_{13} - \sinh^2 \psi} \ln \left(\frac{\sinh \gamma_{13}}{\sinh \psi} \right) . \qquad (D.5)
$$

We analyze I_2 in order to get the high-energy behavior of this amplitude. We start by writing I_2 as

$$
I_2 = I_{cth-1} + I_1 , \qquad (D.6)
$$

where

$$
I_{cth-1} = \int_0^{\gamma_{13}} d\psi \left[\frac{\sinh 2\gamma_{13}}{\sinh^2 \gamma_{13} - \sinh^2 \psi} \ln \left(\frac{\sinh \gamma_{13}}{\sinh \psi} \right) \right] \times \psi \, (\coth \psi - 1)
$$
$$
= 2 \int_0^{\gamma_{13}} d\psi \left[\frac{\sinh 2\gamma_{13}}{\sinh^2 \gamma_{13} - \sinh^2 \psi} \ln \left(\frac{\sinh \gamma_{13}}{\sinh \psi} \right) \right] \times \psi \frac{e^{-2\psi}}{1 - e^{-2\psi}} ,
$$

$$(D.7)$$

and where

$$I_1 \;=\; \int_0^{\gamma_{13}} d\psi \left[\frac{\sinh 2\gamma_{13}}{\sinh^2 \gamma_{13} - \sinh^2 \psi} \ln\left(\frac{\sinh \gamma_{13}}{\sinh \psi} \right) \right] \psi \,. \qquad (D.8)$$

Note that I_{cth-1} is exponentially suppressed in ψ when $\psi \sim \gamma_{13}$. However, for small ψ the factor $\frac{\sinh 2\gamma_{13}}{\sinh^2 \gamma_{13} - \sinh^2 \psi} = 2 + \mathcal{O}(]^{-\gamma_{\infty\ni}})$. Therefore we can rewrite I_{cth-1} as

$$\begin{aligned}
I_{cth-1} \;&=\; \int_0^\infty d\psi \left[2 \ln\left(\frac{2\sinh \gamma_{13}}{2 \sinh \psi} \right) \right] \psi \left(\coth \psi - 1 \right) + \mathcal{O}(]^{-\gamma_{\infty\ni}}) \\
&=\; 2 \left[\gamma_{13} \int_0^\infty d\psi\, \psi \left(\coth \psi - 1 \right) \right. \\
&\qquad\quad - \int_0^\infty d\psi\, \psi^2 (\coth \psi - 1) \\
&\qquad\quad \left. - \int_0^\infty d\psi\, \psi \ln(1 - e^{-2\psi})\left(\coth \psi - 1 \right) \right] \\
&\equiv\; 2(k_1 \gamma_{13} + k_2 + k_3)\,. \qquad\qquad (D.9)
\end{aligned}$$

We evaluate k_1, k_2 and k_3 separately, starting with

$$\begin{aligned}
k_1 \;&=\; \int_0^\infty d\psi\, \psi \left(\coth \psi - 1 \right) \\
&=\; 2 \int_0^\infty d\psi\, \psi \frac{e^{-2\psi}}{1 - e^{-2\psi}} \\
&=\; 2 \sum_{n=0}^\infty \int_0^\infty d\psi\, \psi\, e^{-2(n+1)\psi} \\
&=\; \frac{1}{2}\zeta(2)\,. \qquad\qquad (D.10)
\end{aligned}$$

We evaluate k_2 and k_3 by using the same expansion with answers

$$\begin{aligned}
k_2 \;&=\; - \int_0^\infty d\psi\, \psi^2 (\coth \psi - 1) \\
&=\; -\frac{1}{2}\zeta(3)\,, \qquad\qquad (D.11)
\end{aligned}$$

and finally

$$
\begin{aligned}
k_3 &= -\int_0^\infty d\psi\, \psi\, \ln(1 - e^{-2\psi}) \,(\coth\psi - 1) \\
&= \frac{1}{2}\zeta(3) \,.
\end{aligned}
\tag{D.12}
$$

Combining these results one finds

$$
I_{cth-1} = \zeta(2)\gamma_{13} \,.
\tag{D.13}
$$

Now let's look at the remaining integral in Eq. (D.6), I_1. After some trivial algebra one can rewrite I_1 as

$$
I_1 = k_4 + k_5 \,,
\tag{D.14}
$$

where

$$
\begin{aligned}
k_4 &= 2\int_0^{\gamma_{13}} d\psi\, \psi(\gamma_{13} - \psi)\, \frac{1}{(1 - e^{-(\gamma_{13}-\psi)})(1 + e^{-(\gamma_{13}-\psi)})} + \mathcal{O}(\rceil^{-\in\gamma_{\infty\ni}}) \\
&= 2\gamma_{13}\int_0^{\gamma_{13}} d\lambda\, \lambda \sum_{n=0}^\infty e^{-2n\lambda} - 2\int_0^{\gamma_{13}} d\lambda\, \lambda^2 \sum_{n=0}^\infty e^{-2n\lambda} + \mathcal{O}(\rceil^{-\in\gamma_{\infty\ni}}) \,,
\end{aligned}
\tag{D.15}
$$

with $\lambda \equiv \gamma_{13} - \psi$, from which

$$
k_4 = 2\left[\frac{\gamma_{13}^3}{6} + \gamma_{13}\frac{\zeta(2)}{4} - \frac{\zeta(3)}{4}\right] \,.
\tag{D.16}
$$

Finally k_5 is given by

$$
\begin{aligned}
k_5 &= -2\int_0^\infty d\psi\, \psi\, \ln(1 - e^{-2\psi}) \\
&= \frac{\zeta(3)}{2} \,,
\end{aligned}
\tag{D.17}
$$

by using same kind of manipulations. Combining the above results one finds

$$I_1 = \frac{\gamma_{13}^3}{3} + \frac{\zeta(2)}{2}\gamma_{13} \,. \tag{D.18}$$

Using Eqs. (D.13) and (D.18), one finds for the asymptotic behavior of I_2

$$I_2(v_1, v_3) = \frac{\gamma_{13}^3}{3} + \frac{3\zeta(2)}{2}\gamma_{13} + \mathcal{O}(]^{-\gamma_{\infty \ni}}) \,. \tag{D.19}$$

By using this result in the expression for the single-pole term, $W^{s.p.}_{2E,3g-D}$, we find

$$
\begin{aligned}
W^{s.p.}_{2E,3g-D} &= \left(\frac{\alpha_s}{\pi}\right)^2 d^{[t]}_{JI} C_A \frac{1}{2}\left\{ -\frac{1}{4\varepsilon}\,\gamma_{13} + \frac{1}{16\varepsilon}\left[\frac{2}{3}\gamma_{13}^3 + 4\zeta(2)\gamma_{13}\right]\right\} \\
&\quad + \mathcal{O}(]^{-\gamma_{\infty \ni}}) \\
&= -\left(\frac{\alpha_s}{\pi}\right)^2 d^{[t]}_{JI} \frac{C_A}{2}\frac{1}{4\varepsilon}\left[-\frac{\gamma_{13}^3}{6} + (1 - \zeta(2))\,\gamma_{13}\right] + \mathcal{O}(]^{-\gamma_{\infty \ni}}) \,.
\end{aligned}
\tag{D.20}
$$

The contribution of the $\bar{V}_{\mu\nu\rho}$ piece to the diagram in Fig. 4.3(f) is given by [99]

$$W^{s.p.}_{2E,3g-\bar{V}} = -\left(\frac{\alpha_s}{\pi}\right)^2 d^{[t]}_{JI} \frac{C_A}{2}\frac{1}{4\varepsilon}\left[-\gamma_{13} + \frac{\zeta(2)}{4} + \frac{1}{2}I_3(\gamma_{13}) + \mathcal{O}(]^{-\gamma_{\infty \ni}})\right] \,, \tag{D.21}$$

where

$$I_3(\gamma_{13}) \equiv \sinh(2\gamma_{13}) \int_0^{\gamma_{13}} d\psi \, \frac{1}{\sinh^2 \gamma_{13} - \sinh^2 \psi} \ln\left(\frac{\sinh \gamma_{13}}{\sinh \psi}\right) \,. \tag{D.22}$$

One can analyze the high-energy asymptotics of I_3 in a similar way as above, with the result

$$I_3(\gamma_{13}) = \gamma_{13}^2 + \frac{3\zeta(2)}{2} + \mathcal{O}\left(]^{-\gamma_{\infty \ni}}\right) \,. \tag{D.23}$$

Combining Eqs. (D.20), (D.21) and (D.23), and letting $\gamma_{13} = T$, we find

$$
\begin{aligned}
W^{s.p.}_{2E,3g} &= -\left(\frac{\alpha_s}{\pi}\right)^2 d^{[t]}_{JI} \frac{C_A}{2} \frac{1}{4\varepsilon} \left\{ \left[-\frac{T^3}{6} + (1 - \zeta(2))\, T \right] \right. \\
&\qquad\qquad \left. + \left[\frac{T^2}{2} - T + \zeta(2) \right] \right\} + \mathcal{O}\left(\gimel^{-\gamma_{\infty\ni}}\right),
\end{aligned}
$$

$$(D.24)$$

which is the result given in Eq. (4.60).

The amplitudes for diagrams (d) and (e) of Fig. 4.3 are given in Ref. [100] and the high-energy asymptotics is obtained with a similar analysis. The results are given in Eq. (4.61). As mentioned above, these contributions cancel the $\bar{V}_{\mu\nu\rho}$ contribution from diagram (f), which is enclosed by the second set of brackets in Eq. (D.24).

Finally, let us look at the crossed-ladder diagram in Fig. 4.3(b). The velocity factor in configuration space is given by

$$
\begin{aligned}
F_{CL,t}(v_1, v_3) = (ig\mu^\varepsilon)^4 \, (v_1 \cdot v_3)^2 \int_0^\infty d\alpha_1 \int_0^{\alpha_1} d\alpha_2 \int_0^\infty d\beta_1 \int_0^{\beta_1} d\beta_2 \\
\times D(v_1\alpha_1 + v_3\beta_2) D(v_1\alpha_2 + v_3\beta_1). \quad (D.25)
\end{aligned}
$$

It is not difficult to show that the single-pole part of the crossed-ladder velocity factor is precisely the negative of that for the uncrossed-ladder diagram in Fig. 4.3(a). Therefore in the combination of the two diagrams the single-pole part of Eq. (D.25) is multiplied by the difference of the respective color factors. Although the individual color factors are not proportional to the one-loop factor $d^{[t]}_{JI}$, their difference evaluates to $d^{[t]}_{JI} C_A/2$. The following result for

the combination of diagrams (a) and (b) can also be found in Ref. [99],[1]

$$W^{s.p.}_{CL+L,t} = -\left(\frac{\alpha_s}{\pi}\right)^2 d^{[t]}_{JI} \frac{C_A}{2} \frac{1}{2\varepsilon} \coth^2 \gamma_{13} I_3(v_1, v_3),\qquad \text{(D.26)}$$

where we define

$$I_3(v_1, v_3) \equiv \int_0^{\gamma_{13}} d\psi\, \psi\, (\gamma_{13} - \psi)\, \coth \psi.\qquad \text{(D.27)}$$

One can investigate the asymptotic behavior of I_3 in a way similar to that presented for the 3-gluon vertex diagram in Fig. 4.3(f). One obtains the result

$$I_3(v_1, v_3) = \frac{\gamma_{13}^3}{6} + \frac{\zeta(2)}{2}\gamma_{13} - \frac{\zeta(3)}{2} + \mathcal{O}(]^{-\gamma_{\infty_3}}).\qquad \text{(D.28)}$$

By using the above relation in Eq. (D.26) we find

$$W^{s.p.}_{CL+L,t} = -\left(\frac{\alpha_s}{\pi}\right)^2 d^{[t]}_{JI} \frac{C_A}{2} \frac{1}{2\varepsilon} \left(\frac{\gamma_{13}^3}{6} + \frac{\zeta(2)}{2}\gamma_{13} - \frac{\zeta(3)}{2}\right) + \mathcal{O}(]^{-\gamma_{\infty_3}}).\qquad \text{(D.29)}$$

Letting $\gamma_{13} = T$, this is the result given in Eq. (4.59), along with the result for diagram (c) [99].

---

[1]Needless to say we can evaluate the integrals in momentum space and get the same result.

Appendix E

The commutator of $\mathbf{I}_{\mathrm{f}}^{(1)\mathrm{fin}}$ and $\boldsymbol{\Gamma}_{S_{\mathrm{f}}}^{(1)}$

The task of this appendix is to evaluate the commutator $\left[\mathbf{I}_{\mathrm{f}}^{(1)\mathrm{fin}}, \boldsymbol{\Gamma}_{S_{\mathrm{f}}}^{(1)}\right]$ appearing on the left-hand side of Eq. (4.99). Note that the pole parts of $\mathbf{I}_{\mathrm{f}}^{(1)}$ can be identified with $\boldsymbol{\Gamma}_{S_{\mathrm{f}}}^{(1)}$, via Eq. (4.89). Writing out the $\mathcal{O}(\varepsilon^0)$ parts of $\mathbf{I}_{\mathrm{f}}^{(1)\mathrm{fin}}$ with nontrivial color structure, the commutator of the finite and pole parts of $\mathbf{I}_{\mathrm{f}}^{(1)}$ becomes,

$$
\begin{aligned}
\left[\mathbf{I}_{\mathrm{f}}^{(1)\mathrm{fin}}, \boldsymbol{\Gamma}_{S_{\mathrm{f}}}^{(1)}\right] = {} & \\
& \frac{1}{4}\left[\sum_{k}\sum_{l\neq k}(\mathbf{T}_k\cdot\mathbf{T}_l)\left(\frac{1}{2}\ln^2\left(\frac{\mu^2}{-s_{kl}}\right)+\frac{\gamma_k}{\mathbf{T}_k^2}\ln\left(\frac{\mu^2}{-s_{kl}}\right)\right)\right. \\
& \left. \qquad\qquad , \sum_{i}\sum_{j\neq i}(\mathbf{T}_i\cdot\mathbf{T}_j)\ln\left(\frac{\mu^2}{-s_{ij}}\right)\right] \\
= {} & \mathcal{C}_{3,\mathrm{f}} + \mathcal{C}_{2,\mathrm{f}},
\end{aligned}
\tag{E.1}
$$

where in the second equality we introduce notation to separate the terms with three logarithms ($\mathcal{C}_{3,\mathrm{f}}$) from those with two ($\mathcal{C}_{2,\mathrm{f}}$).

In the case where all external lines are gluons, or all are quarks and/or antiquarks, all the ratios $\gamma_k/\mathbf{T}_k^2$ in the left-hand side of the commutator are

equal. This term is then proportional to $\mathbf{\Gamma}_{S_f}^{(1)}$, and $\mathcal{C}_{2,f}$ vanishes. This argument does not apply, of course, to mixed processes, such as $q\bar{q} \to gg$. For the latter case, however, and for any other $2 \to 2$ process, we may use the color conservation identity $\sum_k \mathbf{T}_k = 0$ and the simplicity of the kinematics to show that $\mathcal{C}_{2,f}$ vanishes. The argument is simple, and may be given for the case $q\bar{q} \to gg$ without loss of generality. In this case, we may take $k = 1, 2$ in Eq. (E.1) to correspond to the incoming quark and antiquark, and we consider just these terms in the double-logarithmic part of the commutator in Eq. (E.1). We focus first on the terms with prefactor $\gamma_q/\mathbf{T}_q^2 = 3/2$. (The same argument applies to the remaining terms, with prefactor $\gamma_g/\mathbf{T}_g^2$.) These terms are proportional to

$$\left[\sum_{k=1}^{2} \sum_{l \neq k} \mathbf{T}_k \cdot \mathbf{T}_l \ln\left(\frac{\mu^2}{-s_{kl}}\right) , \sum_{i=1}^{4} \sum_{j \neq i} \mathbf{T}_i \cdot \mathbf{T}_j \ln\left(\frac{\mu^2}{-s_{ij}}\right) \right] . \qquad \text{(E.2)}$$

This commutator would vanish if the sum over index k were extended to $k = 3$ and 4. But this can by done by observing that $\sum_k \mathbf{T}_k = 0$ implies that, for example,

$$\mathbf{T}_1 \cdot \mathbf{T}_2 = \mathbf{T}_3 \cdot \mathbf{T}_4 + \frac{1}{2}\left(T_3^2 + T_4^2 - T_1^2 - T_2^2\right) , \qquad \text{(E.3)}$$

where the squared terms commute with all combinations of generators. At the same time, we have $s_{12} = s_{34}$. As a result, in the left-hand term of the commutator (E.2), we may make the replacement

$$\mathbf{T}_1 \cdot \mathbf{T}_2 \ln\left(\frac{\mu^2}{-s_{12}}\right) \to \mathbf{T}_3 \cdot \mathbf{T}_4 \ln\left(\frac{\mu^2}{-s_{34}}\right) . \qquad \text{(E.4)}$$

Analogous reasoning for each of the terms in the sum over k and l in Eq. (E.2) shows that for $2 \to 2$ scattering the sum of the missing terms with $k =$

$3, 4$ is identical in the commutator to the sum from $k = 1, 2$. Inserting the missing terms, at the price of an overall factor of $1/2$, the two entries of the commutator become identical and it vanishes. This argument, of course, is heavily dependent on the specifics of $2 \to 2$ scattering. We know of no general argument that would eliminate all double-logarithmic terms in the commutator in $2 \to n$ processes; indeed such terms are generically present.

We now consider the triple-logarithmic terms in Eq. (E.1),

$$
\begin{aligned}
\mathcal{C}_{3,\mathrm{f}} &= \frac{1}{8} \left[\sum_k \sum_{l \neq k} \mathbf{T}_k \cdot \mathbf{T}_l \, , \, \sum_i \sum_{j \neq i} \mathbf{T}_i \cdot \mathbf{T}_j \right] b_{kl} \, a_{ij} \\
&= \frac{1}{2} \sum_{i \neq j \neq k} \left[\mathbf{T}_k \cdot \mathbf{T}_j \, , \, \mathbf{T}_j \cdot \mathbf{T}_i \right] b_{kj} \, a_{ij} \\
&= \frac{1}{2} \sum_{i \neq j \neq k} i \, f_{a_1 a_2 a_3} \, \mathbf{T}_k^{a_1} \, \mathbf{T}_j^{a_3} \, \mathbf{T}_i^{a_2} \, b_{kj} \, a_{ij} \, ,
\end{aligned}
\tag{E.5}
$$

where in the first equality we have introduced the notation $b_{kl} = \ln^2(\mu^2/(-s_{kl})) = b_{lk}$ and $a_{ij} = \ln(\mu^2/(-s_{ij})) = a_{ji}$. In the second equality in Eq. (E.5) we have identified the nonvanishing terms in the commutator, for which one and only one pair of generators is matched between the two entries of the commutator. Because the scalar products are symmetric, there are four ways in which this matching may occur, for fixed indices $i \neq j \neq k$. Finally, the third equality shows the result of performing the commutator explicitly for the generators on the j line. This form is reminiscent of the color structure of $\hat{\mathbf{H}}_{\mathrm{f}}^{(2)}$, Eq. (4.94), although the triple-logarithmic momentum factors are different, and depend on the renormalization scale, μ.

To make contact between Eq. (E.5) and the explicit expression (4.94) for $\hat{\mathbf{H}}_{\mathrm{f}}^{(2)}$, we convert the sum of unequal choices of i, j and k into a sum over

distinguishable triplets, denoted (i, j, k). For each such choice, there are six permutations of the indices i, j and k in the final expression of Eq. (E.5). These can be thought of as three cyclic permutations, which leave the structure constants the same, but change the momentum factors, and three more (exchanges of i and k for fixed j, plus cyclic permutations), which change the sign of the structure constants, and change the kinematic factors.

Following this path, we define

$$c_{[kj,ji]} \equiv b_{kj} \, a_{ji} \; - \; b_{ij} \, a_{jk} \tag{E.6}$$

and rewrite $\mathcal{C}_{3,\mathrm{f}}$ as

$$\mathcal{C}_{3,\mathrm{f}} \;\; = \;\; \frac{1}{2} \sum_{(i,j,k)} i \, f_{a_1 a_2 a_3} \, \mathbf{T}_k^{a_1} \, \mathbf{T}_j^{a_3} \, \mathbf{T}_i^{a_2} \left[c_{[kj,ji]} + c_{[ik,kj]} + c_{[ji,ik]} \right]. \tag{E.7}$$

A straightforward calculation shows that all of the μ-dependence cancels in this expression. Relabelling the indices, and using the antisymmetry of the structure constants, we derive

$$
\begin{aligned}
\mathcal{C}_{3,\mathrm{f}} \;\; &= \;\; -\frac{i}{2} \sum_{(i,j,k)} f_{a_1 a_2 a_3} \, \mathbf{T}_i^{a_1} \, \mathbf{T}_j^{a_2} \, \mathbf{T}_k^{a_3} \, \ln\left(\frac{-s_{ij}}{-s_{jk}} \right) \ln\left(\frac{-s_{jk}}{-s_{ki}} \right) \ln\left(\frac{-s_{ki}}{-s_{ij}} \right) \\
&= \;\; -\frac{1}{2} \, \hat{\mathbf{H}}_{\mathrm{f}}^{(2)}, \tag{E.8}
\end{aligned}
$$

which establishes the result of Eq. (4.99). We emphasize that, unlike our demonstration that $\mathcal{C}_{2,\mathrm{f}}$ vanishes, this result holds for an arbitrary $2 \to n$ process.

Bibliography

[1] E. Fermi, Ric. Sci. **4**, 491 (1933); reprinted in E. Fremi, *Collected Papers*, edited by E. Segre *et al.* (University of Chicago Press, Chicago, 1962), Vol. 1, p. 538.

[2] E. Fermi, Z. Phys. **88**, 161 (1934).

[3] G. F. Chew, *S-Matrix Theory of Strong Interactions* (W. A. Benjamin, INC., New York, 1962).

[4] R. J. Eden, P. V. Landshoff, D. I. Olive and J. C. Polkinghorne, *The Analytic S-Matrix* (Cambridge University Press, Cambridge, 1966).

[5] T. Regge, Nuo. Cim. **14** 951 (1959).

[6] T. Regge, Nuo. Cim. **18** 947 (1960).

[7] M. Gell-Mann and Y. Neeman, *The Eightfold Way* (W. A. Benjamin, INC., New York, 1962).

[8] T. P. Cheng and L. P. Li, *Gauge Theory of Elementary Particle Physics* (Oxford University Press, New York, 1984).

[9] O. W. Greenberg, Phys. Rev. Lett. **13**, 598 (1964).

[10] M. Y. Han and Y. Nambu, Phys. Rev. **B139**, 1006 (1965).

[11] C. N. Yang and R. L. Mills, Phys. Rev. **96**, 191 (1954).

[12] E. D. Bloom *et al.*, Phys. Rev. Lett. **23**, 930 (1969).

[13] M. Breidenbach *et al.*, Phys. Rev. Lett. **23**, 935 (1969).

[14] J. I. Friedman and H. W. Kendall, Ann. Rev. Nucl. Part. Sci. **22**, 203 (1972).

[15] R. P. Feynman, Phys. Rev. Lett. **23**, 1415 (1969).

[16] J. D. Bjorken and E. A. Paschos, Phys. Rev. **185**, 1975 (1969).

[17] C. G. Callan and D. G. Gross, Phys. Rev. Lett. **22**, 156 (1969).

[18] G. t' Hooft, Nucl. Phys. **B33**, 173 (1971).

[19] G. t' Hooft, Nucl. Phys. **B35**, 167 (1971).

[20] G. t' Hooft and M. Veltman, Nucl. Phys. **B50**, 318 (1972).

[21] K. Wilson, Phys. Rev. **D3**, 1818 (1971).

[22] L. D. Fadeev and V. N. Popov, Phys. Lett. **B25**, 29 (1967).

[23] G. Sterman, *An Introduction to Quantum Field Theory* (Cambridge University Press, Cambridge, 1993).

[24] K. Wilson, Phys. Rev. **D10**, 2445 (1974).

[25] J. Kogut and L. Susskind, Phys. Rev. **D11**, 395 (1975).

[26] M. Creutz, *Quarks, Gluons, and Lattices* (Cambridge University Press, Cambridge, 1983).

[27] D. J. Gross and F. Wilczek, Phys. Rev. Lett. **30**, 1343 (1973).

[28] D. J. Gross and F. Wilczek, Phys. Rev. **D8**, 3633 (1973).

[29] H. D. Politzer, Phys. Rev. Lett. **30**, 1346 (1973).

[30] G. Sterman and S. Weinberg, Phys. Rev. Lett. **39**, 1436 (1977).

[31] L. Landau, Nucl. Phys. **13**,181 (1959).

[32] S. Coleman and R. E. Norton, Nuovo Cimento **38**, 438 (1965).

[33] G. Sterman, Phys. Rev. D **17**, 2773 (1978).

[34] S. B. Libby and G. Sterman, Phys. Rev. D **18**, 3252 (1978).

[35] D. Amati, R. Petronzio and G. Veneziano, Nucl. Phys. **B140**, 54 (1978).

[36] A. H. Mueller, Phys. Rev. **D18**, 3705 (1978).

[37] R. K. Ellis, H. Georgi, M. Machacek, H. D. Politzer and G. G. Ross, Nucl. Phys. **B152**, 285 (1979).

[38] A. V. Efremov and A. V. Radyushkin, Theor. Math. Phys. **44** 664,774 (1981).

[39] J. C. Collins and G. Sterman, Nucl. Phys. **B185**,172 (1981).

[40] G. Sterman, Phys. Rev. **D17**, 2773 (1977), *ibid.* 2789

[41] J. C. Collins, D. E. Soper and G. Sterman, Nucl. Phys. **B261**, 104 (1985).

[42] J. C. Collins, D. E. Soper and G. Sterman, Nucl. Phys. **B308**, 833 (1988).

[43] R. Basu, A. Ramalho and G. Sterman, Nucl. Phys. **B244**, 221 (1984).

[44] G. T. Bodwin, S. J. Brodsky and G. P. Lepage, Phys. Rev. Lett. **47**, 1799 (1981).

[45] W. W. Lindsay, D. A. Ross and C.T. Sachrajda, Nucl. Phys. **B214**, 61 (1983).

[46] A. Sen and G. Sterman, Nucl. Phys. **B229**, 231 (1983).

[47] J. C. Collins, D. E. Soper and G. Sterman, Nucl. Phys. **B223**, 381 (1983).

[48] J. C. Collins, D. E. Soper and G. Sterman, Phys. Lett. **B134**, 263 (1984).

[49] J. C. Collins, D. E. Soper and G. Sterman, Phys. Lett. B **438**, 184 (1998) [arXiv:hep-ph/9806234].

[50] G. t' Hooft, Nucl. Phys. **B33**, 173 (1971).

[51] G. t' Hooft and M. Veltman, Nucl. Phys. **B50**, 318 (1972).

[52] R. Tucci, Argonne report ANL-HEP-PR-84-70.

[53] S. J. Chang and S. K. Ma, Phys. Rev. **180**, 1506 (1969).

[54] J. B. Kogut and D. E. Soper, Phys. Rev. **D1**, 2901 (1970).

[55] G. Grammer, Jr. and D. R Yennie, Phys. Rev. **D8**, 4332 (1973).

[56] J. C. Collins and D. E. Soper, Nucl. Phys. **B193**, 381 (1981).

[57] J. C. Collins and D. E. Soper, Nucl. Phys. **B194**, 445 (1982).

[58] W. Zimmermann, in: *Lectures on elementary particles and quantum field theory*, eds. S. Deser, M. Grisaru and H. Pendleton (MIT Press, 1970).

[59] G. T. Bodwin, Phys. Rev. **D31**, 2616 (1985), *ibid.* **D34**, 3932 (1986).

[60] A. Sen, Phys. Rev. **D28**, 860 (1983).

[61] J. Botts and G. Sterman, Nucl. Phys. **B325**, 62 (1989).

[62] N. Kidonakis, G. Oderda and G. Sterman, Nucl. Phys. **B531**, 365 (1998) [hep-ph/9803241].

[63] N. Kidonakis, G. Oderda and G. Sterman, Nucl. Phys. **B525**, 299 (1998) [hep-ph/9801268].

[64] N. Kidonakis and J. F. Owens, Phys. Rev. **D63**, 054019 (2001) [hep-ph/0007268].

[65] A. Banfi, G. P. Salam and G. Zanderighi, JHEP **0408**, 062 (2004) [hep-ph/0407287].

[66] R. Bonciani, S. Catani, M. L. Mangano and P. Nason, Phys. Lett. **B575**, 268 (2003) [hep-ph/0307035].

[67] M. Dasgupta and G. P. Salam, Phys. Lett. **B512**, 323 (2001) [hep-ph/0104277].

[68] G. Sterman and M. E. Tejeda-Yeomans, Phys. Lett. **B552**, 48 (2003) [hep-ph/0210130].

[69] C. Anastasiou, E. W. N. Glover, C. Oleari and M. E. Tejeda-Yeomans, Nucl. Phys. **B601**, 318 (2001) [hep-ph/0010212].

[70] C. Anastasiou, E. W. N. Glover, C. Oleari and M. E. Tejeda-Yeomans, Nucl. Phys. **B601**, 341 (2001) [hep-ph/0011094].

[71] C. Anastasiou, E.W.N. Glover, C. Oleari and M.E. Tejeda-Yeomans, Nucl. Phys. **B605**, 486 (2001) [hep-ph/0101304].

[72] Z. Bern, A. De Freitas and L. J. Dixon, JHEP **0306**, 028 (2003) [hep-ph/0304168].

[73] E. W. N. Glover, JHEP **0404**, 021 (2004) [hep-ph/0401119].

[74] A. De Freitas and Z. Bern, JHEP **0409**, 039 (2004) [hep-ph/0409007].

[75] E. W. N. Glover, C. Oleari and M. E. Tejeda-Yeomans, Nucl. Phys. **B605**, 467 (2001) [hep-ph/0102201].

[76] Z. Bern, A. De Freitas and L. J. Dixon, JHEP **0203**, 018 (2002) [hep-ph/0201161].

[77] S. Catani and M. H. Seymour, Phys. Lett. **B378**, 287 (1996) [hep-ph/9602277];

[78] S. Catani and M. H. Seymour, Nucl. Phys. **B485**, 291 (1997) [Err.-ibid. **B510**, 503 (1997)] [hep-ph/9605323].

[79] S. Catani, Phys. Lett. **B427**, (1998) 161 [hep-ph/9802439].

[80] W. T. Giele and E. W. N. Glover, Phys. Rev. **D46**, 1980 (1992).

[81] Z. Kunszt, A. Signer and Z. Trócsányi, Nucl. Phys. **B420**, 550 (1994) [hep-ph/9401294].

[82] S. M. Aybat, L. J. Dixon and G. Sterman, hep-ph/0606254.

[83] B. Jantzen, J. H. Kühn, A. A. Penin and V. A. Smirnov, Nucl. Phys. **B731**, 188 (2005) [hep-ph/0509157].

[84] L. W. Garland, T. Gehrmann, E. W. N. Glover, A. Koukoutsakis and E. Remiddi, Nucl. Phys. **B627**, 107 (2002) [hep-ph/0112081];

[85] L. W. Garland, T. Gehrmann, E. W. N. Glover, A. Koukoutsakis and E. Remiddi, Nucl. Phys. **B642**, 227 (2002) [hep-ph/0206067].

[86] Z. Bern, L. J. Dixon and D. A. Kosower, JHEP **0408**, 012 (2004) [hep-ph/0404293].

[87] R. Akhoury, Phys. Rev. **D19**, 1250 (1979).

[88] L. Magnea and G. Sterman, Phys. Rev. **D42**, 4222 (1990).

[89] L. Magnea, Nucl. Phys. Proc. Suppl. **96**, 84 (2001) [hep-ph/0008311];

[90] L. Magnea, Nucl. Phys. **B593**, 269 (2001) [hep-ph/0006255].

[91] J. C. Collins, Adv. Ser. Direct. High Energy Phys. **5**, 573 (1989) [hep-ph/0312336].

[92] R. J. Gonsalves, Phys. Rev. **D28**, 1542 (1983).

[93] G. Kramer and B. Lampe, Z. Phys. **C34**, 497 (1987) [Erratum-ibid. **C42**, 504 (1989)].

[94] T. Matsuura and W. L. van Neerven, Z. Phys. **C38**, 623 (1988).

[95] T. Matsuura, S. C. van der Marck and W. L. van Neerven, Nucl. Phys. **B319**, 570 (1989).

[96] R. V. Harlander, Phys. Lett. **B492**, 74 (2000) [hep-ph/0007289].

[97] S. Moch, J. A. M. Vermaseren and A. Vogt, JHEP **0508**, 049 (2005) [hep-ph/0507039];

[98] S. Moch, J. A. M. Vermaseren and A. Vogt, Phys. Lett. **B625**, 245 (2005) [hep-ph/0508055].

[99] G. P. Korchemsky and A. V. Radyushkin, Nucl. Phys. **B283**, 342 (1987).

[100] I. A. Korchemskaya and G. P. Korchemsky, Nucl. Phys. **B437**, 127 (1995) [hep-ph/9409446].

[101] J. Kodaira and L. Trentadue, Phys. Lett. **B112**, 66 (1982).

[102] N. Kidonakis, hep-ph/0208056.

[103] G. Sterman, in *AIP Conference Proceedings Tallahassee, Perturbative Quantum Chromodynamics*, eds. D. W. Duke, J. F. Owens, New York, 1981, p. 22.

[104] J. G. M. Gatheral, Phys. Lett. **B133**, 90 (1983).

[105] J. Frenkel and J. C. Taylor, Nucl. Phys. **B246**, 231 (1984).

[106] C. F. Berger, hep-ph/0305076.

[107] C. F. Berger, Phys. Rev. **D66**, 116002 (2002) [hep-ph/0209107].

[108] S. Catani, B. R. Webber and G. Marchesini, Nucl. Phys. **B349**, 635 (1991).

[109] L. J. Dixon, in *QCD & Beyond: Proceedings of TASI '95*, ed. D. E. Soper (World Scientific, Singapore, 1996) [hep-ph/9601359].

[110] V. Ravindran, J. Smith and W. L. van Neerven, Nucl. Phys. **B704**, 332 (2005) [hep-ph/0408315].

[111] Y. L. Dokshitzer and G. Marchesini, Phys. Lett. **B631**, 118 (2005) [hep-ph/0508130].

[112] Y. L. Dokshitzer and G. Marchesini, JHEP **0601**, 007 (2006) [hep-ph/0509078].

[113] M. H. Seymour, JHEP **0510**, 029 (2005) [hep-ph/0508305].

[114] A. Kyrieleis and M. H. Seymour, JHEP **0601**, 085 (2006) [hep-ph/0510089].

[115] J. M. Cornwall and G. Tiktopoulos, Phys. Rev. **D15**, 2937 (1977).

[116] J. Frenkel and J. C. Taylor, Nucl. Phys. **B124**, 268 (1977).

[117] D. Binosi and L. Theussl, Comput. Phys. Commun. **161**, 76 (2004) [hep-ph/0309015].

[118] J. A. M. Vermaseren, Comput. Phys. Commun. **83**, 45 (1994).